University of South-Eastern Norway
Faculty of Technology, Natural Sciences and Maritime Studies

Doctoral dissertation no. 101
2021

Mahesh Ediriweera

Impact erosion by solid particles in gas-particle flows

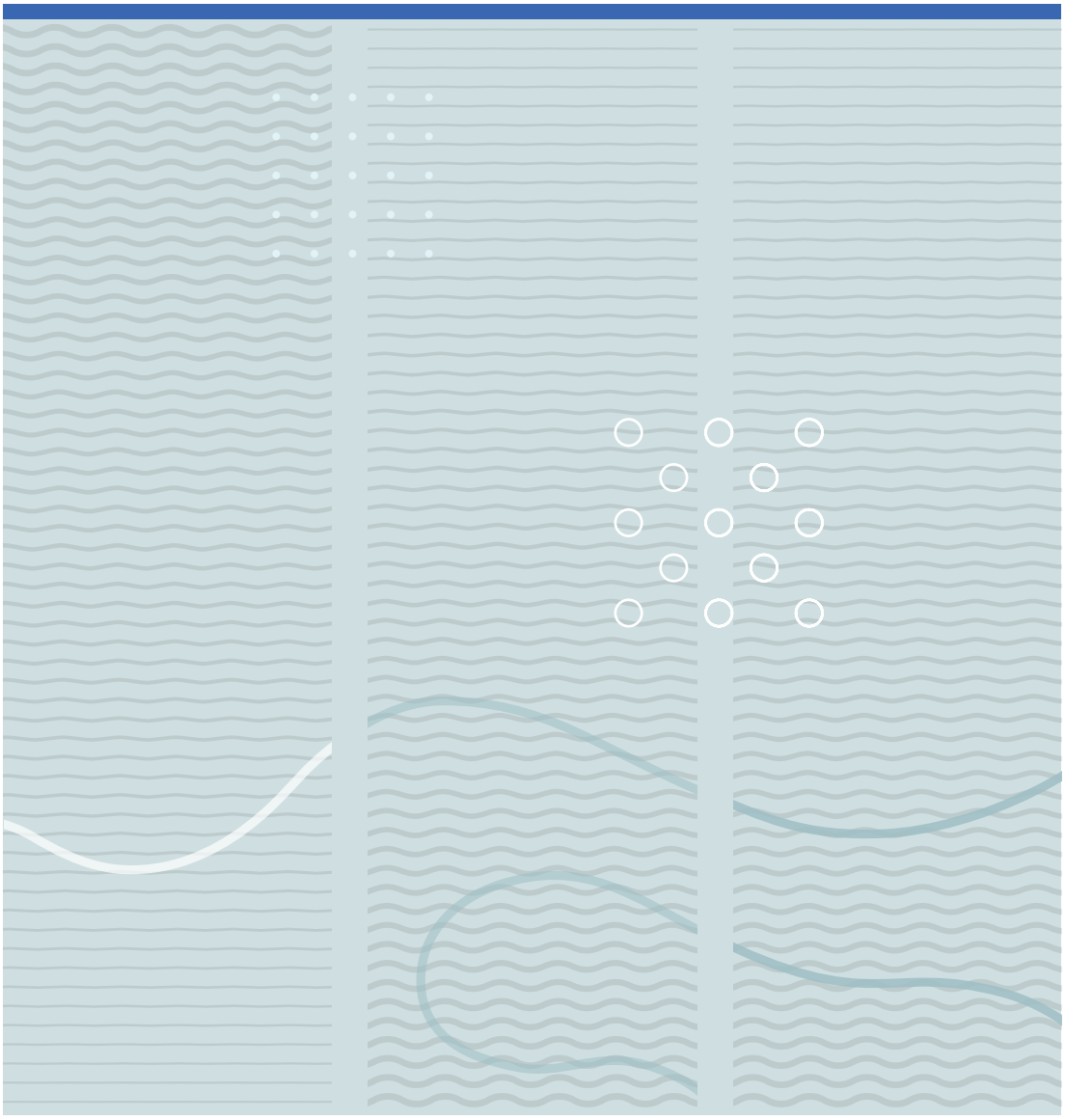

Mahesh Ediriweera

Impact erosion by solid particles in gas-particle flows

A PhD dissertation in
Process, Energy and Automation Engineering

Faculty of Technology, Natural Sciences and Maritime Studies
University of South-Eastern Norway
Porsgrunn, 2021

Doctoral dissertations at the University of South-Eastern Norway no .101

ISSN: 2535-5244 (print)
ISSN: 2535-5252 (online)

ISBN: 978-82-7206-608-5 (print)
ISBN: 978-82-7206-609-2(online)

Print: University of South-Eastern Norway

Dedicated to my parents, wife, son, daughter, family members and friends.

Preface

This thesis is submitted to University of South East Norway (USN) as a partial fulfilment of the degree of Doctor of Philosophy to the Department of Process, Energy and Automation Engineering under the Faculty of Technology, Natural Sciences and Maritime Sciences. I had the pleasure of working as a PhD candidate at SINTEF Tel-Tek and USN from August 2015 to January 2019. Professor Chandana Ratnayake was the main supervisor and Dr. Jana Chladek and Dr. Sivert Ose (GE Power Norway AS) were co-supervisors.

The study related to the impact erosion in gas particle systems was conducted under the project of "Effective handling of bulk solids with focus on reduction of erosion and scale formation". The project was mainly funded by the Research Council of Norway together with Hydro Aluminium AS, GE Power Norway AS and Omya Hustadmarmor AS through the BIA program (Project No, 247789).

Acknowledgements

The experimental study described under this thesis would not have become a reality without the support of many individuals and organisations. Therefore, I would like to take this as an opportunity to acknowledge and express my gratitude towards them. Firstly, I would like to express my sincere gratitude to my main supervisor Prof. Chandana Ratnayake and the co-supervisor Dr. Jana Chladek for selecting me for this project, their excellent guidance, encouragement and immense support given from the beginning to the end. I am forever grateful to their kindness, patience and tremendous moral support given whenever needed and for sharing their academic as well as practical knowledge. Their guidance throughout the project helped me in planning the project work, correcting publications and writing the thesis and most importantly widening my knowledge in powder technology. My sincere thanks also goes to co-supervisor Dr. Sivert Ose for sharing his expert industrial knowledge related to impact erosion. His constructive comments and fruitful discussions helped me keeping the focus on subject matters.

I would like to thank Dr. Maths Halstensen for his proficiency on modelling and data handling which enhanced the quality of the final outcome. I sincerely thank Dr. Arne Røyset for his excellent work in analysing eroded samples and his dedication for the publication. Further, I would like to thank Dr. Ali Ghaderi for the interesting discussions on mathematics. I am grateful to Prof. Gisle Enstad for his instructions to overcome practical problems on experiments.

This project is a collective effort of team SINTEF Tel-Tek. My heartfelt gratitude goes to them for employing me and offering the PhD position. The guidance from Dr. Reidar Arneberg to perform the multivariate test campaign is highly appreciated. Dr. Arneberg was exceptionally kind to guide me even after his retirement. Further, I acknowledge useful instructions given by the department head, Dr. Frode Brakstad and Dr. Sailesh Abburu on application of multivariate data. Dr. Kristian Aas supported in arranging test facilities during his period as the project leader. I am grateful to Franz Otto Hafenbrädl for his generous support at powder hall. He and Tonje Thomassen helped me to conduct

simultaneous laboratory tests. I thank my fellow PhD partner, Dr. Ingrid B. Haugland for her company throughout the project. I am grateful to Hans Aksel Haugen, Liv Axelsen, Dr. Klaus Schöffel, Marit Larsen, Hallgeir Kjeldal, Eksath de Silva for supporting me in many ways during my stay at Tel-Tek.

I acknowledge all the representatives from industrial partners for the shared knowledge, valuable discussions and the great support. I specially thank Gunn Iren Müller and Marina Zinchenko for providing bulk material on time. I am grateful to Marcus Adam for his valuable comments on publications.

There is a lot who deserves special thanks from USN. I should mention Unni S. Kaasin, Prof. Britt E. Moldestad, Prof. Lars A. Tokheim, Asanthi Jinasena, Per M. Hansen, Mariken Røsand and Øyvind Johansen for their support during the project and opening me new doors in academia. I am also grateful to the PhD committee, library, IT department and print shop at USN.

I convey my gratitude to all my friends in Norway for their social support during my stay in Norway. Special thank goes to Deshaka Kottage, Chameera Jayarathna, Ajith Pitigala, Anjana Malagalage, Sithara Dayarathna and their families who were with me from the very first day I arrived in Norway. I am also thankful to my housemates at the student house, Robin Wold and Anushka Perera who made it an interesting experience.

I would like to thank my parents, my siblings for their moral support. They are the people who moulded up me to the person who I am today. I am also grateful to parents-in law for their dedication during the hectic period of my life. Last but not the least, I would like to express my heartful gratitude to my loving wife Dilini, who was always by my side and taking care of me and my two precious kids. She always believed in me and was holding my hand during all the difficult times. A big hug to my little Oneth & Oneli for being my stress relievers during this restless period. I love you so much!

Abstract

Mass loss of inner wall surface due to particle impact, also referred as erosive wear, is a common challenge encountered in industrial pneumatic conveying systems. Previous studies have shown that erosion is a process involving many parameters and a combination of several wear mechanisms. Though a large number of fundamental and analytical mechanisms/models are available to explain the phenomena, there is no fully defined comprehensive description to predict erosion rate accurately.

In the present study, a sand blast type erosion tester was used to investigate the erosion process on mild steel (DOMEX 355MC) surface. The effect of particle size, impact angle, exposure time (amount of erodent) on impact erosion was analysed by univariate tests. Morphology of the eroded craters produced by a stream of air-borne dolomite particles were studied by a surface profilometer. Topographic measurements of the profilometer provided the dimensions of the surface profile, estimation of maximum penetration and slope inside the crater. Based on univariate tests, multivariate analysis was carried out with six variables to determine significant variables using the Design of Experiments methodology. This methodology resulted in selection of four significant variables which were used to calibrate a Partial Least Squares Regression (PLS-R) model that allows a closer study of the influence of the main variables and their interactions.

Mass loss against impact angles changed considerably with exposure time due to changes of the surface during the erosion process. It was noticed that the effective impact angle (impact angle measured inside the crater) had changed with the expansion of the crater. The change of effective impact angle causes to change the dominance of the erosion mechanism on the eroded surface and consequently the erosion rate. The effective impact angle was calculated for different exposure times to understand the change of erosion rate with time. The penetration depth was highest at low impact angles. The critical impact angle corresponding to the maximum penetration depth changed with the exposure time. The knowledge of how the particles penetrate into the surface as a function of exposure time can be useful in determination of the material thickness when designing equipment with longer durability.

The effects of four significant main variables were identified by the statistical model. The model predicted promising results, however, the validity of the model is limited to the tested conditions and the materials. Impact angle and impact velocity had high effects on erosion. Generally, erosion increased with higher impact velocity and decreased with increase in impact angle. Impact velocity had a higher effect at low impact angles than at high impact angles, revealing an interaction between the two variables. Increase in surface temperature and particle size of bulk material also resulted in higher erosion, however, the effects of these two variables were lower compared to the effects of the impact velocity and the impact angle. Surface temperature had a higher effect on erosion than the particle size within the tested conditions.

List of papers

Paper 01

Ediriweera M., Chladek J., and Ratnayake C. (2019) Effect of impact angle, exposure time, and particle size on impact erosion. Particulate Science and Technology: p. 1-9. doi: 10.1080/02726351.2019.1663328.

Paper 02

Ediriweera M., Chladek J., Røyset A., and Ratnayake C. (2020) The progression of impact erosion with exposure time. Submitted to Particulate Science and Technology.

Paper 03

Ediriweera M., Arneberg R., Chladek J., Røyset A., and Ratnayake C. (2018) Multivariate analysis of impact erosion by Dolomite particles. The International Conference on Conveying and Handling of Particulate Solids (CHoPS, 2018). doi: 10.2139/ssrn.3293018.

Paper 04

Ediriweera M., Halstensen M., Arneberg R., Chladek J., Røyset A., and Ratnayake C. (2019) Multivariate modelling of key variables in solid-particle erosion. Submitted to Tribology - Materials, Surfaces & Interfaces.

List of tables

List of figures

Nomenclature

C_d	Drag coefficient
d	Perpendicular penetration depth of the crater
d_{max}	Maximum penetration depth
E	Deformation wear factor
f_c	Full penny median crack
h_c	Half-penny crack
K	Kinetic energy of the particle
l_c	Lateral crack
M	Total particle mass
m_{loss}	Mass loss
P	Plastic flow stress
Q	Removed material volume
r	Radius of the particle
u	Air velocity
V	Particle velocity
v_{loss}	Volume loss
W_D	Removal volume due to deformation wear
W_C	Removal volume due to cutting wear
W_{t0}	True erosion rate when the particle concentration tending to zero
θ	Impact angle
θ_e	Effective impact angle
θ_i	Initial impact angle
p	Density of material
p_a	Density of air
p_p	Density of particle
2Ψ	Angle of indenter
ω	Rotational speed

Table of contents

Part A: Overview

1 Introduction

1.1 Background

Pneumatic transportation of granular and powdered solid is a well-known technique used in the industry due to its attractive flexible and environment friendly behaviour. Wide range of solid particles can be successfully conveyed by carrier gas under variety of conditions [1]. Pneumatic conveying systems are comprised with several components such as compressors, valves, pumps, conveying pipelines, cyclones, etc. Although there are number of benefits, material removal on the surface by erosive wear has been identified as a major challenge in the industrial pneumatic conveying systems which causes many unnecessary effects such as unplanned plant shutdowns, hazardous material leakages, undesired or dangerous metal particle contaminations in the transported material and also huge cost for maintenance and labour.

Material removal on the surface also known as surface wear affects the durability of the components and is a main cause of material wastage in components [2]. Wear is the removal of material from the surfaces by physical separation due to micro-fracture or plastic deformation, or by chemical dissolution at the contact interface. There are three major types of wear mechanisms, which can be identified as follows.

- Abrasive wear
- Erosive wear
- Corrosive wear

Both abrasion and erosion are mechanical processes, while corrosion is related to chemical processes. Abrasive wear takes place when a harder material slips over a relatively soft surface [3]. It can also be described as the loss of material due to a harder material being forced against and rubbing along a soft surface. The impingement of solid particles or small drops of liquid often causes erosion of surfaces of the components. When a particle is impacted on a surface with a significant velocity, dents and large scale subsurface deformation occur on the surface [4]. Corrosive wear is typically caused by

chemical and electro-chemical reactions between the surface and the surrounding environment. Oxygen or other reactive gases present in the environment react with the top layers of solid surface and resulting products of the reaction are formed on the surface [5]. The corroded layer then removes from the surface and the process is called corrosive wear.

The contact between the wall surface and the transported particulates causes wear of the inner surface of pipe walls in pneumatic conveying systems. Mainly, the wear of pneumatic conveying systems occurs due to the high velocity impact of the suspended particles and therefore it is called impact erosion [6]. Impact erosion can be seen in variety of industrial applications. As an example, smaller particles escaping from gas-cyclones cause considerable damage to the turbine stator and rotor blades in a coal gasification plant and reduce the durability of equipment drastically [7] due to the impact erosion. Impact erosion of the inner surface can be severe, depending on influential parameters. Thus, better understanding of impact erosion mechanisms and analysis of influential parameters are essential to control the erosion process effectively in handling abrasive materials.

With the progression of scientific studies, more and more aspects were considered to control erosion. Most of the research works have been developed on the basis of experimental results and analytical investigations [7-13]. Although many researchers have suggested a number of wear mechanisms, models and correlations to understand the phenomena [11, 14-17], no comprehensive description of the erosion mechanisms is available to address industrial challenges and a big knowledge gap still exists. Also, there are no effective methods available to reduce/control, or accurately predict the amount of wear. Thus, real-time observation and prediction models have been recognised as effective techniques to monitor erosion at industrial applications. A comprehensive understanding of effects of influential parameters on erosion is essential in developing prediction models or measurement methods.

This PhD study has been part of a knowledge-building research project no. 247789 funded by the Research Council of Norway and industry, including Hydro Aluminium AS,

GE Power Norway AS and Omya Hustadmarmor AS. In metal and mineral industries, pneumatic conveying is commonly used as the main bulk transfer method [18-21]. In aluminium production, primary alumina is used as a sorbent in dry scrubbers to capture off-gases containing fluoride. While chalk, limestone, marble and dolomite are used as raw materials in calcium carbonate production. It is generally accepted that alumina and dolomite with high content of hard mineral contamination are highly erosive [18, 22]. In both alumina and dolomite processing, handling of abrasive particles cause frequent wear of conveying equipment and therefore, there is a need to better control and minimise erosive damage.

In the present study, impact erosion in pneumatic transport of dolomite particles was investigated in detail. The findings of the study will be useful for further development of impact erosion mitigation mechanisms and for improved equipment designs in the processing plants. It is also expected that the research findings will be useful for other industries which handle different types of bulk solids but experience similar challenges.

1.2 Research problem

The main objective of the research study was to find the effects of influential variables and to investigate the process and propagation of impact erosion in pneumatic conveying systems, through a systematic experimental procedure using a lab scale erosion tester. The knowledge gained from univariate tests led to execution of a multivariate analysis on effects of main variables and their interactions to develop a predictive model including significant variables. In order to achieve the main objectives of the study, the project work was divided into several tasks and their interaction and connection to each other are shown in Figure 1.1. The scientific publications made during the study and their relevance to the different tasks are also indicated in the figure.

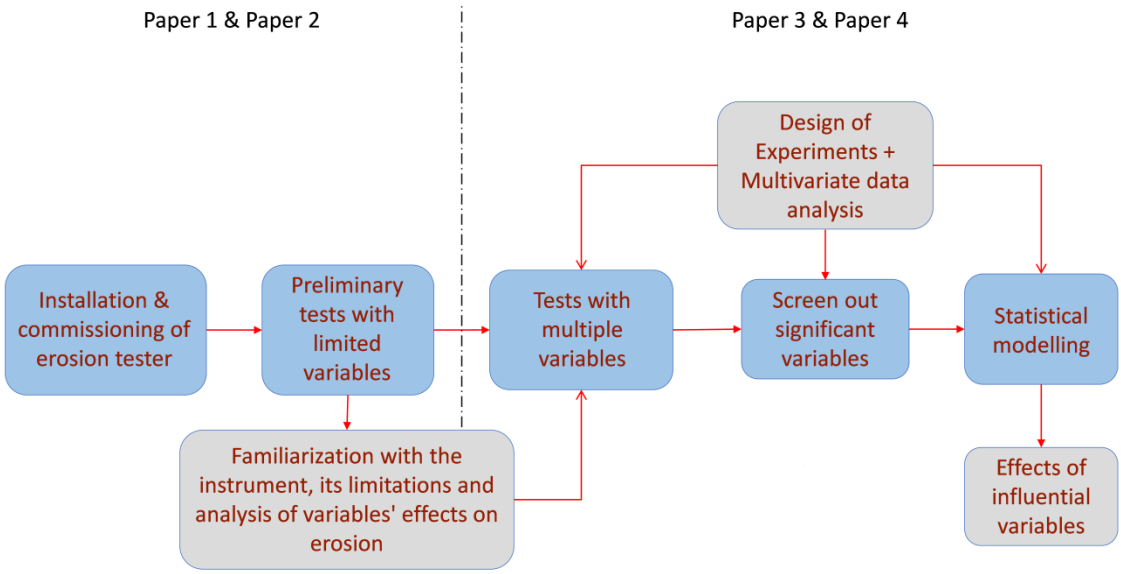

Figure 1.1: Schematic diagram of scientific approach followed during the present investigation.

Initially, a literature review related to gas-particle erosion and powder technology was performed to learn about the previous research. After the erosion tester (sand blast type) was installed at the powder hall at SINTEF Tel-Tek, preliminary tests were performed to identify the limitations and calibration conditions of the instrument related to the industrial process conditions. The preliminary tests were carried out as univariate tests with several variables such as particle size, impact angle and exposure time, correlating them to the resulting impact erosion. Under the context of the present study, the impact angle is defined as the angle between the target surface and the trajectory line of the particle coming towards the target. Commission and familiarisation of the tester and analysis of influences of the variables on erosion were also accomplished in this stage. The findings of the preliminary tests were utilized to perform experiments with multiple variables. Design of Experiments (DOE) method was used to reduce the number of tests with many variables. The most significant variables on impact erosion were identified by screening design. Finally, multivariate analysis was performed to reveal underlying correlations between variables and to build the predictive model with significant variables.

1.3 Structure of the thesis

The thesis is divided into two main parts. Part I gives the overview of the research study, divided into several chapters. The state of the art is presented under the literature review in Chapter 2. An overview of the experimental setup and a description of the calibration methods are given in Chapter 3. Further, Chapter 3 describes how to obtain a controlled gas-particle stream in the erosion tester. Different measurement methods to monitor and quantify the amount of erosion are described in Chapter 4. In Chapter 5, the observations of the experiments and findings are presented, correlating them with the scientific articles published during the study. The main conclusions and the future recommendations are presented in Chapter 6 and Chapter 7 respectively.

Part II presents the selected scientific publications made during the present study. Paper 1 presents the influence of impact angle and exposure time on impact erosion using the experimental results in the preliminary study. The propagation of eroded craters is discussed in Paper 2. Paper 3 discusses the identification of the significant variables among several variables through a screening design. Development of a predictive model by revealing underlying correlations between the variables and validation of the model are discussed in Paper 4.

2 Impact Erosion

In this chapter, a general overview is presented to understand the fundamentals of the erosion process related to pneumatic conveying of particulate materials. A review of previous investigations on particle impact erosion is also described simultaneously.

2.1 Overview

Removal of material by particle impact erosion is experienced in many fields such as pneumatic conveying systems, rotor blades or space crafts. Impact erosion is considered as a serious problem in industry due to material loss on the surface of equipment, which ultimately leads to complete wear of components with time. In components where the flow direction changes rapidly (turbine blading, valves, bends, etc.), erosion is considerably more significant than in straight sections. Local turbulences due to the roughened surface or misaligned parts may greatly expedite the process. There are also useful applications related to impact erosion such as sand blasting which is used to smoothen rough surfaces. The regulation and control of erosion processes are vital, in terms of both desirable and undesirable erosion. A thorough understanding of the process is essential to regulate the surface erosion in industrial capacity.

The amount of erosion (W) is commonly denoted by the ratio of mass loss on the surface by the unit mass of erodent. Occasionally, it is convenient to present the amount of erosion as a volume ratio instead of mass ratio. In either case, the parameter is dimensionless.

$$W = \frac{Mass\ loss\ on\ the\ surface}{Mass\ of\ erodent\ material}$$

The scientific literature on erosion dates back to the late 19th century [23]. Many experimental investigations on solid particle erosion against various materials have been carried out since then to analyse surface erosion [7, 8, 10-12, 14, 17, 23-37]. The dynamic forces between the surface and the erodent particles were extensively analysed to understand the process. At early studies, the interest on wear of ductile materials such as metals and alloys was rather more dominant than that on brittle

materials and also single grain studies were popular to predict erosion by multiple particles [14, 24, 38, 39]. Later, studies on erosion mechanism in brittle materials [39-41] such as glass and ceramic could also be found in the literature. The research studies to understand the basic mechanisms involved in the erosion process have been continued to the present date.

2.2 Mechanisms of erosion

The experimental analysis over the years showed a significant difference between ductile and brittle wear characteristics. Typically, ductile materials showed the highest erosion rate around 20^o to 30^o of impact angle [42], while the brittle materials generally have a peak erosion at impact angle of 90^o [23]. The wear of ductile materials is mainly caused by plastic deformation where the surface material is removed by cutting or ploughing actions of the erodent particles. Whereas in brittle materials, the energy transformation from particles to the surface of the target material induces material deformation, crack formation and propagation. Figure 2.1 shows the variation of erosion against impact angle for ductile and brittle materials.

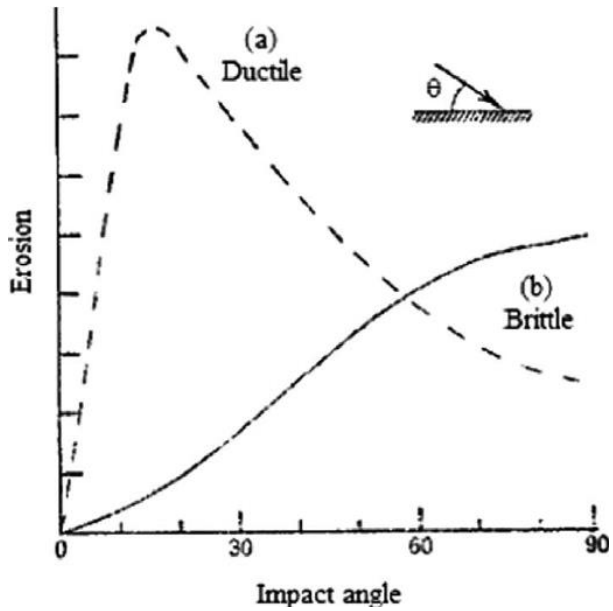

Figure 2.1: Schematic figure showing variation in erosion with impact angle for ductile and brittle materials [9].

The present study mainly focused on erosion in the ductile surface. Therefore, all the experiments were carried out using a ductile material. However, a fundamental understanding of erosion mechanism in brittle material is also important to understand the erosion process in ductile materials particularly at high impact angles. Figure 2.2 shows the erosive failure of both ductile and brittle materials due to different mechanisms acting on respective surfaces.

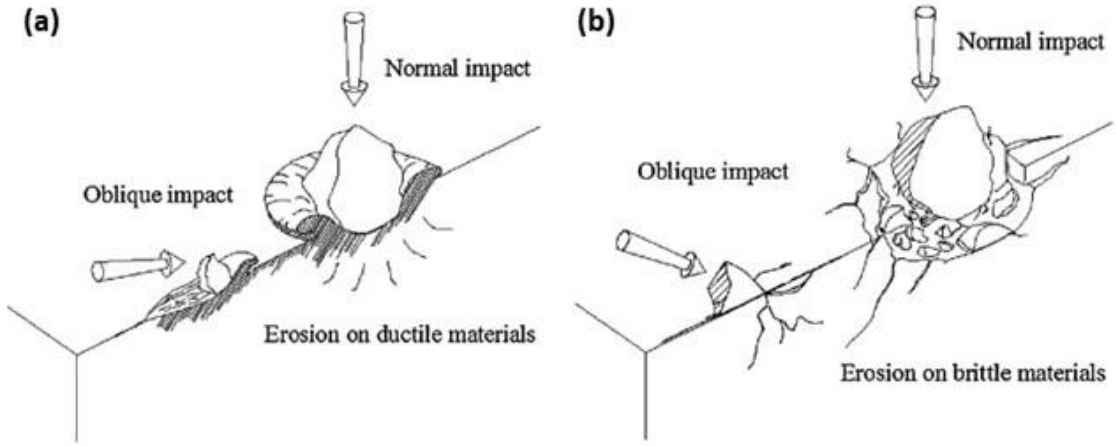

Figure 2.2: The erosive failure of (a) ductile materials and (b) brittle materials [43].

2.2.1 Brittle erosion

The wear mechanism applicable to brittle materials, e.g. glass, ceramic, is markedly different from ductile materials. The major cause of material removal on brittle surfaces is due to the formation and propagation of cracks when a relatively harder object strikes the surface. This mechanism is proposed based on the patterns of cracks formed by single particle indentation. The Cavendish laboratory, University of Cambridge, UK has studied high speed impact erosion to understand single particle and multiple particle crack formation for decades using light gas guns, different shapes of solid particles and high speed photographic sequences [39]. Quasi-static or dynamic loading of a hard particle forms cracks on a brittle surface. However, the load should exceed the critical limit for cracking. Figure 2.3 shows the cracks generated on a brittle surface due to strike of a hard particle. The labels in the figure show half-penny crack (h_c), full penny median crack (f_c), lateral crack (l_c), depth of median crack perpendicular to surface (d) and angle

of indenter (2Ψ). Median, radial and lateral cracks are formed during indentation load cycle where lateral cracks are more damaging as they effectively propagate underneath before returning to the surface.

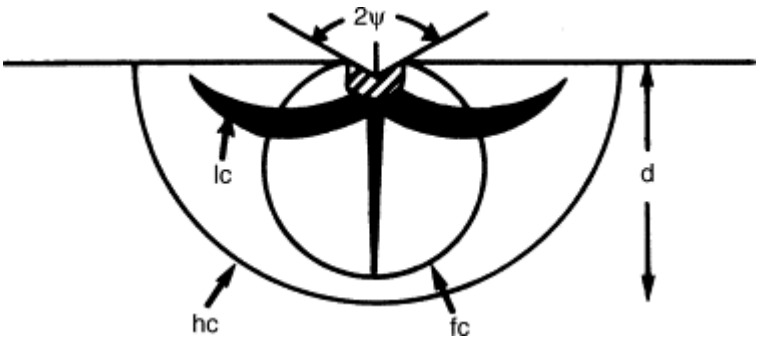

Figure 2.3: Schematic diagram of the side view of the cracks generated in glass by a pointed indenter [44].

As explained, erosion in brittle materials is mainly due to the crack formation following high compressive and shear stresses at particle impacts. However, if the particle velocity is low and the average particle size is small, the impact area becomes smaller and kinetic energy is not powerful enough to generate cracks on the brittle surface. Therefore, the chance of lateral crack initiation drops. Low energized particles only plastically deform the contact area by scribing with no formation of cracks, eventually displaying a ductile wear on brittle surface and this shift of erosion mode is called the brittle-ductile transition [45]. The transition is not only fundamentally interesting, but it may also cause the erosion rate to drop dramatically. Wensink [46] carried out experiments to explain brittle-ductile transition using sharp particles with different sizes and velocities, for brittle materials. Even though different materials displayed the same qualitative result, the energy of transition to achieve ductile manner was different from each other. Wensink concluded that the transition is very sensitive to material properties and different crack initiations due to material structure. Figure 2.4 shows the ductile transition of glass surface eroded by smaller SiC particles.

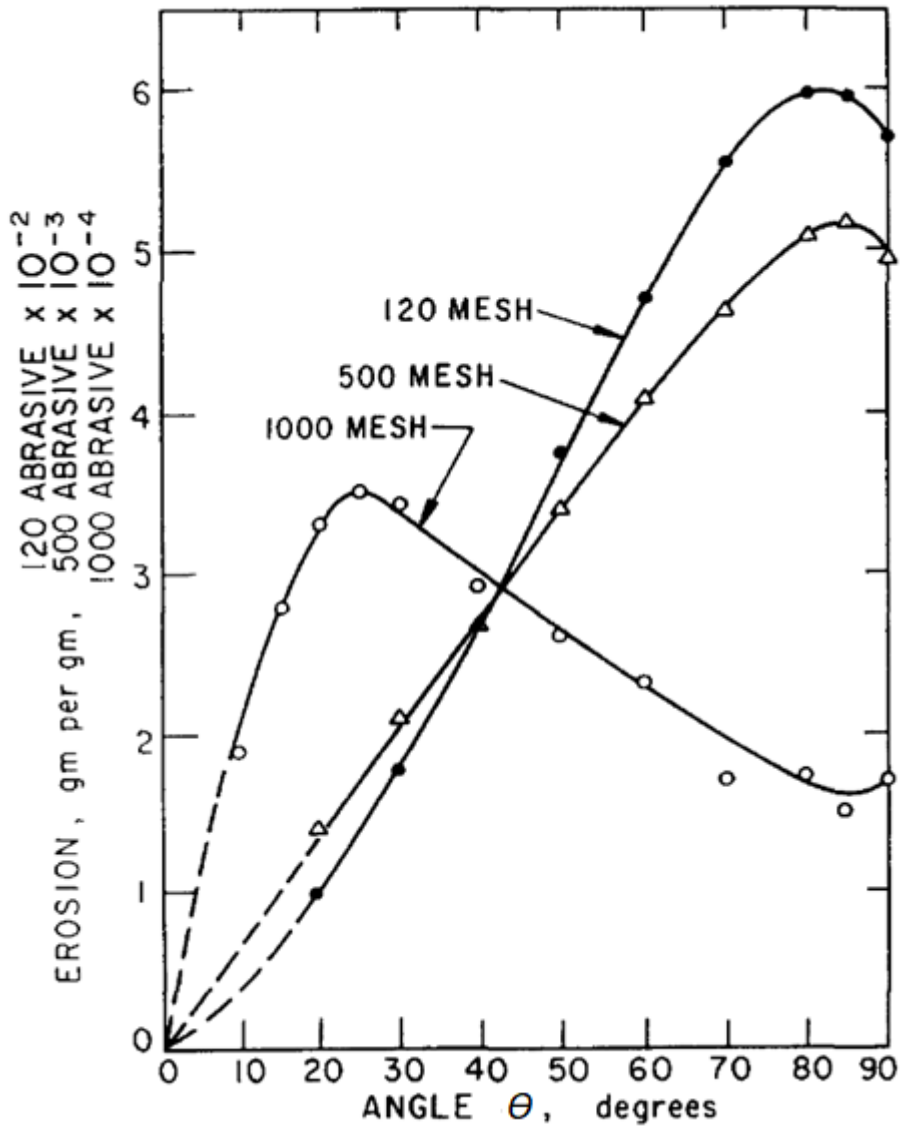

Figure 2.4: Erosion as a function of angle for glass eroded by SiC particles of 120 mesh (127 µm), 500 mesh (21 µm) and 1000 mesh (9 µm) [23].

2.2.2 Ductile erosion

An early model to predict the removed surface volume of ductile materials was published in 1958 by Finnie [8, 9]. The analytical model was developed mainly analysing 2-D rigid particle trajectory on the surface. Figure 2.5 shows the trajectory of the particle in contact with the surface. He considered that solid particles hit and cut down the surface as teeth of a milling cutter or grains of a grinding wheel. The resistance to the cutting action was designated as dynamic flow pressure of the surface material. The

surface cutting and ploughing by the abrasive particle are the leading contributions to the erosive wear as per Finnie's hypothesis. The material is subjected to shear over an area equal to the vertical cross section of the particle which penetrates the surface. If the shear strength exceeds the strength of the surface material, plastic deformation occurs. Shear and extrusion of the surface by the particle in the cutting mechanism cause removal of the material as a chip from the surface. Later studies using stereo scanning electron microscopy showed that some particles remove chips while others form piles at the end of the crater which can be easily removed by subsequent particles [23]. The removed material volume due to the particle trajectory was calculated by considering pure plastic deformation [8]. The equation of momentum was used to describe the mechanism. The initial velocity has an angle (Θ) with the surface which is the impact angle of the particle. Several assumptions were made in Finnie's explanation such as;

- Less rotational movements of the particle during the cutting process
- Angular shape of the particle
- The constant ratio of the vertical and horizontal force components
- The constant ratio of contact length and depth of the cut

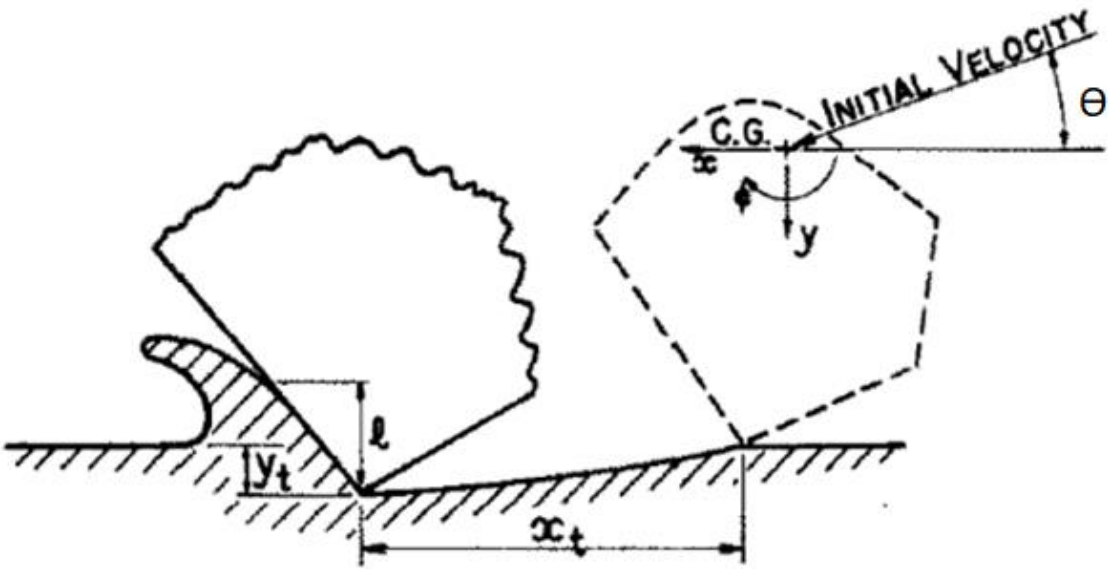

Figure 2.5: The trajectory of the particle in contact with the surface [8].

The model contained two equations to estimate the removed volume in the surface for different impact angles as shown by Equation 2.1 and Equation 2.2.

$$Q \approx \frac{MV^2}{8p}[sin\ sin\ 2\Theta - 3sin^2\Theta] \quad \Theta \leq 18.5^o \tag{2.1}$$

$$Q \approx \frac{MV^2}{24p} cos^2\Theta \qquad \Theta \geq 18.5^o \tag{2.2}$$

where, removed material volume (Q) is expressed by the mass of the particle (M), velocity of the particle (V), plastic flow stress (p) and the impact angle (Θ). The model presented by Finnie [8] was mostly applicable for lower impact angles and greatly underestimated the erosion of impact angles above 45°. However, the effort by Finnie inspired the investigation of particle erosion on target materials. The equations were modified numerous times over the years by several investigators. A summary of such updated analytical models was presented by Levy in 1995 [29].

The cutting mechanism is inadequate to explain erosive wear for high impact angles. In order to investigate the erosion process at high impact angles, another mechanism was suggested by Bitter to illustrate the normal erosion [10]. As per Bitter's explanation, deformation of the material due to the repeated collisions with particles eventually results in breaking loose pieces on the surface. When particles strike on a surface with normal impact angle and do not reach the strength of the target material, only the elastic deformation occurs. Elastic impact does not damage the surface and causes no wear. If the elastic limit exceeds, repeated collisions of multiple particles cause permanent deformation and harden the surface. The surface then becomes relatively hard and brittle which is no longer plastically deformable. Further increment of load results in breakage of the surface and its fragments will be removed. This type of material removal on the surface is called deformation wear. Bitter's model [10] for deformation wear, as shown in Equation 2.3, was developed focusing on impact of elastic state and plastic-elastic state:

$$W_D = \frac{M[Vsin\,\Theta - K]^2}{2\varepsilon} \tag{2.3}$$

where removal volume (W_D) correlates with total particle mass (M), velocity (V), impact angle (Θ) and deformation wear factor (ε). Deformation wear factor was defined as the energy needed to remove a unit volume of the surface by deformation wear. Constant (K) is related to the elastic limit. Equation is valid only if $V sin\ \Theta$ > K. At low values of $V sin\ \Theta$, no deformation wear occurs, meaning that the deformation wear is negligible at low impact angles. Bitter proposed that the total wear at every instant is a sum of two mechanisms which are the cutting (W_C) and the deformation (W_D) wear. The cutting mechanism is dominant at low impact angles while at high angles close to normal impact, the effect of the cutting mechanism is small and deformation wear becomes dominant. Both cutting and deformation mechanisms are considered as the main reasons for impact wear though several other erosion mechanisms can be found in the literature.

2.2.3 Energy transformation and crack formation during collision

The energy transformation by particles to the target material is an important analysis in developing wear mechanisms. Transformation of kinetic energy was studied by Neilson and Gilchrist [47] in their study and further extended the findings of Bitter through a general model. Hutching [15] introduced unit-less Best number (B_e) also called Metz number, correlating the impact velocity and yield stress of the target material when a particle hits a massive target. The value of B_e was high at high impact velocities and plastic deformation was expected. He further indicated that only 1-10% of the initial kinetic energy conserved in rebounding particles, while 1-5% transmitted into elastic waves. Approximately, 90% of the kinetic energy caused plastic deformation, most of which transferred into heat. Ben-Amy and Levy [48] studied shear energy transformation during the collisions. They suggested that the removal of material depends largely on the shearing action of the particle. The frictional forces between the particles and the target material introduce very high shear strains in the near surface region of the eroded material, which leads to highly deformed lip formation [49-51]. In this region, shear strains result in formation of adiabatic shear bands, which ultimately cause the failure in ductile materials [48].

Material removal also caused crack formation and propagation on the subsurface of ductile material [20, 21]. Cenna et al [20] studied the wear mechanisms in ductile surfaces and described that wear proceeds mainly by the mechanism of delamination via subsurface crack growth. They explained this phenomenon considering the effects of work hardening and the formation of transfer film on the surface. When the work hardened layer is subjected to repeated collisions, micro-cracks propagate over the surface.

Fundamental awareness of erosion mechanisms is important in identifying prominent properties that control the erosion process. The knowledge can be used to improve the performance of erosion affected systems by employing more suitable structural materials or operating in resistive conditions. The erosion mechanisms are usually undertaken by studying the dependence of erosion behaviour upon angle of impact. Material that shows the highest erosion rate at low angles is said to exhibit ductile mode of erosion. On the other hand, if maximum erosion rate is observed at 90° angle, the removal of material is said to be in brittle mode of erosion.

2.3 Influential factors in erosion by solid particles

The rate of mass loss during an impact erosion process depends on the characteristics of the carrier flow as well as the particle and the solid surface properties. Thus, in order to design equipment to minimise particle erosion, it is important to understand how impact erosion is influenced by different influential variables. A brief review of the influential variables is provided below.

2.3.1 Influence of flow properties

Depending on the application, regulation of fluid stream characteristics and impact conditions occasionally provides better results in erosion controlling, rather than focusing on properties of the surface and particulate materials. The characteristics of the flow influence the surrounding conditions (i.e., temperature, humidity, etc.) in the vicinity where erosion takes place and vice versa. It can be expected that some fluid flow

properties such as direction, velocity and temperature affect the mass removal on the target surface.

2.3.1.1 Impact angle

The direction of the gas flow indirectly determines the impact angle at which the particle strikes the surface. A number of studies [8-10, 12, 20, 23, 52-55] showed how the damage of metals by erosion can widely vary depending on the impact angle. The influence of impact angle on erosion is crucial at low angles on ductile surfaces from 20 to 40 degrees where the cutting mechanism is dominant. The dominant mechanism of the erosion process is mainly decided by the impact angle. Section 2.2 discussed how the erosion profile changes against the impact angle due to the various mechanisms acting on ductile and brittle surfaces, as depicted in Figure 2.1, which shows the dependency of erosion rate on impact angle. Many predictive models have included impact angle as a trigonometric function in the model, which illustrates the importance of the impact angle [55]. Oka [55] showed that both maximum erosion and the corresponding impact angle tend to change with hardness of the target material. He found that the impact angle at the maximum erosion associates with the shear strength to cut the material and its resistance is indicated by the compressive strength or hardness of the surface material.

2.3.1.2 Impact velocity

The particle velocity is generally considered as one of the most influential parameters associated with the impact erosion. The velocity of the carrier flow indirectly influences the wear rate since the impact velocity of a particle depends on the flow velocity. Most of the research investigations [7, 28, 30, 56] have studied erosion with flow velocity rather than individual particle velocity. The studies have mostly shown that the mass removal from the surface per unit mass of erodent particles has an exponential relation with impact velocity which lies between 2 to 4 for gas-borne particles [57]. The exponential relationship indicates the significance of the particle velocity on erosion. Ductile material shows exponential values between 2 to 2.5 whereas brittle material has high exponent values up to 4 [57]. Based on the kinetic energy of the particles, the

exponential value of 2 would be expected. A variation of the exponential value might be caused by other influential properties of the target material and the particles [30]. Figure 2.6 shows the influence of impact velocity for Fe-C (quenched) and brass surfaces. The graph is drawn in logarithmic scale and the exponential values for Fe-C and brass are 2.64 and 2.62, respectively. The surrounding temperature has also been found to influence the exponential value of the velocity in fluidized bed type testing [58]. The value is also dependent on other test conditions. Sundararajan and Shewmon [59] compared results from a number of researchers and found that the velocity exponent changed as the particle size increased. It is also expected that the flow regime, average distance of particles and flow patterns vary with the flow velocity and influence the erosion process accordingly.

Further, studies for fracture of particles have shown that particles only deform elastically at low incident velocity whereas many of them tend to fracture at increased velocities. The transition from no-damage to fragmentation of particles occurs at a threshold velocity. Small particles showed more resistivity to fracture than larger particles depending on the velocity [34, 60]. A fraction of kinetic energy deficit due to the fragmentation of particles may reduce the erosion on the surface [61]. According to previous experimental studies [34, 60], the particle fragmentation is strongly proportional to the velocity and the calculations of erosion rate must focus on fragmentation effect to obtain results of higher accuracy.

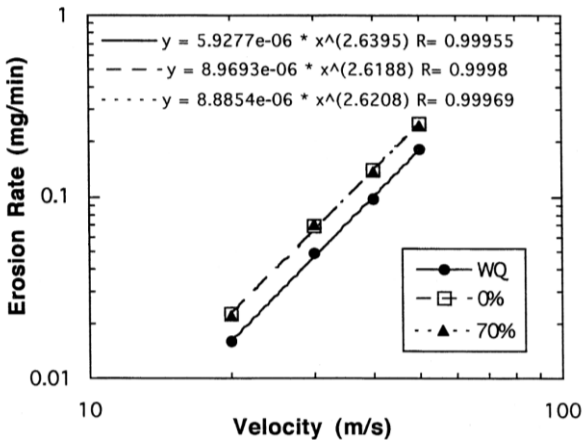

Figure 2.6: Erosion rate against the particle velocity for Fe–0.6%C (WQ) and brass with 0% and 70% cold work. Conditions: impact angle: 90°; erodent: 355 µm Al_2O_3 [30].

2.3.1.3 Temperature

The effect of temperature on the erosion rate has been investigated by several researchers [13, 42, 62-64]. In general, it was found that severity of erosion damage differs as the temperature increases, depending on the testing temperature and the impact angle [13]. Yerramareddy [63] and Zhou and Bahadur [42] showed the peak erosion rate of Titanium alloy was at 20^{o} impinge angle for elevated temperature at 500^{o}C while at ambient conditions peak erosion appeared at 30^{o}. Therefore, it can be considered that the maximum erosion rate shifts towards low angles at elevated temperatures for ductile materials. Tabakoff [64] showed that erosion rate increases for elevated surrounding temperatures for given velocities.

Zhou [42] studied the surrounding temperature from 25^{o}C to 800^{o}C and three different regions were highlighted in the profile of erosion rate against the surrounding temperature. Figure 2.7 shows the different regions in erosion rate against the temperature. The first region is the temperature independent range of wear, which spans from the room temperature to approximately 200^{o}C. The second range is the moderate region, where the erosion rate increased moderately with the temperature beyond 200^{o}C. After 650^{o}C, it shows rapid increment with rising temperature. Zhou suggested two ways to explain this behaviour with respect to the temperature; with physical and chemical changes of the material. In Titanium alloys, mechanical properties are unstable after 550^{o}C which may cause a rapid rise in erosion rate at high temperatures. As an example, tensile strength of titanium at 600^{o}C is about half of the corresponding value at room temperature. The elongation of Titanium alloy against the tensile strength initially increases with temperature, displays a drop between 200^{o}C and 400^{o}C, and again increases rapidly for further increments [62]. At high temperatures, oxidation of metal is rapid and the oxide layer weakly binds to the alloy which can be easily cracked on particle impacts.

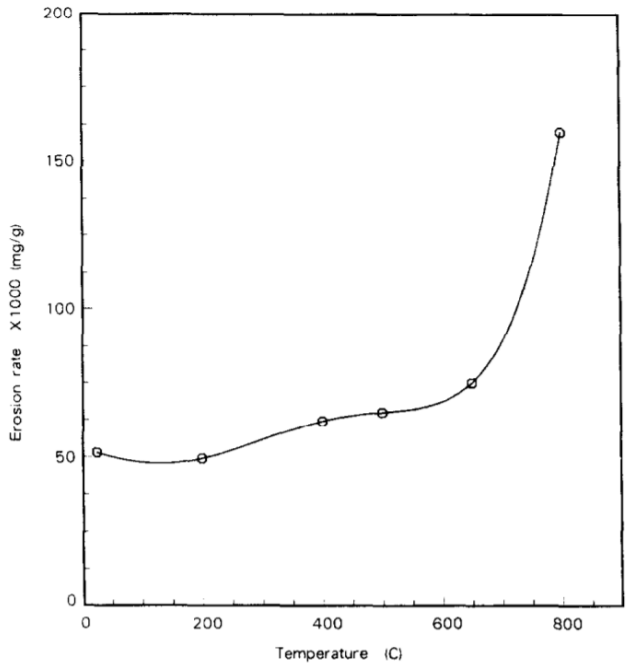

Figure 2.7: The erosion rate and different regions against the temperature [42].

2.3.2 Influence of particle properties

The influence of properties of air-borne solid particles is of great interest with respect to erosion problems. Some properties such as particle size, shape and hardness play prominent roles in the erosion process. Kinetic energy of particles and the interference by particles are main characteristics which influence the material removal process [65]. Experimental, analytical and simulation based studies have been reported in literature [17, 52, 56] to understand the behaviour of particle properties and their effect on erosion rate. Some studies and their findings on particle size, shape and flux are briefly discussed in the following sections.

2.3.2.1 Particle size

Tilly [66] worked on the influence of high velocity (240 ms^{-1}) erodent particles and found that particles below 100 µm exhibit decrease in erosion rate with the reduction of particle size, while the particle size between 100 to 200 µm has no significant effect on erosion. The decline in erosion rate for smaller particles can be described by lower impact stresses formed on the surface due to the low kinetic energy conserved in

erodent material. If a given mass of erodent is considered, it contains a larger number of particles when the particles are smaller and a lower number of particles when the particles are bigger. Though the number is higher for a constant mass, experimental results reveal that the increased number of impacts of small particles does not compensate for the influence of low kinetic energy on the erosion process and thus erosion is comparatively less harmful. In Markus's study [56], the erosion rate showed a peak at a critical particle size and dropped later with increasing particle sizes (Figure 2.8). The results demonstrated that bigger particles are not always responsible for higher damages. The observation also revealed that, even though individual bigger particles may have high kinetic energy conserved, the number of impacts on the surface is also a significant factor for the erosion rate. Therefore, both kinetic energy and a number of impacts combinedly influence the erosive wear process. The observation of highest erosion at a certain critical particle size as a result of kinetic energy and the number of strikes can be effectively utilized in controlling the wear process. For spherical particles, the kinetic energy (K) has a cubic relationship against the particle size as shown in Equation 2.4.

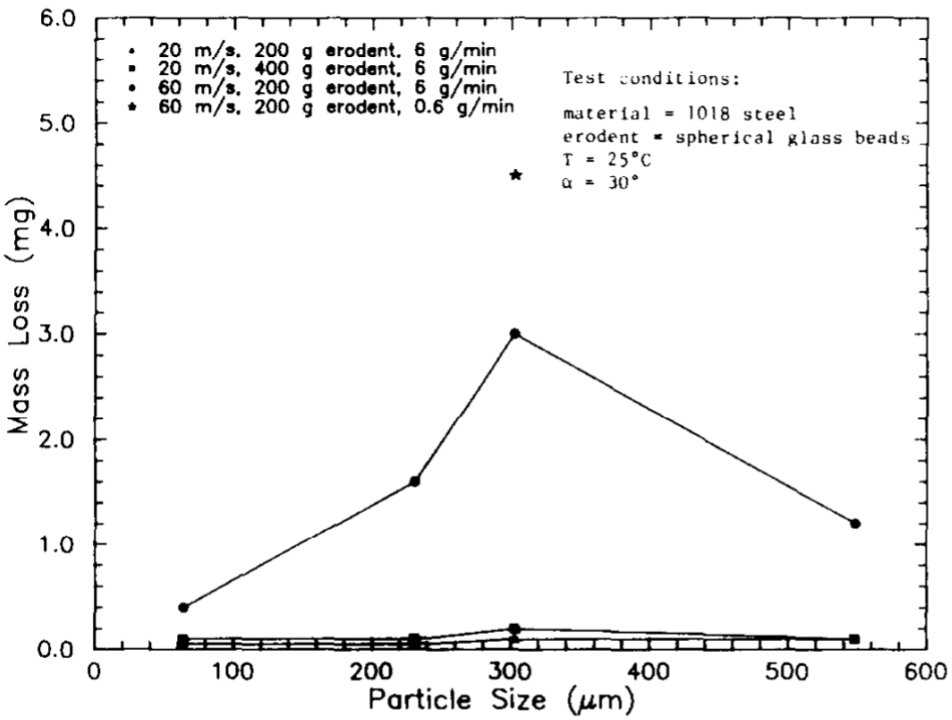

Figure 2.8: The mass loss against the particle size of spherical glass beads [56].

$$K = \frac{2}{3}\pi r^3 \mathrm{p} V^2 \tag{2.4}$$

Moreover, selecting an exact sized set of particles for tests is still a challenge, generally the median of mass distribution is taken as the representative particle size for a collection of particles. If a narrow particle size distribution is used to predict the influence of size, the error associated with different sized particles in the range would be minimized. One deficiency of many studies on particle size was that the velocity was determined by the flow velocity instead of particle velocity. The velocity of the particle varies with particle size in the same carrier flow as explained by the Stokes law. Smaller particles are capable of reaching higher velocities at short time intervals due to less inertia against the gas stream.

2.3.2.2 Particle concentration

The concentration of airborne particles is depicted by the particle mass per unit mass of air in the system. Therefore, the number of collisions and the concentration of transported material directly correlate through the particle size and the particle density. Further, higher number of particles leads to inter-particle collisions that affect the erosion process. In general, there is a tendency of higher erosion in the system with low particle concentrations. With his experimental work Markus [56] showed that low solid feeding rate makes significant damage, indicating the particle-particle interference at high concentrations which reduces the ability to erode the impact surface. An experimental investigation with bends in pneumatic conveying systems [32] also showed a lower trend of reduction of the wall thickness due to particle impact while the particle concentration was increased. In reality, the number of particles striking the surface is not always equal to the number of particles travelling towards the target. This phenomenon can be understood with a shielding effect formed by the rebounding particles [26]. The average distance between the particles is related to the concentration which can be estimated from the particle size, feed rate and the density [56]. As long as the average distance between particles is long enough, inter-particle collisions are minimized, and impacted particles are able to leave the surface as the subsequent particle reaches the target. If the average distance decreases, rebound particles

interfere with the trajectory of other particles or slow them down, resulting in a change of the impact angle or the impact force, even preventing the collisions with the wall material. Therefore, in pneumatic transportation of particulate materials, dilute phase is much more harmful in terms of erosion than dense phase transportation, not only for the higher particle velocities, but also due to the lower particle concentration (i.e., solid loading ratio).

2.3.2.3 Particle shape

The contact area on the impact surface during the particle collision is highly dependent on the shape of the particle which is also a significant characteristic in anticipating the particle's erosive strength [27]. Particulate materials with sharp edges are capable of penetrating the surface and remove material as cutting tools. Hutchings and Oka [52, 67] carried out investigations to predict the influence of erodent shape on wear process. The difference in magnitude of erosion rate between angular and round particles was greater than a factor of ten [67]. Figure 2.9 presents the simulation profiles of erosion rates for various shaped erodent particles acting on a ductile material. Generally, spherical particles are the least damaging ones as shown in Figure 2.9. Oka [16, 37] has done a series of experimental studies and found that spherical particles hardly remove material from the surface at low impact angles though the angular particles remove material by cutting action. It would be expected that the spherical particles slip over the surface while particles with sharp edges penetrate the surface at low angles.

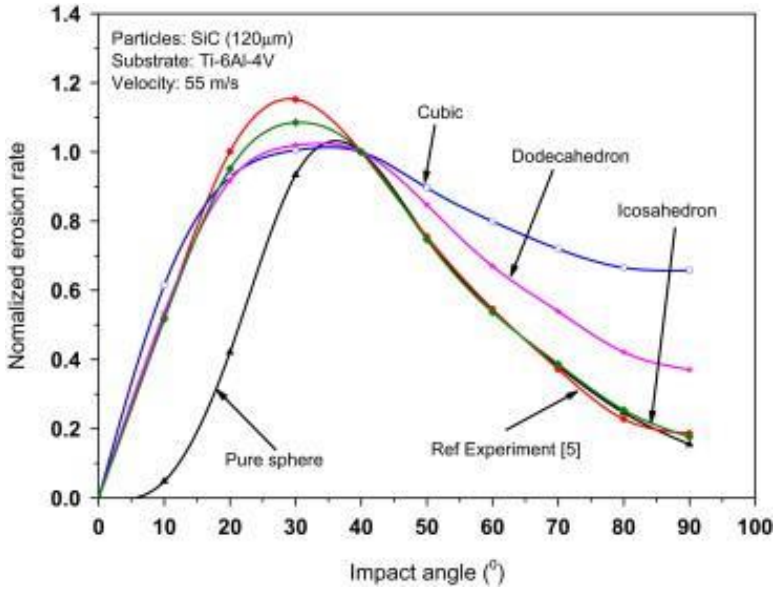

Figure 2.9: Normalized erosion rate under multiple impacts with different particle shapes [17].

2.3.3 Influence of surface material properties

Impact erosion is a mechanical phenomenon. Hence, the consideration of mechanical properties of the surface material is crucial in investigating erosion processes. The substantial difference of erosion mechanisms between ductile and brittle surfaces was discussed early in this chapter. In general, mechanical properties of material are measured in large scale test models while the erosion takes place in a localized area related to smaller scale changes and thereby, the local properties of the surface are much influential in the erosion process. One of the most important surface properties is hardness of the target material [8, 52].

The effect of particle hardness should be considered in relation to the surface hardness in context of particle impact erosion, since it is the ratio of particle to surface hardness that influences the erosive wear. When selecting resistive materials against erosion, relative hardness of particles with respect to the surface material is practically meaningful. Hardness indicates the resistance of solid material to withstand a compressive force without being permanently deformed. Hutchings [52] observed that cutting effectiveness of abrasive particles decreased notably when the particle hardness

was less than 1.2 times of surface hardness. If particles are softer than the target material, they may deform during the impact without doing much harm, because they are unable to transfer their kinetic energy effectively. Under such situations, material removal occurs only by minor chipping with no secondary crack formation for soft particles [31]. However, if the particle hardness is significantly higher than that of surface material, relative hardness of particles becomes less important and wear rate is independent of the particle hardness. Figure 2.10 shows the relative erosion for hardened carbon steel against particulate materials of different hardness values [52].

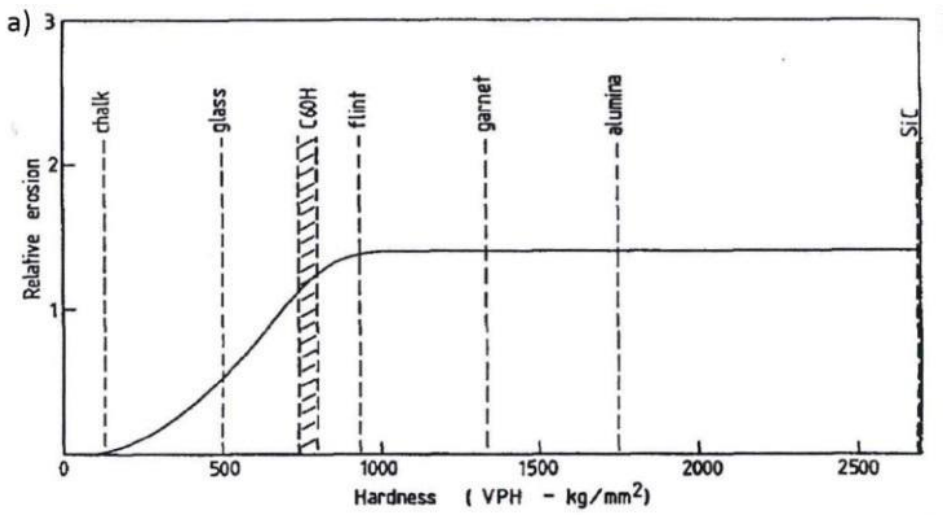

Figure 2.10: Influence of particle hardness on the erosion of carbon steel [52].

Nevertheless, Levy [68] demonstrated that harder material can also be less erosive resistant and suggested that the ductility of the material is important in the manner that the material can suffer larger deformation without material removal. Further, Hutchings [69] and Hornbogen [70] claimed that fracture toughness is a dominant factor which affects the impact erosion process. A model was developed by Ben-Ami [53] to correlate hardness and toughness to predict the critical angle which provided the maximum erosion against impact angle. The ratio of the target material's fracture toughness to its hardness was the parameter which governed the erosion mechanism and consequently the critical angle for the maximum erosion, as per his explanation [53].

2.4 Impact erosion in pneumatic conveying systems

Mass removal of the inner surface causes the reduction of wall material thickness of the pneumatic conveying pipes that are used to transport particulate materials. Ultimately, a possible puncture of the pipe system by impact of solid particles results in bulk material leakages into the surrounding. Frequent maintenance and regular costly replacements of components due to surface erosion may be hampering reliable operation of the conveying system and consequently, disrupting continuous operation of the relevant production processes. Plants need to shut down or re-route for considerable time periods to deal with such situations and the plant could lose a lot of productive operational time. Among other components, bends of pneumatic conveyors can be susceptible to a high level of erosive damage. Many studies have been done to recognise the conditions which critically influence the surface erosion of pneumatic conveying components [32, 71-75].

The understanding of impact erosion by particles in pneumatic conveying systems includes the complex geometries of components in the system, difficulty of measuring or modelling 3-D turbulent motion of particles and wide range of angles due to flow patterns. A particle is driven by the balance of the forces acting on it and the velocity of the particle is induced by the flow conditions. Figure 2.11 illustrates a schematic diagram of force balance on a particle in contact with a horizontal surface. If the particle is suspended in the air, it experiences a drag force due to the relative motion of fluid, the gravitational force and the buoyancy force apart from the inter-particle contact forces. However, the directions of gravitational force and the buoyancy force relative to the direction of the drag force depend on the orientation of the pneumatic conveying pipe segment. Therefore, the locations of possible puncture in the pneumatic conveying system might vary with the orientation which significantly influences the motion of the particle.

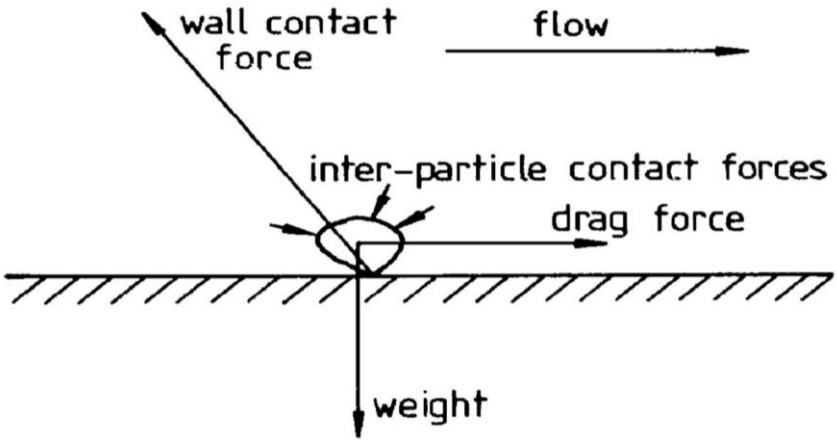

Figure 2.11: Schematic diagram of a force balance on a particle at solid boundary [52].

Pneumatic conveying systems operate in different flow regimes and erosive wear varies with the respective characteristics of the regime. Pneumatic conveying systems are mainly operated under two flow modes which are recognised as dilute and dense phases. The two phases are distinguished based on the particle concentration and transport velocity. In pneumatic conveying, systems with the solid loading ratio of less than 15 are typically said to operate in dilute phase while the dense phase systems are defined as the ratio of greater than 40 [76]. Generally, dilute phase systems are associated with high gas velocities and thereby erosion can be often a significant defect in those systems. In dilute phase conveying, particles are suspended in the carrier gas-stream and distributed more homogeneously across the cross section of a pipe segment. Particle-particle interaction is comparatively insignificant in these systems.

Mitigation and control of pipe erosion is needed in ensuring reliable operation of pneumatic conveying systems. An understanding of how the particle behaves/moves under different flow conditions/patterns would be useful in designing components for pneumatic conveyors. A thorough investigation under controlled conditions is needed to identify the significance of influential variables and to correlate them to impact erosion. In general, obtaining stable conditions is always challenging in pneumatic conveying. Thereby, the selection of experimental procedure is critically important, if the investigation involves an experimental approach.

2.5 Pneumatic conveying systems vs erosion testers

Though it is interesting to perform the experiments of impact erosion in full scale or pilot scale pneumatic conveying systems, such trials are expensive, time consuming and difficult in establishing as a repeatable test procedure, due to their inherent complexity. Therefore, the bench scale erosion testers are used as alternative experimental techniques to study the erosion under the conditions that occur in real life pneumatic conveying systems. Such erosion testers offer inexpensive and fast data acquisition in better controlled experimental conditions with high prospects of repeatability. However, the erosion process by airborne particles in pneumatic conveying systems is more complicated than that of erosion on test pieces in the tester due to many reasons. The prediction of failure due to impact erosion in pneumatic conveying systems is not the same as the prediction of erosion of test pieces in the bench scale erosion testers. The developed empirical models based on the data from bench scale tests are limited in use, because they are not capable of accounting for the variables such as rebounding of particles, directional changes, etc., occurred in real life pneumatic conveying systems. Therefore, establishment of a strong link between bench scale testers and the real system performance to predict erosion is a challenging task. Those comparative variations are required to include in the model when predicting actual erosion accurately in real life conveying systems [77]. Empirically derived constants and relationships are typically used to correlate the findings from bench scale erosion testers with the actual erosion damage in the industrial pneumatic conveying systems.

Particle impact velocity is considered as one of the most influential factors in erosion [30]. However, assuming that one can ensure identical particle velocity in both the bench scale erosion tester and the pneumatic conveying bend, wear results obtained from the two systems can be directly compared without having a correction factor. Attaining identical particle velocity in both systems is still a challenge because impact velocity of a particle can be better controlled in a bench-scale erosion tester than in a pneumatic conveying system [71]. Another difficulty is that the particles travel with a wide distribution of velocities in pneumatic conveying systems due to the uncontrolled

influence of air flow patterns. The knowledge of flow dynamics is important in identifying the flow patterns of a closed system [71].

The convergence and dispersion of the particle flow due to the directional changes and geometrical changes leads to localised or distributed erosion, respectively, on the surface of the conveying systems. Further, rebounding particles are not present in the erosion tester as much as in the pneumatic conveying components. A comparison between erosion in a pneumatic conveying system and a small scale erosion tester shows that the influence of particle concentration is significantly higher in pneumatic conveying systems than in erosion testers [32]. The reason considered is the increased inter-particle collisions in closed surroundings of a pneumatic conveying system. In order to avoid the effect of particle concentration, erosion rates for very low concentration can be determined. Deng [32] suggested a method to determine erosion rate (W_t) for different concentrations using the following equation:

$$W_t = W_{t0} e^{(-f C_p)} \tag{2.5}$$

Where W_{t0} is the true erosion rate when the particle concentration is approaching zero, f is a fractional constant and C_p is the particle concentration.

Erosion occurs on the surface of different geometrical shapes in pneumatic conveying systems whereas mostly flat surfaces are used for the tests in erosion testers. The multiphase flow is guided through enclosed paths of the pneumatic conveying system where the erosion process takes place at the wall of the pipework. In erosion tester, a free jet of airborne particles discharged from a nozzle strikes on a test piece. The erosion rate on test pieces by the free jet of airborne particles can be measured against specific impact angles in the erosion tester. However, erosion occurs under a variety of impact angles in pneumatic conveying systems depending on the geometrical shape of the component. If a bend is considered, particles strike at a range of impact angles. The range of impact angles in conveying bend starts 0° up to some degree that depends on the bend R/d ratio. The range of impact angles decreases when the bend radius increases [78]. In order to correlate the bench scale test results to pneumatic conveying

systems, an integration method of a series of weighted single angle impacts was suggested [71]. The erosion in bend using single angle impacts can be expressed as follows:

$$W_{t0} = f(\sum W_{\theta}\, a_{\theta}) \tag{2.6}$$

Where, W_{θ} is the erosion rate at each individual impact angle obtained from small scale erosion tester and a_{θ} is the weighted coefficient at respective impact angle. The weighted coefficient depends on the particle distribution along the bend, subsequently the number of impacts at the respective impact angle.

2.5.1 Particle stream of the erosion tester

Accelerated airborne particle stream created through the nozzle in erosion tester has specific characteristics. The free jet after the nozzle tip is subjected to surrounding air entrainment. The diameter of the jet increases and velocity of the air jet decays as it travels away from the nozzle, due to the entrainment of surrounding air [79]. The changes of air flow of the free jet cause the changes of particle velocity. Lindsley and Marder [30] reported the velocity distribution of a particle stream 25 mm away from the exit of a 15 mm diameter acceleration tube. The particle stream has spread out from the exit of the tube and the particles on the outer edge of the stream have lost their momentum. Figure 2.12 shows the bell shape velocity profile normal to the particle stream. Relative particle flux is represented by the data rate (number of counts) which also has the similar profile as the velocity profile.

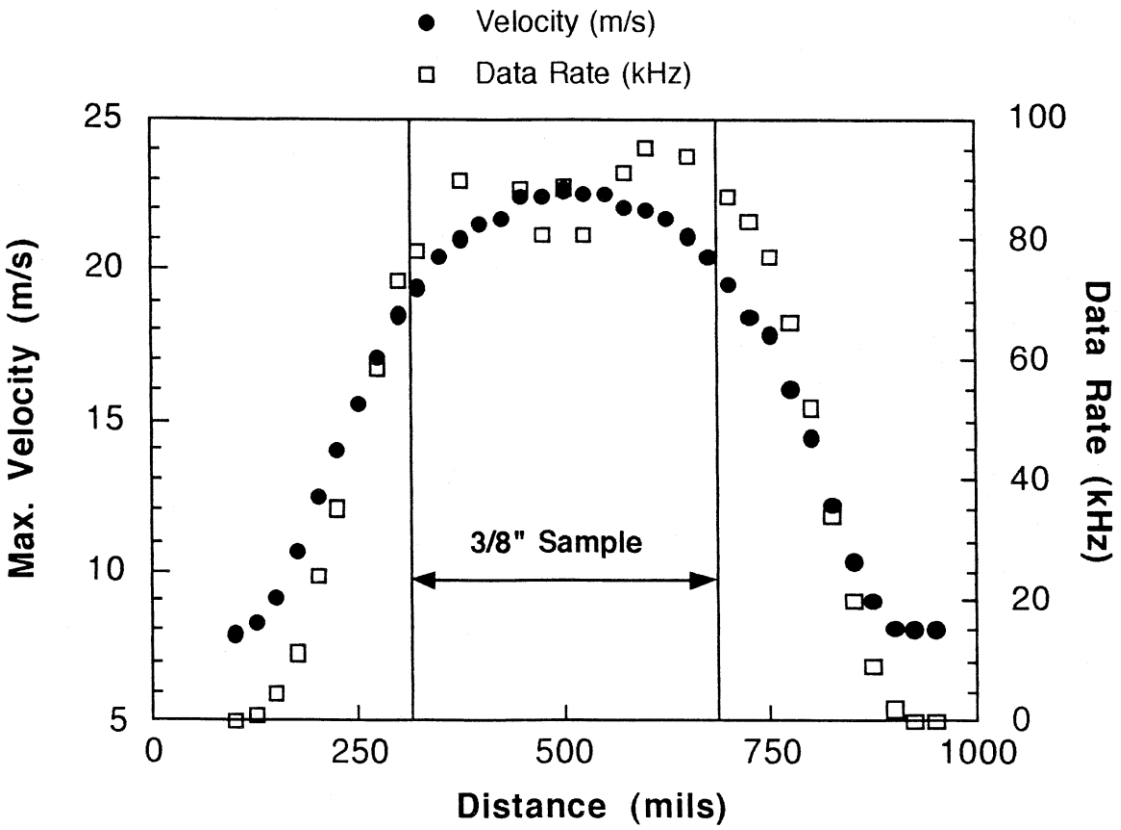

Figure 2.12: Particle velocity and data rate across the erodent stream [30].

In the present study, the effects of influential variables on impact erosion were investigated in an erosion tester. The experiments were carried out using a sand-blast type erosion tester which is built with features to obtain different test and controlled surrounding conditions. A description of the experimental set up and its operation is given in chapter 3. The test results are assumed to correspond to the conditions in pneumatic conveying systems. Thus, tested conditions were selected as close as possible to the conditions in selected industrial settings. The findings of the experiments were correlated to calibrate a predictive model for impact erosion within the tested range of significant influential variables. However, building a link between the bench scale test rig and actual pneumatic conveying system is challenging.

3 Experimental setup and calibration of the apparatus

Empirical investigation of impact erosion in pneumatic conveying pipelines can be carried out by setting up a small scale experimental rig under controlled conditions. Precise and accurate control methods for variables should be ensured in this experimental approach, which is not a straightforward and easy task. Thus, researchers have used two main types of bench scale testing rigs to predict and quantify impact erosion as described in literature [80-82]. Those are called a sand blast type erosion tester and a centripetal effect accelerator erosion tester. In both testers, pre-testing and post-testing procedures are similar and the change in mass of a target material is measured off-line. In this study, the sand blast type erosion tester was used to investigate the effects of impact erosion on target surfaces.

3.1 Sand blast type erosion tester

A sand blast type bench scale erosion tester located at the powder research laboratory of SINTEF Tel-Tek (formerly Tel-Tek) was used to perform experiments during the present investigation. The erosion tester (Ducom Instruments, India) was installed during the start of the PhD work. Figure 3.1 (a) shows a picture of the erosion tester and Figure 3.1 (b) shows a schematic image of the tester. The tester is capable of eroding a target material continuously with a defined amount of erodent particles under pre-decided controlled conditions.

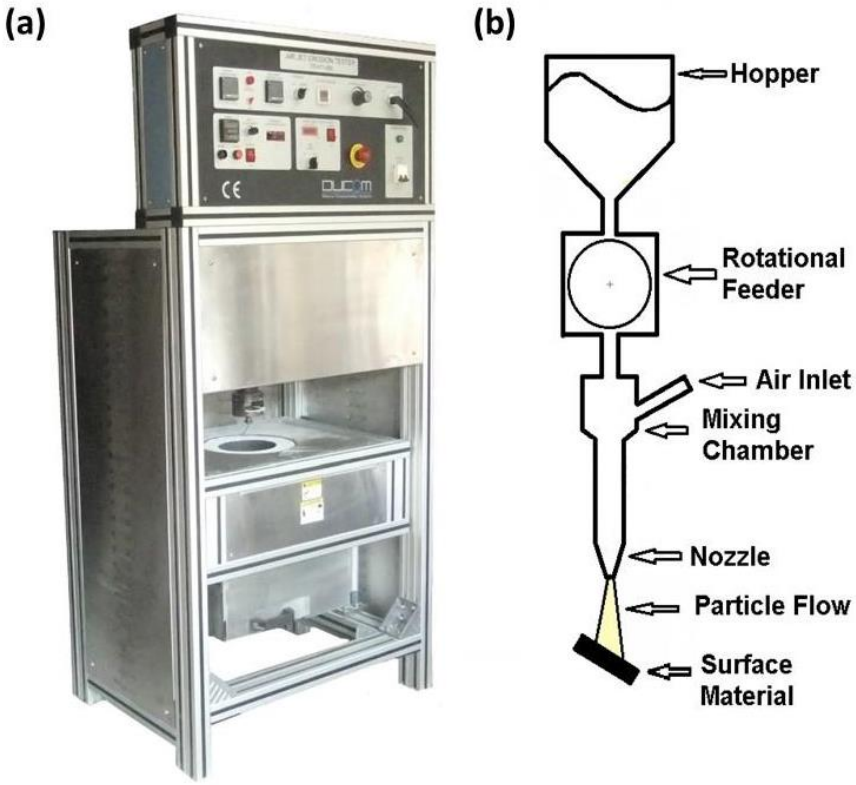

Figure 3.1: (a) Sand blast type erosion tester (b) schematic image of the tester.

3.2 Operation of the erosion tester

The main components of the erosion tester are shown in Figure 3.2. Functions of each component are listed as follows,

- Hopper – to store powdered material
- Rotational feeder – to feed powder from the hopper
- Mixing chamber – to mix powder with a pressurised air stream
- Acceleration tube – to accelerate air-particle mixer
- Nozzle – to shoot particle laden air stream towards the test piece
- Testing chamber – to hold the test piece under required experimental conditions
- Dust collector – to collect downstream particles, after impact with the test piece
- Double disk assembly – to measure the particle velocity

Apart from the nozzle, the central part (d) in Figure 3.2 cannot be reached from the outside of the erosion tester. A five-litre hopper located on top of the instrument, is

filled up with pre-prepared bulk material. Heated particles should not be filled in the hopper, that could possibly damage the interior of the tester. There is an opening to the rotational feeder at the funnel shaped bottom of the hopper. The hopper and the rotational feeder are connected through a tube. Particles from the bottom port of the hopper flow to the top of the rotating wheel under gravity. The gap between the end of the guided port and the top surface of the rotating wheel limits the maximum particle size of the powder sample which can be used in the erosion tester. The feeder is driven by an external AC motor which is connected through a synchronous belt. Speed of the motor is reduced using a gear box. The mass flowrate of the powder material is controlled by the rotational speed of the feeder, the higher the speed, the greater the mass flowrate is and vice versa. Three replaceable AC motors are available with different speeds to obtain different mass flowrates. The motor is connected to electrical supply through a Variable Frequency Drive (VFD). The VFD unit allows the operator to control the rotational speed (RPM) of the motor manually and thereby, the flowrate of the powder material is controlled. The hopper and the chamber of the rotating wheel are connected through a narrow tube to maintain equal air pressure which is important to obtain a stable erodent flow from the hopper to the rotating wheel under gravity.

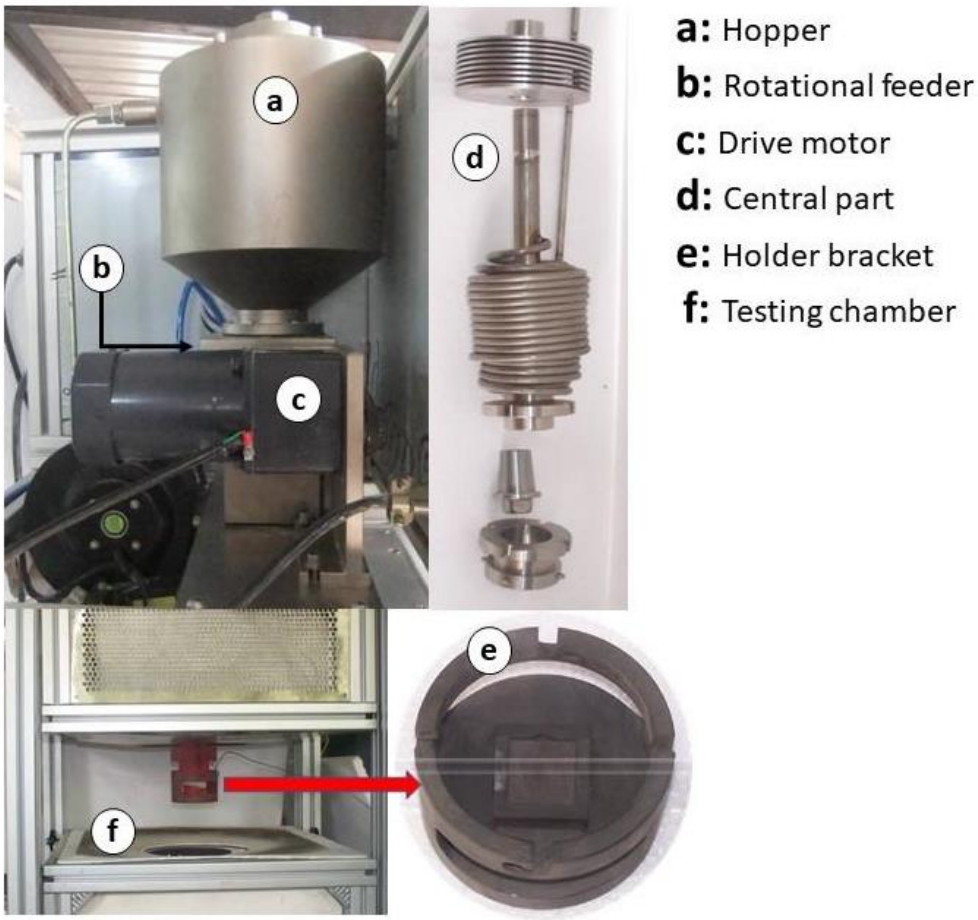

Figure 3.2: Main components of the erosion tester.

The mixing chamber is located beneath the rotary feeder where particles can be well mixed with a stream of compressed air supplied from an external source. Particles fall through the connecting tube and enter the mixing chamber while the wheel of the feeder rotates. Conditioned compressed air of maximum pressure of 6 bars can be supplied into the chamber. The water vapour in compressed air is removed by an air dryer which is connected to the air supply prior to entering the tester. The dryer is able to maintain the relative humidity of compressed air below 1% and the pressure dew point is -40 ^{o}C at 7 bars. The air passes through a spiral tube surrounding the mixing chamber as shown in Figure 3.2 (d) before entering the mixing chamber. A heating coil is also installed around the spiral tube where compressed air can be heated while passing through the spiral. An airflow meter is located at the air inlet just before the spiral tube to monitor the flow conditions of pressurised air.

Figure 3.3: Specimen and 15^{o} holder fixed in the holder-bracket.

Airborne particles are necessary to accelerate up to the required velocity before striking on the surface material sample (test specimen). An acceleration tube is used to increase the velocity of particles in the sand blast type tester. After the mixing chamber, gas particle mixture flows through the acceleration tube located below the chamber. A converged ceramic nozzle of 3 mm is fixed at the end of the tube to further accelerate the air borne particle stream while passing through the nozzle.

Accelerated particles discharged by the nozzle tip strike on the surface of the test piece placed below the nozzle. The test specimen is placed on a holder which is located in the holder-bracket as shown in Figure 3.3. The distance from the nozzle tip to the surface along the centreline of the nozzle is approximately 12 mm. The inclination of the selected holder decides the specific impact angle for the test. The impact angle is measured by the surface tangent of the test specimen against the flow direction of particles. Seven holders used in the study were able to attain 7^{o}, 15^{o}, 30^{o}, 45^{o}, 60^{o}, 75^{o} and 90^{o} impact angles. After striking the surface of the test piece, the erodent material falls into the conical shaped bottom section of the testing chamber, which is connected to the downstream particle collector. The particles in the collector can be taken for further analysis of the used particles. The air with small suspended particles then passes

through a dust cyclone-filter system and cleaned air is discharged to the surrounding by a blower. The filter is cleaned with a reversed air flow from time to time.

There are two heater elements to heat up air, particles and the test specimen for high temperature experimental conditions. The top element is located around the spiral tube of the air inlet to heat up inlet air as well as the airborne particles while passing through the spiral and acceleration tube. Rotational feeder is heat sensitive. Hence, there is a heat sink (Figure 3.2 (d)) with a fan above the mixing chamber in order to prevent propagation of heat towards the rotational feeder. The testing chamber is installed in a movable bed, which can be moved up and down positions by two pneumatic cylinders. The specimen bracket is exposed to ambient air while the bed is in its down position. When the bed is lifted, the nozzle and the holder bracket with the test specimen are positioned inside the test chamber. The specimen is mainly heated by the bottom heat element around the testing chamber. The temperature of both top and bottom heat elements can be regulated individually by the operator during the elevated temperature tests. Both heaters are covered by insulation material in order to minimize the heat transfer to the surrounding.

3.2.1 Air flow meter

An air flow meter, as shown in Figure 3.4, is installed just before the air inlet of the mixing chamber of the erosion tester. It can be used to measure supply air pressure, temperature and flowrate. The technical specifications of the flow meter are given below.

Manufacture	: Alicat Scientific
Model	: M-1000SLPM-D
Range	: 1000 SLPM
Supply voltage	: 15 to 30 V DC
Electric output	: 4 to 20 mA
Pressure accuracy	: +/- 0.5%

Figure 3.4: Air flow meter.

3.2.2 Length of the acceleration tube

The length of the acceleration tube must be very long for the particle to achieve a considerable percentage of the air velocity. Finnie [8] has derived an equation to correlate the distance of the tube with the particle velocity as shown in Equation 3.1.

$$x = \frac{8rp_p}{3C_d p_a}\left[\frac{v}{(u-v)} - ln\left(\frac{u}{u-v}\right)\right] \tag{3.1}$$

where, the particle must travel the distance of x to achieve a velocity of v in an air stream which has a velocity of u; the radius of the particle is r; the density of particle and air are p_p and p_a, respectively and the drag coefficient is C_d. Equation describes a distance that a particle needs to travel in order to achieve a given percentage of velocity of air stream. Generally, the acceleration tube of the testers used for research purposes is not so long and particles may not attain a considerable percentage of the gas velocity.

3.3 Calibration of mass flowrate

The speed of the rotating wheel (erodent feeder) is regulated through the drive motor as explained earlier. The feed rate of the erodent is directly proportional to the rotational speed of the external motor. The feeding process needs to be pre-calibrated according to the speed of the motor to control the feed rate. The set frequency of the drive motor is displayed on the panel board. A timer module is connected to regulate the running time of the motor. In order to find the relationship of the discharge rate of erodent to the set frequency, the discharged amount of erodent material is collected for a known period and weighed. A container is placed under the acceleration tube to collect powder material while the motor is running. The particles are freely flowing down under gravity from the rotary feeder to the collector while the compressed air supply is switched off. The nozzle is removed to obtain a stable particle flow by avoiding possible clogging inside the nozzle during the calibration process.

Table 3.1: Erodent discharge rate against frequency of Motor-1.

Frequency (Hz)	Erodent mass (g)			Discharge rate (g/min)
	Run 01	Run 02	Average	
2	8.5	8.6	8.6	0.9
3	13.0	12.8	12.9	1.3
6	24.5	24.6	24.6	2.5
8	32.0	33.0	32.5	3.3
10	40.5	41.0	40.8	4.1
12	48.0	48.2	48.1	4.8
14	55.0	55.4	55.2	5.6

The mass of the collected erodent particles is measured using a weighing scale. The mass flowrate through the feeder for the unit time can be calculated by dividing the amount of mass collected by the time spend. The procedure is repeated several times and the average mass flowrate is recorded against the set frequency as shown in Table 3.1.

Figure 3.5 shows the calibrated graph against the frequency display of the VFD. Once the relationship of mass flowrate against the set frequency is known, a desired value of

mass flowrate can be obtained by adjusting the frequency on the panel board. Consequently, the amount of erodent mass for the test can be fixed by setting the test duration in the timer module.

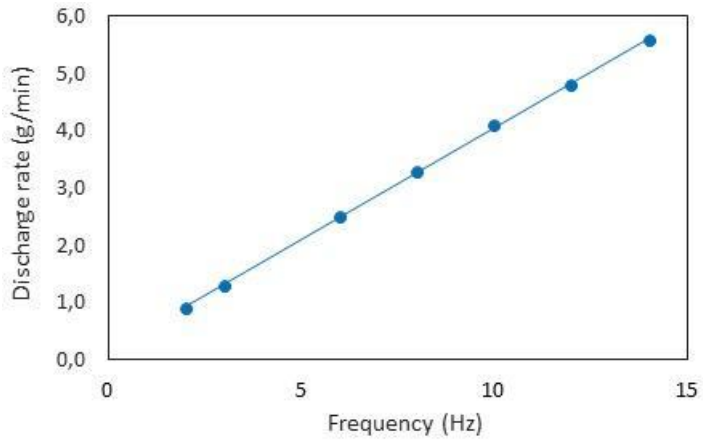

Figure 3.5: Calibration of erodent mass rate against the frequency of the motor.

3.4 Calibration of particle velocity

The accurate measurement of particle velocity during the test is critically important due to the significance of particle velocity as one of the main influential variables in impact erosion. The length of the acceleration tube of the erosion tester is not sufficient for particles to attain the air velocity of the air flow as explained in section 3.2.2. Further, acceleration of particles in the convergent nozzle makes it difficult to calculate particle velocity. The calculation of particle velocity based on carrier air flow is not straight forward as per previous research studies [83]. Hence, an accurate practical technique is required to determine or control the velocity of particles. A special mechanical arrangement is used offline with the erosion tester to overcome this obstacle through a specific pre-calibration method coupled with the supply air pressure to the tester. The Figure 3.6 (a) shows the calibration utility called the double disk assembly.

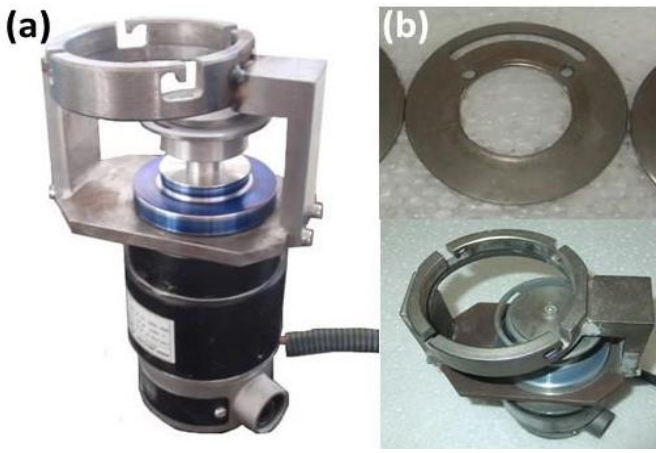

Figure 3.6: (a) Double disk assembly and (b) upper disk of the assembly.

As shown in the Figure 3.6, two metal disks are attached to a common shaft of the drive DC motor in this assembly. The top disk has a 90-degree arc shape slit as shown in Figure 3.6 (b). The assembly is mounted under the discharge nozzle tip during the pre-calibration process. The slit is aligned with the nozzle centre when it is mounted to the erosion tester. The distance between the top disk and the nozzle tip along the centreline of the nozzle, is the same as the distance to the target test piece when the target piece is positioned in the holder. Thus, it can be assumed that the particle passing through the slit of the top disk has similar velocity as the impact velocity on the test piece during the tests. In pre-calibration, a part of discharged particle stream from the nozzle passes through the slit and strikes on the bottom disc, when the disc rotates.

The striking particles leave an arc shape scar on the surface of the bottom disk. Typically, the scar has an angular displacement relevant to the ends of the slit in the upper disk. This angular displacement is the measure of time-of-flight of the particle stream as it travels the space between two disks. A formula for the particle velocity is developed considering the time-of-flight of the particles and the rotational speed of disks [83]. The formula is shown in Equation 3.2. The angular displacement is measured using a protractor and the value is substituted in the equation to find the velocity of particles. The rotational speed of the disks is measured using a laser tachometer.

$$V = (H * \emptyset)/(360 * \omega) \quad (3.2)$$

Where, the particle velocity is V; the space between two disks is H; the measured angular displacement on the lower disc is $\emptyset$ degrees and the rotational speed is ω.

3.4.1 Particle velocity with particle size

Particles of different sizes do not achieve the same acceleration in an air stream due to the different drag forces acting on them according to the Stokes' law in Equation 3.3. Further, the acceleration tube of the erosion tester is not long enough to achieve the fully developed velocity of the particles. Thus, bigger particles achieve lower velocity than smaller particles in the air flow. A relationship of particle size, the particle velocity and the travelled distance is given in Equation 3.1.

$$F_d = 6\pi\mu r u \tag{3.3}$$

Where, F_d is the Stokes' drag force; μ is dynamic viscosity of the fluid; r is radius of the spherical particle and u is the flow velocity relative to the particle. Individual relationships were obtained for particle velocity against the absolute air pressure for different size classes using the velocity calibration assembly. The calibrated velocities for different size classes are graphed against the median particle size in the respective class as shown in Figure 3.7.

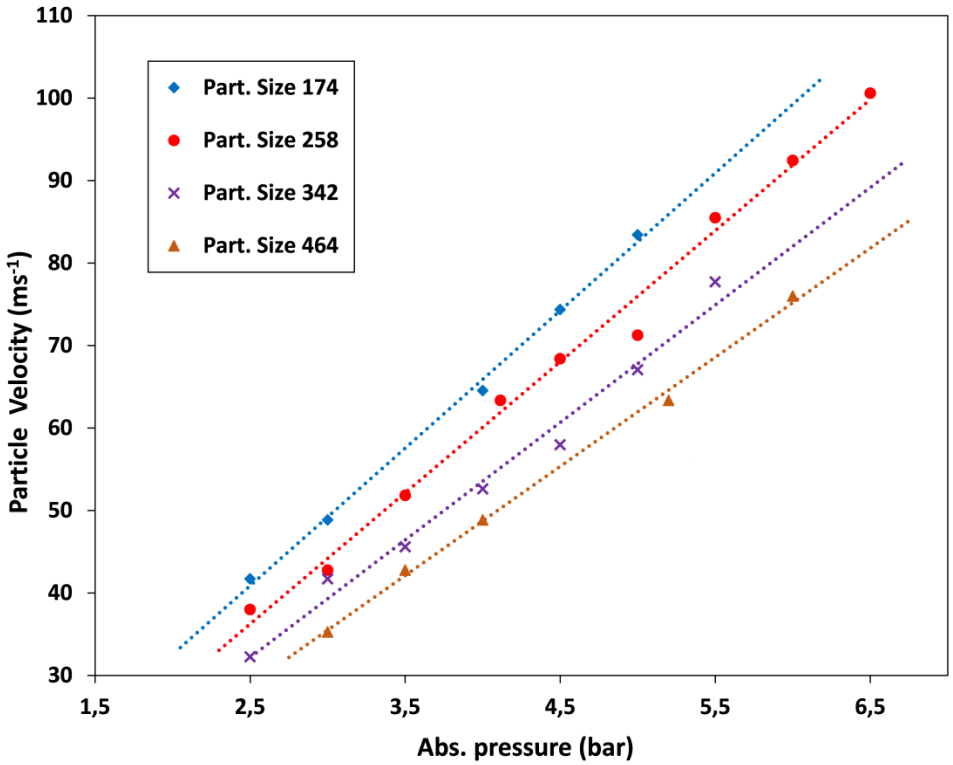

Figure 3.7: Particle velocity against absolute air pressure.

3.5 Regulation of temperature

The control and monitoring of temperature are essential in experiments at elevated temperatures. There are two thermocouples used to measure the temperature in the erosion tester. One sensor is placed in-touch with the heater element to monitor the temperature of the heater. The other sensor, whose tip is positioned in-touch with the material specimen, measures the test specimen temperature. The holder of the test specimen has a hole to insert the probe of the thermocouple. Prior to the test, the probe is inserted through the hole such that the tip is in-tough with the opposite side of the surface of the specimen. Figure 3.8 shows the positioning of the specimen temperature sensor.

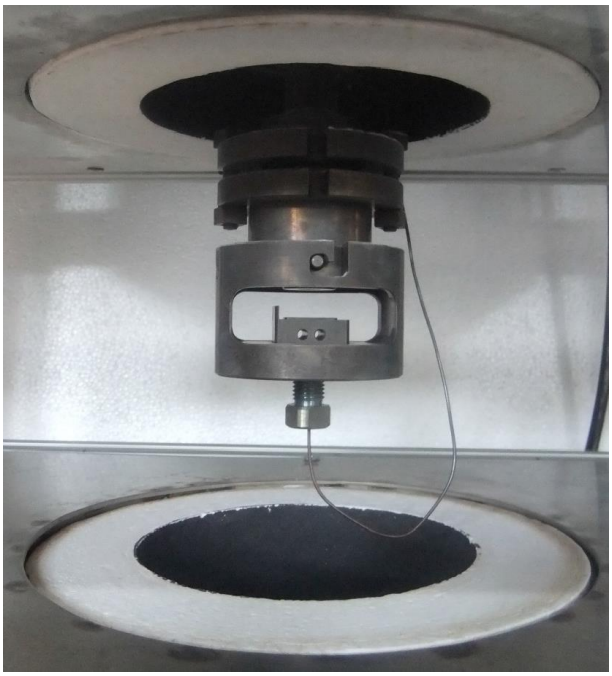

Figure 3.8: The tip of the thermocouple is in-touch with the specimen.

During the elevated temperature tests, the temperature of particles and air are not controlled, but the surface temperature of the specimen is regulated and monitored regularly. The particles and air get heated while passing through the central part of the erosion tester. The surface temperature of the specimen is maintained by the dissipated heat from the heating element. The heater can achieve maximum temperature up to 1100^{o}C. Maintenance of heater temperature below 1100^{o}C, is important to prevent overheating of the element. The measured temperature of the specimen and the heater are displayed on respective PID screens as shown in Figure 3.9. The desired surface temperature for the test is entered to the PID controller of the specimen as the set temperature. The measured (actual) surface temperature is displayed on the same digital screen. Depending on the difference of the set and the actual temperature of the specimen, the PID controller sends a signal to the relay of the power supply of the heaters in order to maintain the temperature at the set value. The actual surface temperature of the test specimen is usually influenced by the mass flowrate of the air-solids stream, and therefore it is necessary to perform some preliminary trials to attain the set value of the specimen temperature at different mass flowrates.

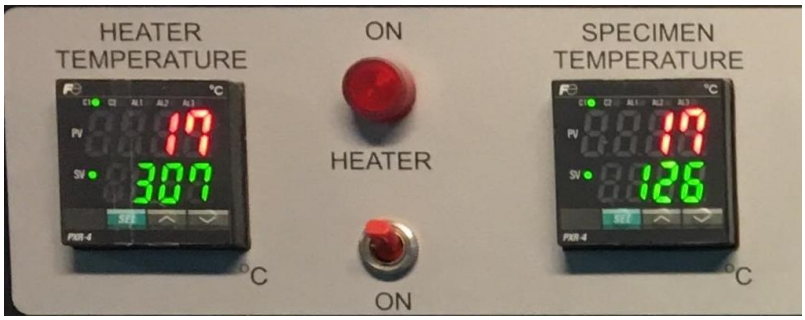

Figure 3.9: Digital display of PID controllers used for temperature control of the heater and the test specimen.

3.6 Material

The research study was carried out as a part of a comprehensive project, partially funded by industries, as described in section 1.1. The erodent material and the target wall material for the tests were selected satisfying the requirements of the relevant industrial applications. Dolomite, $CaMg(CO_3)_2$, (99+%) particles from Omya Hustadmarmor AS were used for all the erosion tests in the present study. Omya Hustadmarmor AS is a $CaCO_3$ manufacturing plant in Norway. Several samples of bulk powder were received in different particle sizes. The sample preparation procedure of the erodent particles for the test is explained in section 4.3. Average particle density and Mohs scale hardness of tested Dolomite particles are 2.85 g/cm3 and 3.50, respectively. A product information technical data sheet of the dolomite particles used for commercial purposes is provided in Appendix I, as received from the material supplier, Omya. The tests of multivariate analysis (section 5.3) were carried out using the powder sample, whose Particle Size Distribution (PSD) is shown in Appendix I. The PSD curve of dolomite particles that was used to carry out preliminary tests (section 5.1) is provided in Appendix II, as received from the supplier.

SSAB DOMEX 355MC mild steel bricks (25X25mm and 70X25mm) of 5 mm thickness were used as the target materials. This is hot rolled mild steel [84] which is used in industrial plants since it is relatively cheap. The material is commonly used in construction of equipment where corrosion is not a serious challenge. The data sheet of the material is attached in the Appendix III.

4 Measurement methods

As described in the literature, it is a known challenge to quantify mass loss and investigate the relevant topographical damage of the metal surfaces with real time measurements at the site. In this chapter, the experimental procedure used to study impact erosion on the surface of a test piece under controlled experimental conditions is explained. The methods to quantify mass loss and to evaluate the topography of eroded craters are presented. Particle size and shape characterisation measurements are explained as a part of the experimental procedure. Design of Experiment (DOE) method is used to perform experimental investigation covering vast range of test parameters effectively. The importance of DOE method in a multivariate analysis is also briefly summarized under this chapter.

4.1 Experimental procedure

Impact erosion tests were performed in three steps:

1) Calibration of the tester to predetermined experimental conditions
2) Execution of the test for the required duration
3) Obtaining the measurements and data analysis

A number of variables can be studied in the erosion tester such as impact angle, impact velocity, surface temperature, concentration of particles (i.e., Solids Loading Ratio - SLR), amount of particle mass, target material properties and particle properties. Some variables are controlled directly in the tester while others are indirectly controlled by changing the material or by regulating a secondary variable, e.g., SLR is controlled by regulating the air flowrate and the feed rate of erodent. The predetermined values of variables are controlled within the ranges of achievable limitations of the tester. The tester must be calibrated to predetermined conditions to maintain those conditions during the test.

As explained in section 3.2, the impact angle is changed by replacing the respective specimen holder in the bracket. Different impact velocities are achieved by regulating

the supply air pressure through a flow valve. Calibration of particle velocity against the supply air pressure is explained in section 3.4. Section 3.5 explains the control of heater temperature to achieve the desired surface temperature. Surface temperature is sensitive to the mass flowrate of erodent and air flowrate. When the required air mass flowrate is known for the test according to the predetermined particle velocity, correspondent mass flowrate of erodent particles can be calculated in order to maintain SLR at the desired value. The erodent mass flowrate is achieved by controlling the calibrated frequency of the drive motor of the rotational feeder. The calibration process of the erodent mass rate against the speed of motor is described in section 3.3. Further, total amount of erodent mass used for the test is also a significant parameter in an experiment. When the mass flowrate is decided, the amount of erodent mass can be limited by setting the duration of the test.

The effects of the target material properties and the particle properties on impact erosion can be determined by testing the materials with desired properties. In the present study, only one type of target material, SSAB DOMEX 355MC mild steel, was tested under different conditions. Dolomite, $CaMg(CO_3)_2$, (99+%) was used as the erodent material and different sizes of particles were tested during the test campaign.

During the calibration process, the test variables are adjusted at the desired values as explained in the previous paragraph. The experimental set up is then prepared to conduct the desired test. A sample of sieved particulate material, which is to be tested as the erodent, is fed to the storage hopper of the tester through the top lid. Once the hopper is filled the air-tight lid is closed. Target material specimen is cleaned with an evaporable cleaning agent and then dried using a high-pressure air jet. The mass of the cleaned specimen is carefully measured using a scale and recorded. Figure 4.1 shows the weighing scale in the laboratory. The measurement error of the used scale was 0.1 mg. The weighted specimen is placed in the specimen holder and the holder with specimen is positioned inside the holder bracket. The testing chamber is then lifted to "Up" position by operating pneumatic cylinders of the low bed, to avoid its exposure to ambient air during the tests. The air valve is opened to maintain the adjusted air flow

through the erosion tester. The predetermined duration of the test is entered in the timer module connected to the feed motor. Once the feed motor of solid material is switched on, running time shown on the display starts to count down, while the particles flow through the tester. The erosion tester runs until the timer module counts down to zero. During the test, the operator is able to monitor the conditions on the panel board and the air flow meter. When the timer counts down to zero, the feed motor stops automatically, while the air flow continues passing through the tester. The supply air valve has to be closed to prevent dust spreading in the surrounding, before the testing chamber is brought to its "Down" position.

Figure 4.1: Weighing scale used in the laboratory.

At the end of the test, after letting the instrument cool down for high temperature tests, the eroded target material specimen is taken out from the holder, cleaned again using the cleaning agent and dried using the compressed air. The weight measurement of the

eroded surface after the test is recorded using the same weighing scale. The difference of the weight measurements before and after the test is the mass loss during the test at the respective experimental conditions. The specimen is then stored in a zip lock bag. Figure 4.2 shows zip lock bags with several specimens saved for further analysis by a profilometer to measure the 3D profiles of the eroded surfaces.

The erodent particles used for the test are collected in the downstream container after collision with the test specimen. The tests are always conducted with fresh erodent material. Therefore, the change of particle properties (e.g., size and shape) after striking the surface, i.e. degradation of particles, could be observed by analysing the properties of particles sampled from the downstream container and comparing them to those of fresh particles.

Figure 4.2: Eroded surface specimens stored in airtight plastic bags.

4.1.1 Selection of variable space and reduction of uncertainty

The selection of test variables and the relevant testing ranges of each variable were quite important, since these will be directly influencing the applicability of the outcome and results of the project. The process conditions relevant to the industrial applications were focused in defining the test conditions of bench scale tests. Thus, the variables that can be controlled in the industrial applications were selected as the main influential variables. In addition, the limitations of the erosion tester and the constraints related to

characteristics of bulk materials were taken into consideration. Further explanation of the selection variable space is given later in section 5.3 under the multivariate analysis.

Several steps were taken in the experimental procedure to reduce the uncertainty of the test results. Mainly each and every test was repeated several times to obtain reliable outcome rather than rely on one sample of test. The repetitions were not carried out one after another. Instead, tests with different conditions were carried out in between to avoid possible intermittent and human errors. The test piece which gives the nearest value for the average mass loss was selected to observe under the profilometer. The erodent material was not reused, fresh particles were always used in each test. Target metal brick was cleaned carefully with volatile cleaning agent and dry air before taking weight measurements. The tests were continuously run to minimise the disturbance and metal brick was not taken out during the test. The hopper was topped up at the beginning of every test expecting stable mass flowrate of particles throughout the test. Each test was numbered, and conditions were recorded to avoid confusion at later analysis. Metal bricks were stored in numbered airtight zip locked bags to avoid corrosion in later analysis.

4.1.2 Design of experiments (DOE)

In real-life industrial processes, there are several process parameters varying simultaneously rather than one at a time. Thus, multivariate data analysis on the influential parameters of the erosion process is needed to be adopted and vast number of tests have to be performed to obtain results. Design of experiments technique is used in this study to determine the significance of the effects of influential variables while performing reduced number of experiments. It is a simultaneous study of several process variables instead of having separate study for each variable [85]. Therefore, the testing time is drastically reduced, and abundance of data is limited. Further, one factor at a time studies cannot detect the effects of interactions between the factors [86]. DOE is useful in estimating which factors and interactions have a significant effect on the response variable and in quantifying the magnitude of these effects. The usage of DOE technique in this study is explained in section 5.3.

4.2 Surface profilometer

Topographic characteristics of the crater on the eroded surface were measured by Alicona Infinitefocus profilometer (Figure 4.3) located at the Norwegian University of Science and Technology (NTNU) in Trondheim, Norway. The technique, based on focus variation principle, analyses the depth of profile through vertical scanning. A beam of light is projected on a relatively small area of the eroded surface of the target material specimen. The reflected light contains the useful information of the surface such as depth, inclination of the focused area, etc., which can be used to generate a 3D image of the profile. The variations in reflected light are analysed to estimate the position of the surface. The instrument provides highly accurate, fast and flexible 3D surface measurements, using a non-contact method to extract data from the eroded profile. The analysis of profilometer measurements to quantify erosion is a relatively time-consuming technique compared with weight measurements.

Figure 4.3: Alicano Infinitefocus profilometer [87].

A 2.5x microscopic objective lens in the instrument was applied to obtain the measurements, which resulted in 1.25 µm vertical resolution, 27 µm lateral resolution, and 14 µm pixel size in the topographic image. The intensity of the reflective light from the surface is maximum, when the surface is in objective focus. Eroded craters with large surface area required stitching of several images together. The images are

generated relative to a virtual 'x-y-z' coordinate system which is aligned so that the uneroded specimen surface is in the z=0 plane. Figure 4.4 shows the xyz coordinate system aligned with the surface. The y-axis is perpendicular to the particle stream, and the x-axis aligns with the incidence plane of the particle stream. The impact angle is the angle between the centreline of the particle stream and the x-axis.

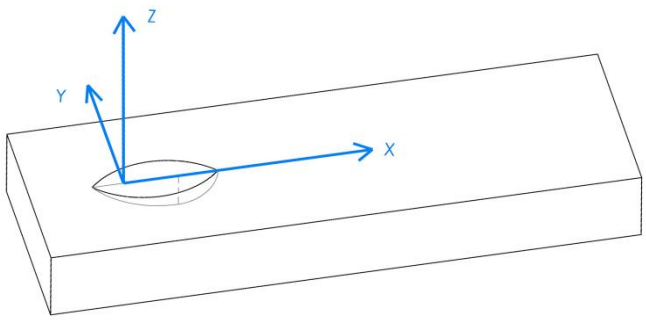

Figure 4.4: The xyz coordinate system aligned with the eroded surface of the specimen.

The well-positioned surface of the specimen in the profilometer is vertically scanned by the produced light beam. The scanning process is performed along a line parallel to x-axis while y-coordinate is constant, and z-coordinate varies in accordance with the depth of the surface profile. When all the x-coordinates are scanned on the selected line, another line is started to scan by changing the y-coordinate (one step away from the previous line). The process is continued until the complete field of view on the surface is scanned. The information collected through the scanning process along a line contains 2D data of the respective line on the surface. The set of 2D data in different line profiles collectively provides 3D data of the eroded surface by xyz coordinates and is recorded in the instrument software. The instrument software is able to generate 3D and 2D pseudo coloured images of the topography and export coordinated data. Numerical values of crater volume and maximum depth, 2D line profiles and 3D surface profiles can be generated using 3D data provided by the surface profilometer.

4.3 Preparation of particles

The erodent material (dolomite) received from the industrial plant, contained different particle sizes as mentioned in section 3.6. As a technical limitation, the particles bigger than 710 microns could not be used in the tester. Particulate material was sieved to remove bigger particles which may clog up the erosion tester. On the other hand, particles smaller than 100 microns tend to form a bridge at the hopper outlet due to their low flowability. Therefore, both finer and coarser particles than the usable range (100-710 micron) were removed using appropriate sieves (sieves of the vibratory column as shown in Figure 4.5) to avoid disturbances of the particle flow from the hopper to the rotational feeder. The particles in the usable range were further classified into several size classes depending on the desired particle size of the test. One known challenge of using a real industrial material as compared to a monodisperse model material is that the material will always have a distribution of particle sizes even within a narrow particle size range. The median value (X50) of the selected size range was used as the nominal particle size for the test.

Figure 4.5: The vibratory sieve-column with different size of sieves.

4.3.1 Measurement of particle size and shape analysis

The particle size distribution of the classified particle size classes was determined using HELOS/KF-MAGIC (Sympatec GmbH), Helium-Neon Laser Diffraction Analyser (Figure 4.6 (a)). A parallel laser beam is focused through particles dispersed in air or liquid. The diffracted spectroscopy of the laser beam passed through the particle dispersion is analysed to obtain information about the size distribution of the measured particles [88]. Measured particle size distributions of classified size classes are shown in Figure 4.7.

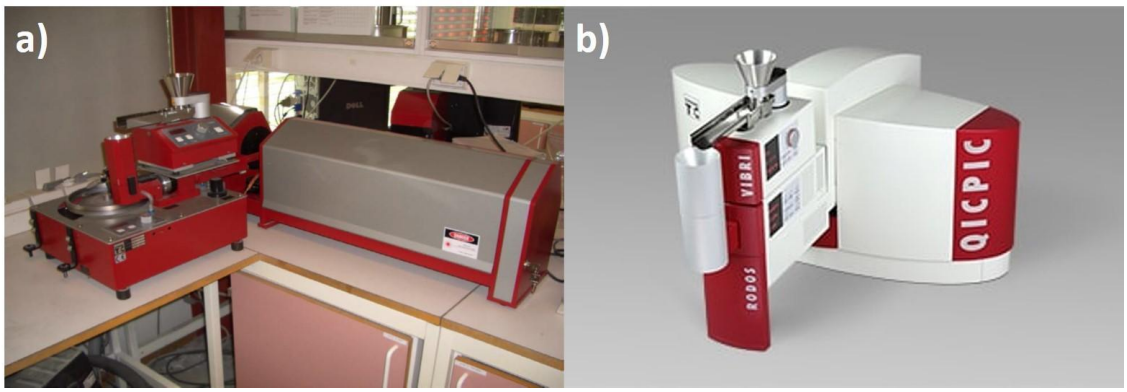

Figure 4.6: (a) Laser Diffraction Analyser (b) Dynamic Image Analyser [89].

The shape of the particles was analysed using QICPIC/L (Sympatec GmbH) Dynamic Image Analyser (Figure 4.6 (b)). Images of the particles obtained by a high speed camera are analysed to provide information about the shape of the particles. The analyser captures the geometrical properties of each single particle among millions of them within a short time. The information is then transmitted to a computer and the distribution of size and shape of the tested particle size class is determined [89].

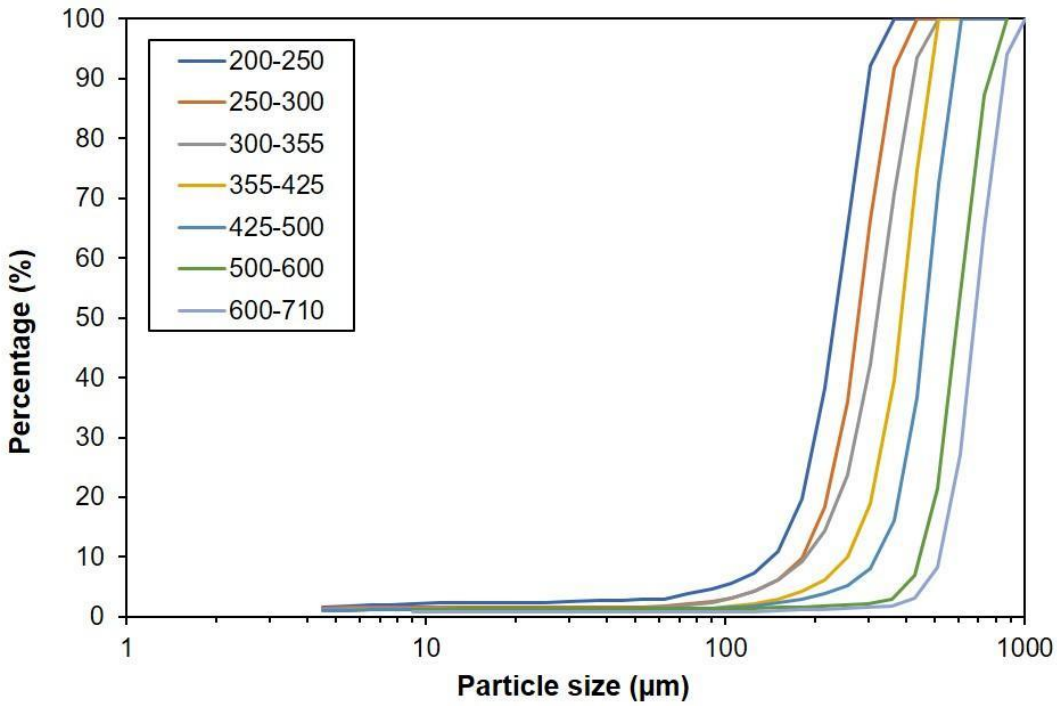

Figure 4.7: Particle size distribution of classified size classes.

5 Results and Discussions

The main objective of the research study was to find the effects of influential variables (e.g., impact angle and velocity, temperature, particle size, exposure time) and to investigate the process and propagation of impact erosion in pneumatic conveying systems, through a systematic experimental procedure using a lab scale erosion tester. Later, a predictive model is built corelating significant influential variables and underlying corelations between the variables were determined. This objective was addressed in a series of experimental tests whose results were described in detail in publications attached in part II of the thesis.

This chapter presents an overview of the major findings and a summary of the articles published under the present study. The results from the preliminary study on the effects of impact angle, particle size and exposure time on erosion are presented (paper 1), followed by the analysis of topographical data obtained by the profilometer from the eroded profiles (paper 2). Screening of significant influential variables (paper 3) on impact erosion through Design of Experiments (DOE) and the model development using multivariate analysis (paper 4) are also presented in this chapter.

5.1 Effects of particle size, impact angle and exposure time (paper 1)

A set of experiments under various experimental settings was conducted to investigate the basic characteristics of the erosion process and to identify technical limitations of the provided test facilities and materials, including erodent material, erosion tester and target material. Another objective of the preliminary study was to identify experimental conditions which provide a measurable mass loss on the surface of the target specimen while maintaining stable experimental conditions during the tests. The results of the preliminary tests provided useful information about the technical limitations of the erosion tester when using the selected erodent material and provided data for calibration of the instrument. The useful information gathered in this stage is as follows:

- Feasible range of mass flowrate depending on the particle size for each drive motor of the rotational feeder
- The relationship between the particle velocity and the supply air pressure
- The maximum and minimum particle size which can be handled in the erosion tester
- The maximum stable surface temperatures under various mass flowrates and the supply air flowrates
- The maximum amount of bulk material which can be handled without disturbing the test dependent on the particle size
- The reliability of the experimental conditions in the erosion tester

After getting to know the limits of the test parameters, a testing procedure was established, and experimental tests were planned accordingly. A number of experiments were carried out to understand the erosion process and how it is affected by influential variables such as particle size, impact angle and exposure time. The amount of erosion was evaluated by measuring the mass loss. The main findings of the preliminary tests are discussed in Paper 1. Following subchapters summarize the observations and discussions of the publication.

5.1.1 Particle size

The effect of particle size on impact erosion was tested with different particle sizes, which were obtained by sieving as explained in section 4.3. Seven different size classes were used for the tests and the influence of particle size for two different impact angles (30^o and 90^o) was studied. Mass loss on the surface at 30^o impact was significantly higher compared to that at 90^o impact (as expected for ductile materials). Mass loss versus particle size at 30^o impact initially increased and then decreased as shown in Figure 5.1 for 35 min exposure. On the other hand, at the 90^o impact, the mass loss increased with increasing particle size, following an insignificant variation at low particle size.

Both the number of collisions on the surface and the kinetic energy of particles influence erosion. The kinetic energy conserved in a particle is the result of particle velocity and

the mass of the particle. In this experiment, similar air velocity was used for the tests and thereby, lower particle impact velocity was attributed for the bigger particles than that for the smaller particles as explained in section 3.4.1. A reduced number of collisions could explain the decline of mass loss with increasing particle size at 30° impact angle (Figure 5.1 (1)).

The increase of mass loss with increasing particle size at the 90° impact (Figure 5.1 (2)) can be explained by an increase of the particle kinetic energy. The kinetic energy conserved in the particles can exceed the elastic limit of the target material, thereby causing damage on the surface. The particles beyond the critical particle size are able to remove fragments on the surface heavily and increase the mass loss as per the deformation wear by Bitter's explanation [10]. The velocity has squared relationship to the kinetic energy and the particle size has cubic relationship. Therefore, it can be shown that kinetic energy for the particle sizes shown in Figure 5.1 (2) continuously increases, displaying an increasing trend of erosion rate even though the impact velocity decreases for the big particles.

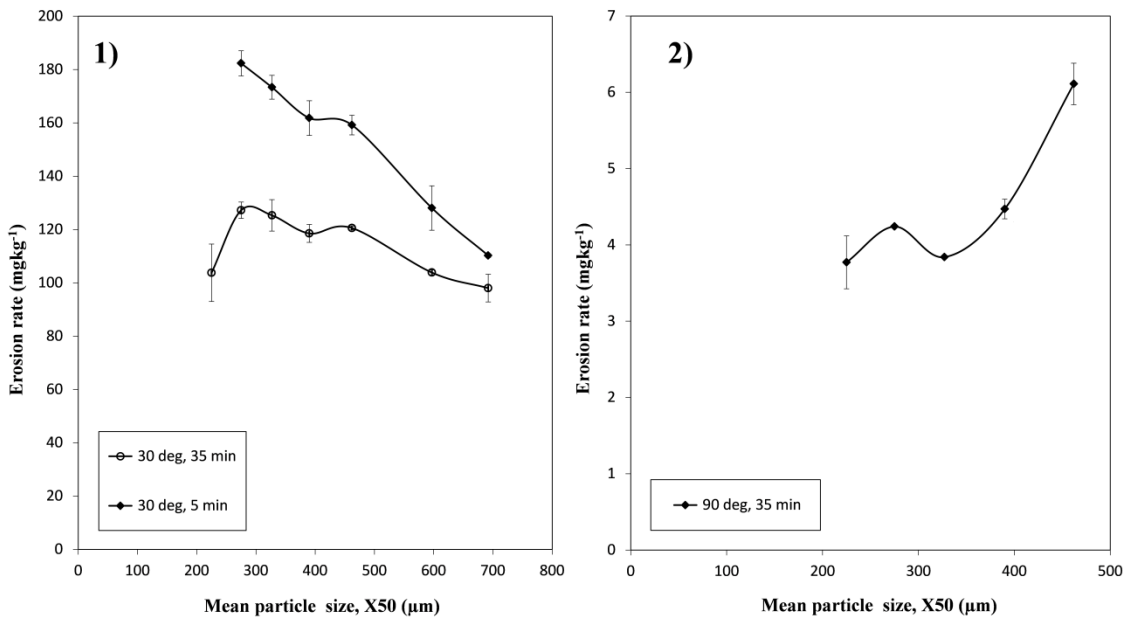

Figure 5.1: Effect of particle size (1) at 30° impact angle for 5 min & 35 min exposure times and (2) at 90° impact angle for 35 min exposure time.

5.1.2 Impact angle and exposure time

The influence of impact angle and the exposure time was tested using seven different impact angles at 7°, 15°, 30°, 45°, 60°, 75°, and 90°. Each impact angle was tested for several exposure times under stable mass flowrate of erodent particles. The mass flowrate of 75 g/min and impact velocity of 70 ms^{-1} were used for the tests. Sieved particles in the size class of 100 to 300 micron (X50 = 168 µm) were tested. The results of the experiment with impact angle and exposure time are published in Paper 1.

Different crater shapes were observed for different impact angles. Projected area of the eroded crater on the surface changes from a channel-like shape at 7° to a more or less elliptical shape at higher impact angles and eventually, it turns into a circular shape at 90° impact as shown in Figure 5.2. The direction of particle velocity relative to the target surface is shown in each subfigure. It is also noticed that the distance from the nozzle tip to the surface increases rapidly at low angles with the growth of the crater due to their prolonged shape.

Contact time of the particles during the collision influences the crater shape apart from the projected area of the particle stream. Impacting particle has a high contact time with the surface at low-impact angles due to the large tangential component of velocity [90]. The contact time between the erodent particle and the target surface is difficult to measure through physical experiments. However, contact time on the surface has been recorded in a numerical model [90]. The study has shown that contact time decreases with increased impact velocity and increased number of impacts. The surface hardening due to multiple particle collisions increases surface hardness and stiffness coefficient, thereby contact time is decreased.

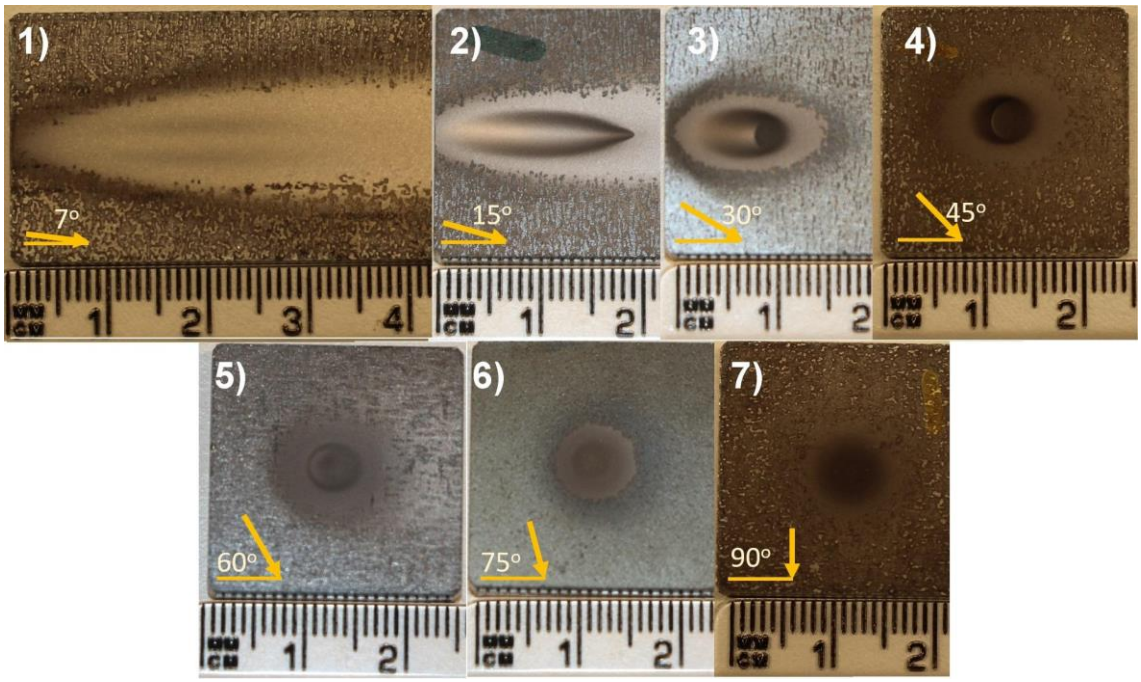

Figure 5.2: Eroded craters after 30 min at (1) 7° (2) 15° (3) 30° (4) 45° (5) 60° (6) 75°, and (7) 90° impact angles.

The mass loss results versus impact angle are in agreement with published studies [10, 23] that reported higher erosion at glancing angles and lower erosion at higher angles on ductile materials. Figure 5.3 (a) shows the mass loss as a function of impact angle. The maximum mass loss was nearly similar at 15° and 30° at shorter exposure times (5 min & 10 min). When the exposure time was increased, the maximum mass loss shifted to 15° and the difference between the mass loss at 15° and 30° increased further with time. This is demonstrated by the change of the gradient in the respective curves in Figure 5.3 (b). At 15° impact, mass loss rate was stable with time, while other impact angles show a decrease of mass loss rate in different magnitudes. The rate is not clear for high impact angles (i.e. 75° and 90°) due to their insignificant mass loss during the tested exposure time.

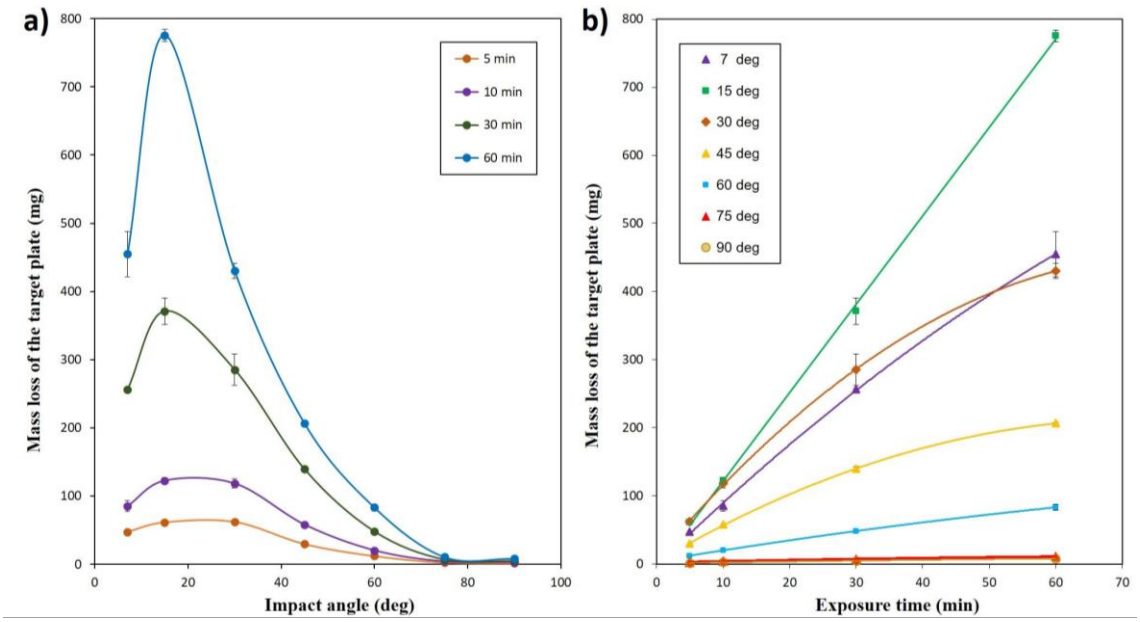

Figure 5.3: (a) Mass loss against impact angle and (b) Mass loss against the exposure time.

Visual observations showed that the impact angle inside the crater (effective impact angle) changed with exposure time as shown in Figure 5.4. The change in mass loss rate with time can be associated with a combination of several factors, such as a change in effective impact angle, enlargement of nozzle distance and work-hardening effects due to the repeated collisions on the surface. The deviation of effective impact angle from the initial impact angle as shown in Figure 5.4 could be associated with the change of erosion mechanism during the erosion process. Thereby, the change of effective impact angle is one possible reason behind the change of mass loss rate with the development of eroded craters with exposure time. The influence of exposure time on morphology of eroded craters is comprehensively discussed in Paper 2 for different impact angles and the main findings are summarized in section 5.2.

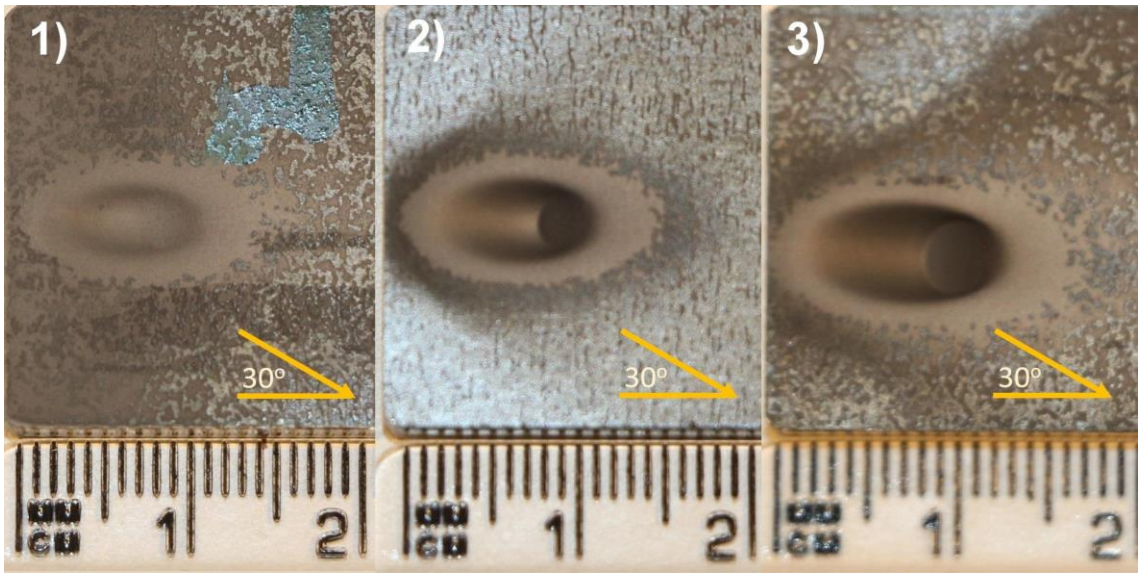

Figure 5.4: Development of the crater with exposure time at 30° impact angle: (1) 10 min, (2) 30 min, and (3) 100 min.

5.1.3 Particle degradation

After colliding with the target surface, erodent particles were collected in the downstream container. It was assumed that the particles settled in the container layer by layer over the testing time. With this assumption, the particles collected in the bottom most layer experienced collision with a fresh or relatively uneroded surface while the particles collected in the topmost layer experienced collision with eroded surface, where the degree of surface erosion increases with longer exposure time. It is expected that the properties of the target plate (impact angle and possibly surface hardness) change with longer exposure time due to erosion influencing the degradation rate of the particles. To determine the degree of particle degradation as a function of exposure time, the particles were sampled from the surface of the downstream container after the tests for different exposure times and the particle size distribution was measured. Mean particle size of the used particles was compared with the fresh particles in the respective size class as shown in Figure 5.5 (a). The degradation is higher at 90° impact angle than at 30° impact. It is also noticed that the higher the particle size, the higher the degradation of particles.

Further, the influence of exposure time on particle degradation was studied by plotting the mean particle sizes versus exposure time as shown in Figure 5.5 (b). The mean particle size of fresh samples was 168 µm for the particles used in this test set. Figure 5.5(b) shows that the mean particle size of the used particles decreases along the exposure time. The high kinetic energy conserved in bigger particles may result in higher degradation of bigger particles. The rapid change of kinetic energy at the collision for higher impact angles [90] or the difference in wear mechanism would result in higher degradation at high impact angles. The increase of degradation of particles against exposure time can be explained by the development of eroded craters. The development of eroded craters during the erosion process will be explained in section 5.2.

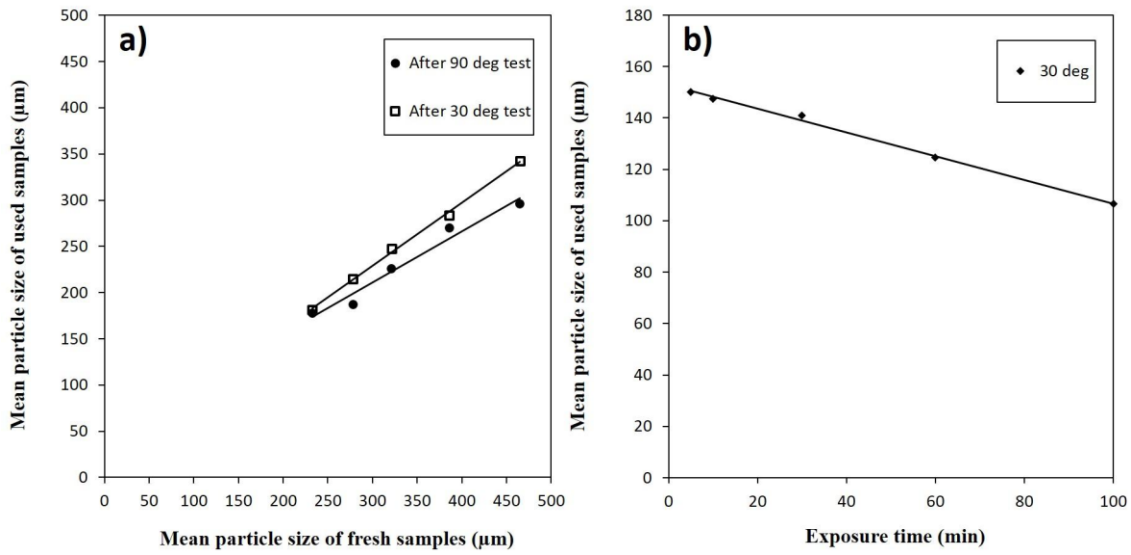

Figure 5.5: (a) Comparison of particle size before and after tests and (b) degradation of particles at 30^{o} as a function of exposure time.

5.2 Time development of eroded crater (paper 2)

The development of eroded craters is dependent on the number of particle collisions with the target surface. Amount of erodent used for the test determines the number of particle collisions during the test. When the mass flowrate is stable, exposure time (testing time) is proportional to the amount erodent. Thus, the effect of exposure time

on erosion is observed to study the evolution of the erosion process with the number of particle collisions. Apart from mass loss measurements as discussed in section 5.1, the change of material surface was examined by analysing the morphology of eroded craters. The morphology was measured by the profilometer as shown in Figure 4.3 which provided images and the 3D coordinated data of the eroded craters on the surface. Figure 4.4 shows the xyz coordinate system aligned with the eroded surface. The operational procedure of the profilometer is discussed in section 4.2. Figure 5.6 shows the optical and pseudo colour images provided by the profilometer.

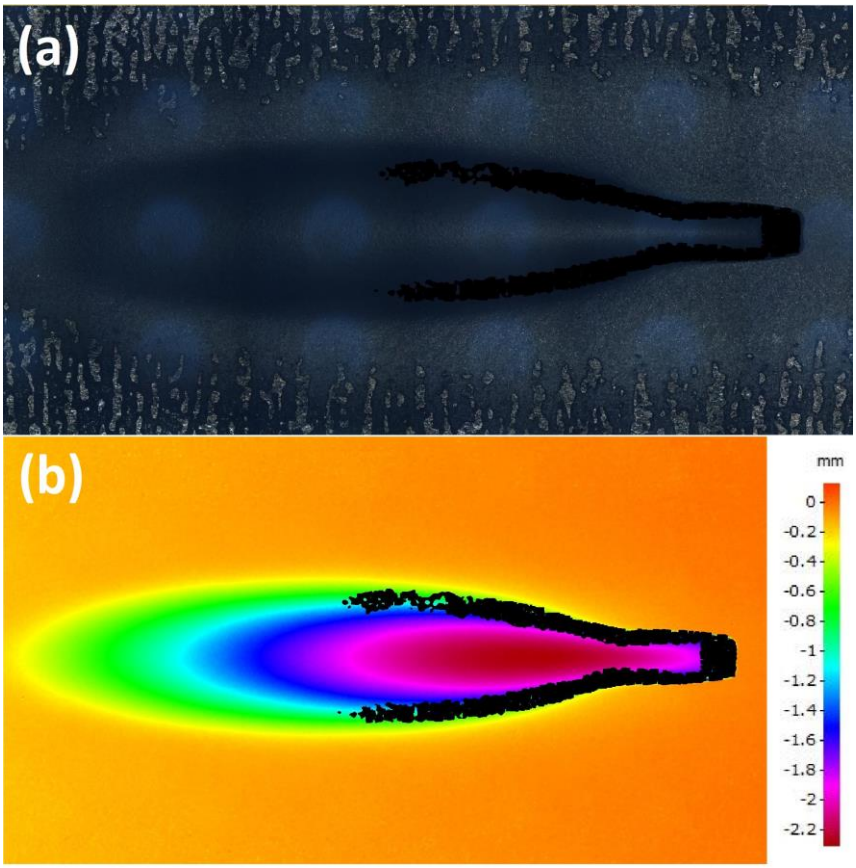

Figure 5.6: (a) An image of the crater and (b) the respective pseudo colour image obtained by the profilometer.

Obtaining surface topographical data by a profilometer is a time-consuming technique. Thus, only a single measurement of the morphology was attained, while average mass loss of several craters was measured for the tests under similar experimental conditions. The depth from the initial surface, volume loss and the inclination of the crater surface

could be evaluated by the profilometer. Figure 5.7 shows the characteristics of the eroded crater on the surface, depicting initial impact angle (Θ_i), effective impact angle (Θ_e) and maximum penetration depth (d_{max}). The analysis of morphology measurements is comprehensively discussed in Paper 2.

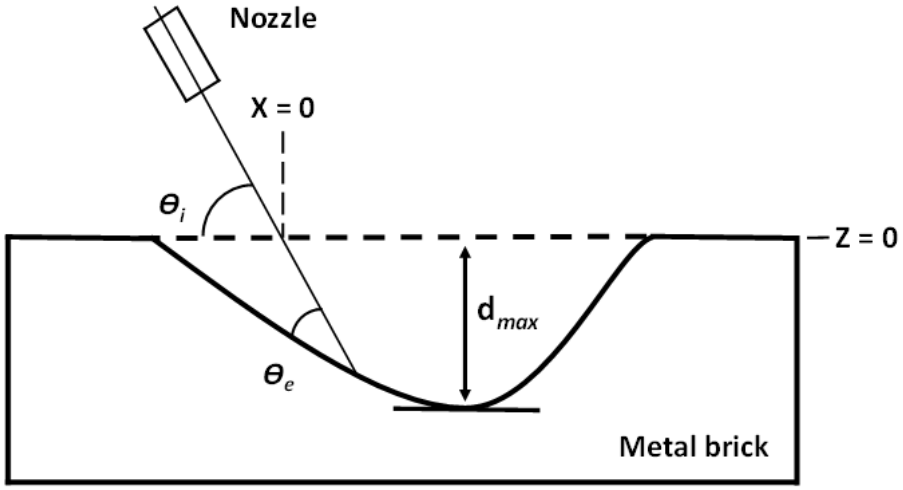

Figure 5.7: The characteristics of the eroded crater on the surface.

5.2.1 Volume loss and the penetration depth

The estimated volume loss by the profilometer was compared with the measured mass losses on the surface. Both volume and mass are proportional to each other in theory. There is a good agreement between measured average mass loss and single volume loss values against the initial impact angle (Θ_i) as shown in Figure 5.8 (a).

The perpendicular depth of the crater from the initial surface is an interesting characteristic in prediction of erosion. The puncture of a wall material in an actual pneumatic conveying system occurs at the point where maximum penetration depth (perpendicular distance to the bottom of the crater) is present. The maximum penetration depth (d_{max}) of the crater versus impact angle was graphed in Figure 5.8 (b) and compared with the mass loss. The graph shows d_{max} at 30^o impact angle at any given time. Further, there is no clear relationship with the mass loss. Thus, it is obvious that the maximum penetration and mass loss do not necessarily coincide at the same impact angle during the tested time (up to 60 min).

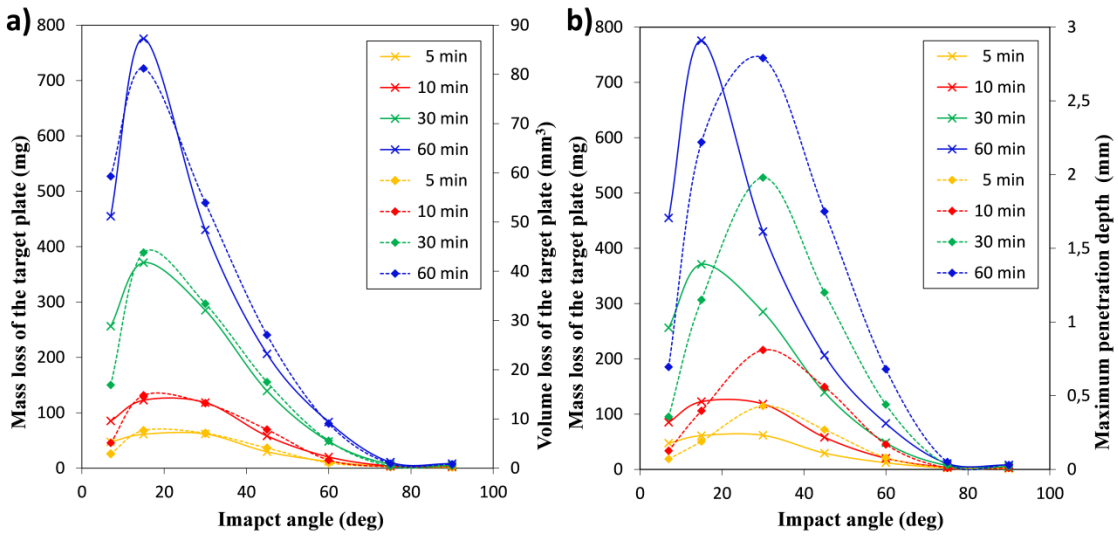

Figure 5.8: Comparison of (a) mass loss (solid line) with volume loss and (b) mass loss with maximum penetration versus impact angle.

However, the profile of maximum penetration depth against the impact angle has also changed with exposure time. The increment of d_{max} from 30 to 60min at 15° was higher than that at 30° impact. The rapid increment of d_{max} at 15° led us to analyse the penetration depth at 15° and 30° impact angles for longer exposure times. Figure 5.9 shows that maximum penetration shifts to 15° from 30° impact angle for increased exposure time. The rate of increment of maximum penetration depth is stabilized for 15° impact while it is decreasing for 30° impact.

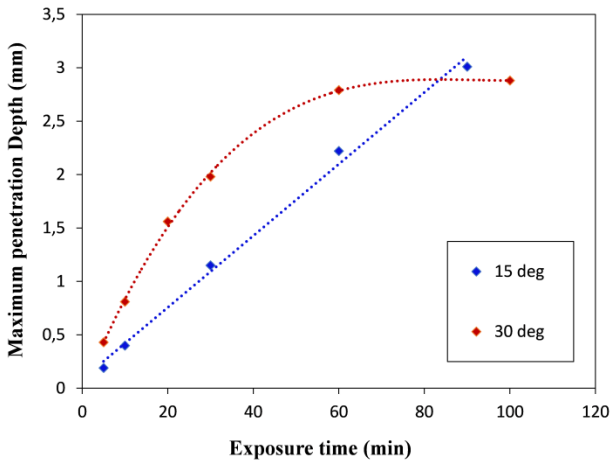

Figure 5.9: Maximum penetration (d_{max}) versus the exposure time at 15° and 30° angles (Θ_i).

5.2.2 Longitudinal profiles of eroded craters

2-Dimensional crater profiles were generated using the 3-Dimensional coordinated data gathered by the profilometer. 2D data of xz coordinate system needs to be filtered in order to attain longitudinal profiles along the centreline of the crater (x-axis). Figure 5.10 (a) shows the generated 2D profile by filtered raw data at 30^{o} impact angle for 60 min of exposure time. Flow direction of the particles-air mixture is from left to right. Two edges of the profile illustrate the uneroded surface and they are supposed to be in line with the x-axis. However, uneroded edges are not in line and even not parallel with x-axis due to the measurement errors during the operation of the profilometer. Thus, data had to be pre-treated to avoid such errors before the analysis.

Pre-treatment of filtered 2D coordinates was done in several steps. Firstly, coordinated raw data of the longitudinal profile were re-filtered to classify 2D data of uneroded surface (both edges of the profile). Classified data were graphed and a trendline was found as shown in Figure 5.10 (b). The slope and y-intercept of the imaginary uneroded surface relative to the xz-coordinate system are shown by the equation of the trendline. The offset values were added to the raw z-coordinates to neutralize the slope and to bring the uneroded surface in line with x-axis. The resulting 2D profile of the eroded crater obtained after elimination of the measurement errors is shown in Figure 5.10 (c).

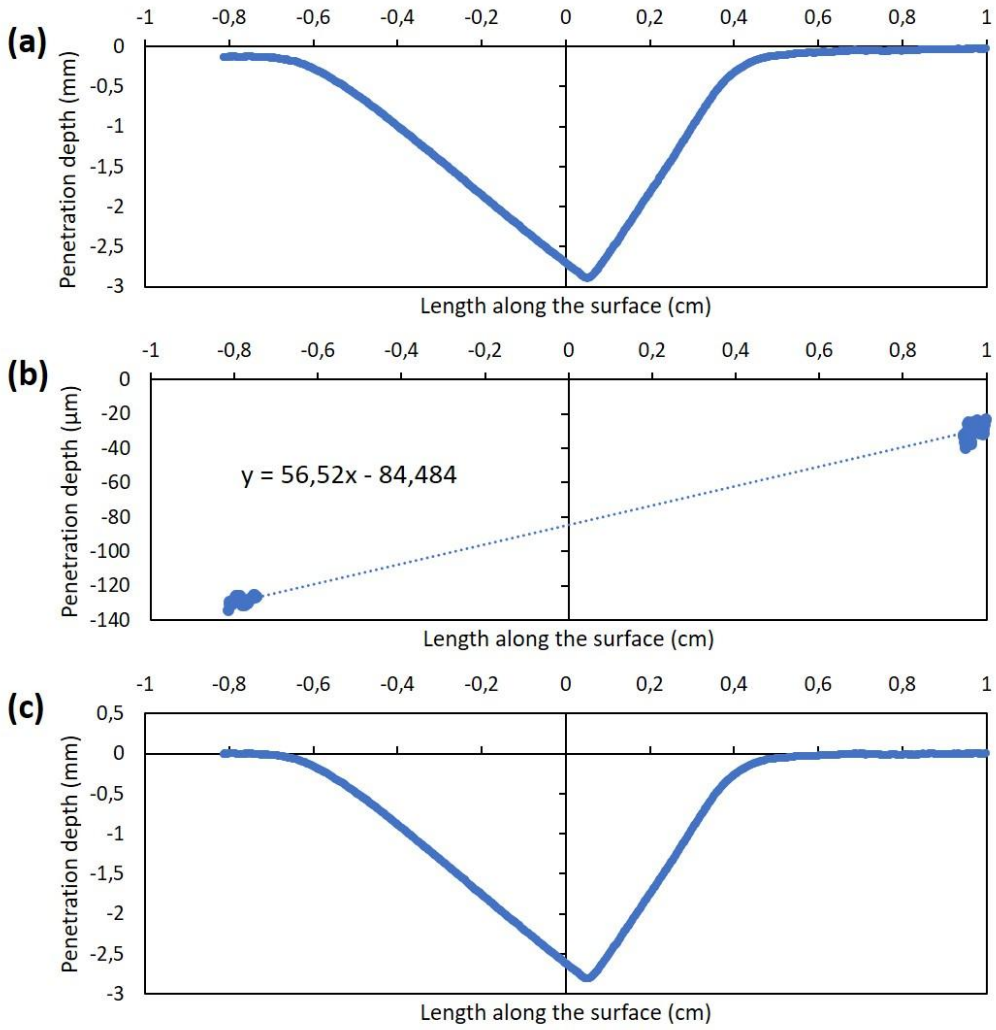

Figure 5.10: Correction of measurement errors occurred in profilometer. (a) Generated 2D profile along x-axis using raw data, (b) inclination of uneroded surface due to the error, (c) corrected profile relative to the x-axis.

5.2.2.1 Eroded 2D profiles

The generated 2D profiles along the centreline of eroded craters at seven different impact angles after 60 min of exposure time are shown in Figure 5.11. The shape of the profile directly influences the penetration depth at each point. The wide spread of the crater profile at glancing angles is clearly visible in the figure. The craters are converged at higher impact angles while at 75° and 90° penetration depth is comparatively insignificant. The effective impact angle inside the crater has changed for developed craters in different magnitudes depending on the impact angle.

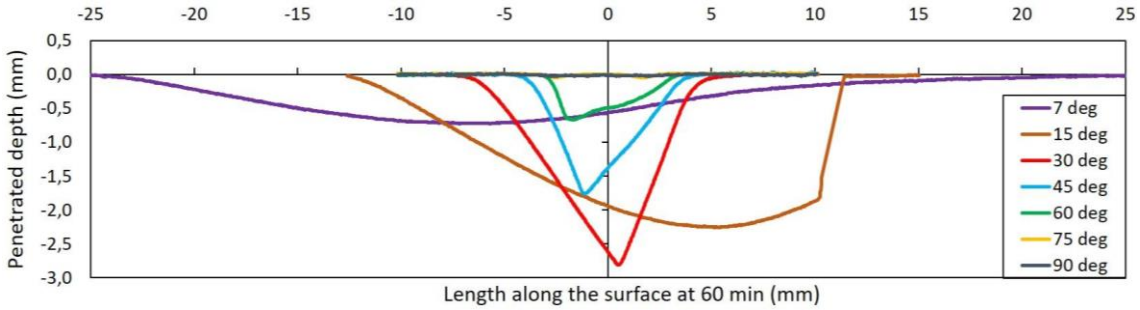

Figure 5.11: 2D profiles along the centre line of eroded craters at different initial impact angles after 60 min of exposure time.

5.2.3 Effective impact angle

The change of 2D profile with growth of the crater was examined by generating longitudinal profiles for different exposure times at a specific impact angle. Particles are in contact with the complete surface of the crater at any given time during the test. Initially, the particles strike on uneroded surface at initial impact angle (Θ_i). When a crater is formed, particles strike under a variety of impact angles inside the crater as can be seen in Figure 5.12. Some particles (to the left of the maximum penetration) strike at lower impact angles than Θ_i while others (to the right of the maximum penetration) strike at higher impact angles of the developed crater. Interestingly, at the point where the maximum penetration appears, particles strike at a similar impact angle as the initial impact angle.

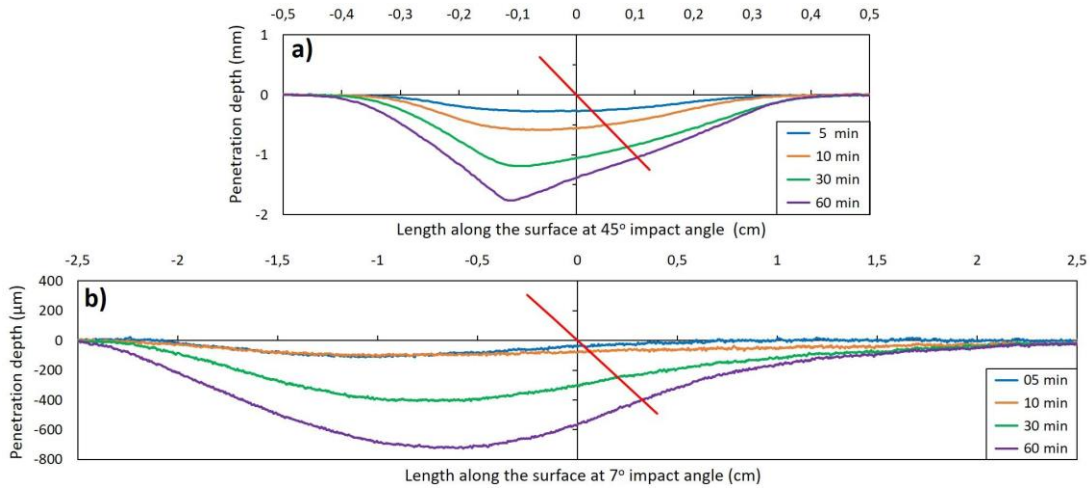

Figure 5.12: Development of craters at (a) 45° impact angle and (b) 7° impact angle.

It was assumed that the change of effective impact angle (Θ_e) resulted in change of erosion rate with the development of eroded crater as explained earlier. Thus, the study focused on analysing the change of effective impact angle with the expansion of the crater. However, due to the complicated behaviour of the particle stream and the large amount of data to analyse from the whole surface area of the crater, the change of effective impact angle along the centreline of particle stream (streamline) was evaluated only at 15° and 30° impact angles as shown in Figure 5.13. Those angles were the most harmful impact angles in terms of both mass loss and penetration depth (Figure 5.8 (b)) during the tested exposure times.

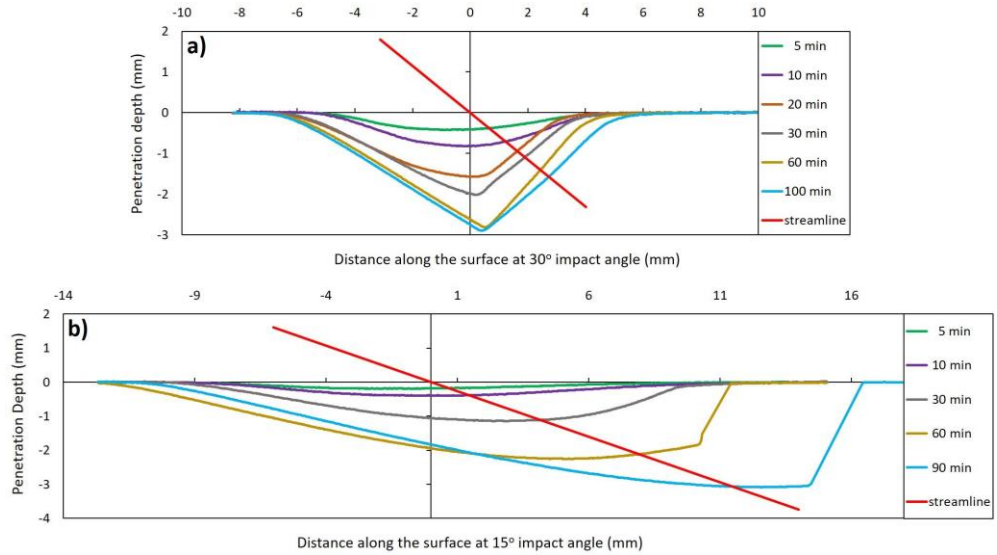

Figure 5.13: Development of craters at (a) 30° impact angle and (b) 15° impact angle.

Both streamlines in Figure 5.13 pass through the profiles under different effective impact angles for different exposure times. Thus, a change of effective impact angle is evident along the streamline with the development of eroded craters at 15° and 30° impact angles. The calculated effective impact angle against the exposure time with the development of the crater is shown in Figure 5.14. The effective impact angle has first increased at short exposure time and decreased later with longer exposures. The deviation of the effective impact angle from the initial impact angle is significant at 30°, while effective impact angle has not changed much from the initial impact at 15°.

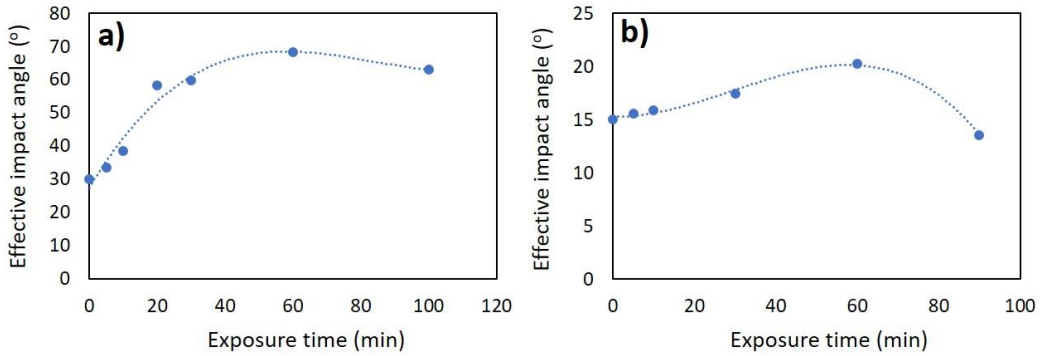

Figure 5.14: Effective impact angle versus exposure time (a) at 30° and (b) at 15° initial impact angle.

5.3 Multivariate analysis

The main objective of the preliminary study (paper 1) was to identify the feasible limitations of the test facilities. In addition, the knowledge gained through the literature review on effects of some influential variables was confirmed by the results of univariate tests under preliminary study. From observations made during the preliminary tests, six influential variables were selected to study further the erosion process by dolomite particles. Multivariate analysis with several variables is a major task in this study that exposes the effect of each variable on impact erosion under different experimental conditions. The selected variables are;

1 - Amount of erodent particles,

2 - Impact angle,

3 - Velocity of erodent particles,

4 - Concentration of erodent particles,

5 - Surface temperature and

6 - Size of erodent particles.

The space of variables (levels) for the tests was selected considering industrial conditions (temperature, velocities) but also the limitations of the erosion tester as explained in section 4.1.1. Design of Experiments (DOE) was employed to study the

effects of multiple variables on impact erosion with a reduced number of tests. The method can be used not only to determine the effect of main variables but also to reveal the effects of interactions between the variables. A short description on DOE method is given in section 4.1.2. DOE consists of three basic stages: screening (to identify significant variables), response surface methodology (to define the optimal space), and model validation (to confirm predictions) [91]. Paper 3 discusses the screening of significant variables while Paper 4 mainly discusses the model development with selected significant variables.

5.3.1 Screening significant variables (paper 3)

The screening analysis was used as a starting point for more detailed designs to model erosion with significant variables. The approach allows one to identify the significant variables among the six variables for further analysis. The screening analysis was started with a reduced quarter fractional factorial design (2^{6-2}). A reduced design generates aliased (confounded) effects which has been briefly discussed in Paper 3. Aliasing or confounding means that the effect of one variable is confounded with the effect of interaction or the effect of interaction is confounded with the effect of another interaction. When aliased effects are present in a design, interpretation of results may become riskier. More details on confounded effects of a reduced factorial design can be found elsewhere [92].

A predictive model for the screening design was developed using Partial Least Square Regression (PLS-R) method and Analysis of Variance (ANOVA). The regression coefficients of the main variables and interactions in Figure 5.15 show their respective effects on predicted mass loss (dependent variable). The corresponding regression coefficients of impact angle and impact velocity show significant effects while regression coefficients of particle size and temperature are relatively less significant. The effects of concentration of particles and the amount of erodent are insignificant compared to the other main variables. The interaction effect of amount of erodent and surface temperature (1x5) is confounded with impact angle and impact velocity (2x3) in the used quarter fractional factorial design. Thus, the regression coefficient of 1x5 can be

expected to be the result of confounding with the interaction of 2x3 (impact angle and impact velocity). However, it is not straightforward to interpret the effects of variables by focusing only the regression coefficients, due to the complexity of the positive influence of the impact velocity, the negative influence of the impact angle and the interaction between them.

The measured mass loss at centre points of the variable space (levels) showed a deviation from predicted results by the screening model. The deviation illustrates a curvature and proves the scarcity of the 2-level design in predicting mass loss by impact erosion. Considering the magnitudes of regression coefficients and the industrial feasibility, four variables were selected as significant variables. Accordingly, concentration of particles and the amount of erodent were discarded in the further analysis.

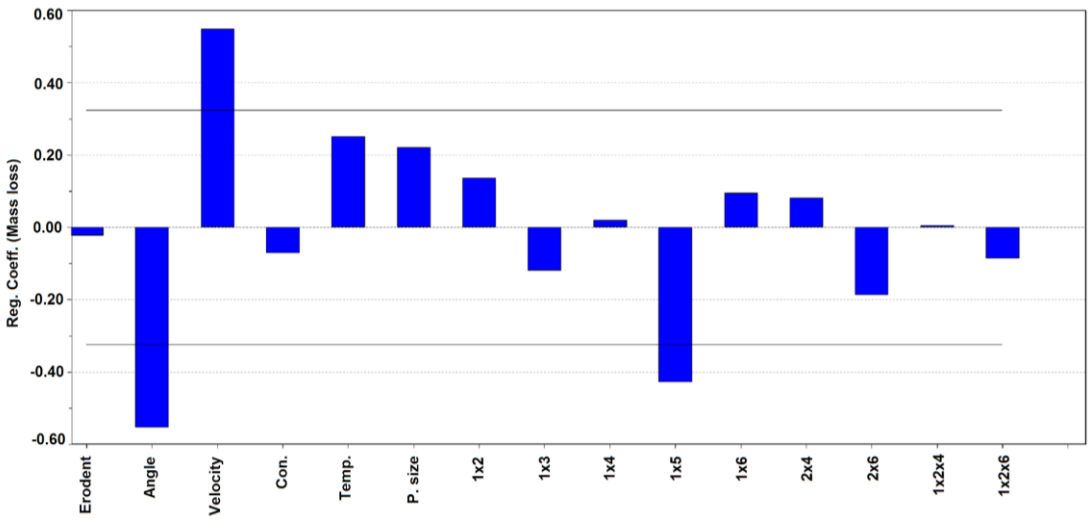

Figure 5.15: Regression coefficients of main effects and interactions.

5.3.2 Model development and significance of the effects (paper 4)

Determination of effects of the significant variable on mass loss and formulation of a predictive model to forecast mass loss caused by impact erosion in multivariate conditions are the main objectives of the study published in Paper 4. The effects of significant variables found in screening analysis (as discussed in section 5.3.1) were investigated in this approach. Four significant variables which are impact angle, impact

velocity, surface temperature and the particle size were used as the main variables in the predictive model. Due to the curvature identified in the 2-level screening design approach, a Regression Surface Methodology (RSM) [93] was used in the new analysis. The testing conditions (e.g. impact velocity, temperature) were selected as close as possible to the relevant industrial process conditions to define the variable space of the tests. PLS-R tool provided in "Unscrambler X 10.3" software package was used for the analysis.

A Central Composite Design (CCD) was used in this study as the RSM among many other designs [93]. The measured mass losses from the tests are spanned over a large range of values and are biased towards the low mass loss region as shown in Figure 5.16. In order to minimize the leaning of mass loss and to enhance the accuracy of prediction at highly erosive conditions, additional tests were added to the initial CCD approach. A total of 87 tests were performed with repetitions covering all the runs suggested in CCD design and the additional tests were also done to minimize leaning behavior. Two independent sets of mass loss results were used for the calibration and the validation of the model. Thus, the model is validated by the test set validation procedure. After removing several outliers, forty-two and forty-one results were used as the calibration set and the validation set, respectively. A second order polynomial relationship was selected as the basis function of the model. Squared terms of the variable were not included and thereby it is a two-factor interaction (2FI) model.

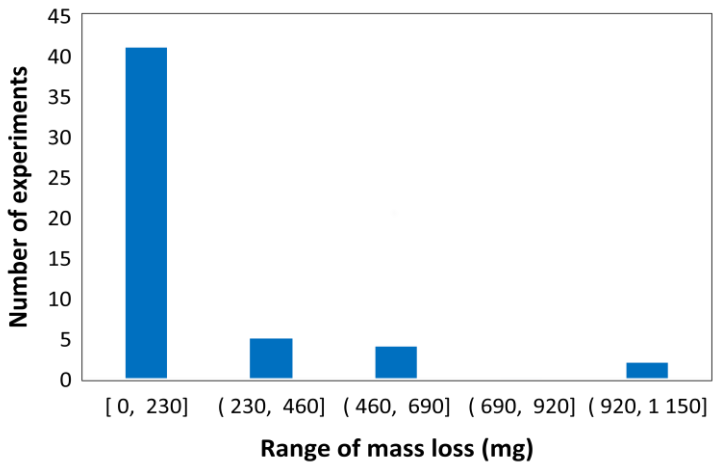

Figure 5.16: The sample count of the response mass loss.

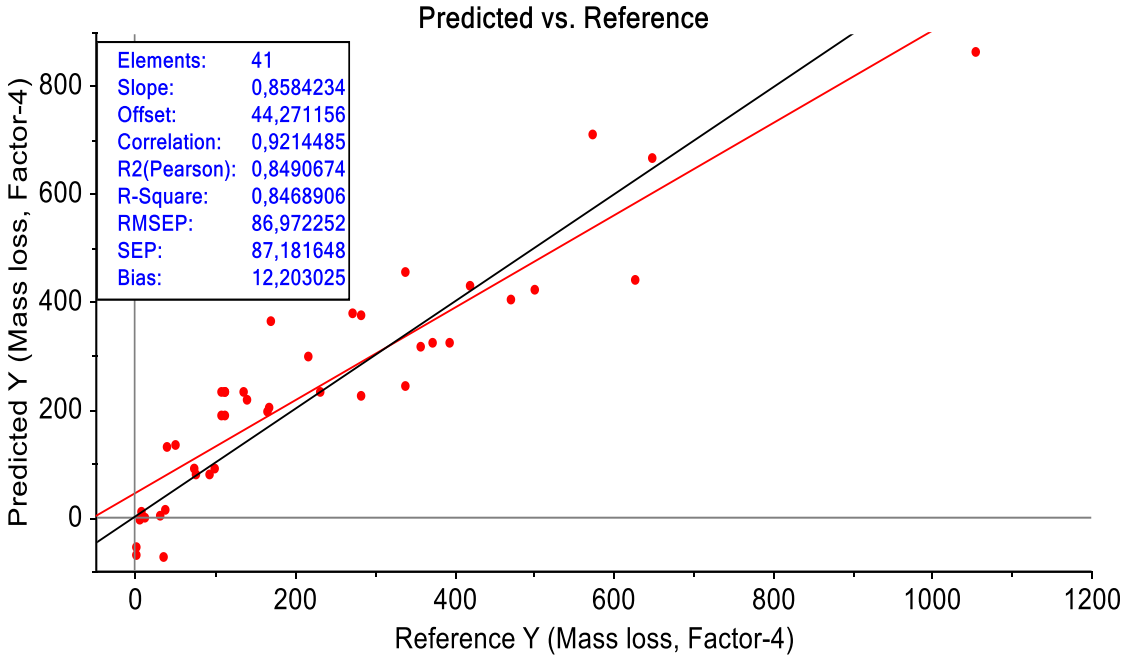

Figure 5.17: Predicted mass loss and measured mass loss (mg) given by PLS-R model.

The predictions based on the model are in good agreement with the measured values as shown in Figure 5.17. The line which goes through the origin represents the perfect match with predicted and measured values of the validation set. The other line with a y-intercept represents the actual regression line of the measured values. The model is not reliable at low mass loss conditions where the measured values are underpredicted. A graphical interpretation of effects of the main variables on the mass loss is presented in Figure 5.18. The poor predictability of the model in the low mass loss region is pronounced in Figure 5.18 (g). Outliers were also found in the same region and eliminated subsequently. Significance of the positive effect of impact angle and the negative effect of impact velocity on mass loss are apparent in Figure 5.18. Both surface temperature and the particle size show positive influences while the effect of surface temperature is higher than that of particle size on mass loss. Further, the effect of impact angle is more pronounced at high velocities and the effect of impact velocity was larger at low impact angles.

The identification of significant variables, their individual and interaction effects on mass loss can be achieved through the model, which is scientifically important to understand

the erosion process. This model was developed by testing industrial materials under the conditions which were selected as close as possible to the industrial applications. Thus, the published model and approaches discussed under the present study can be used in the considered industrial application to control and to minimise impact erosion of pneumatic conveying pipelines used to transport dolomite particles, yet the applicability is very much limited to the materials used for the relevant experiments and tested ranges.

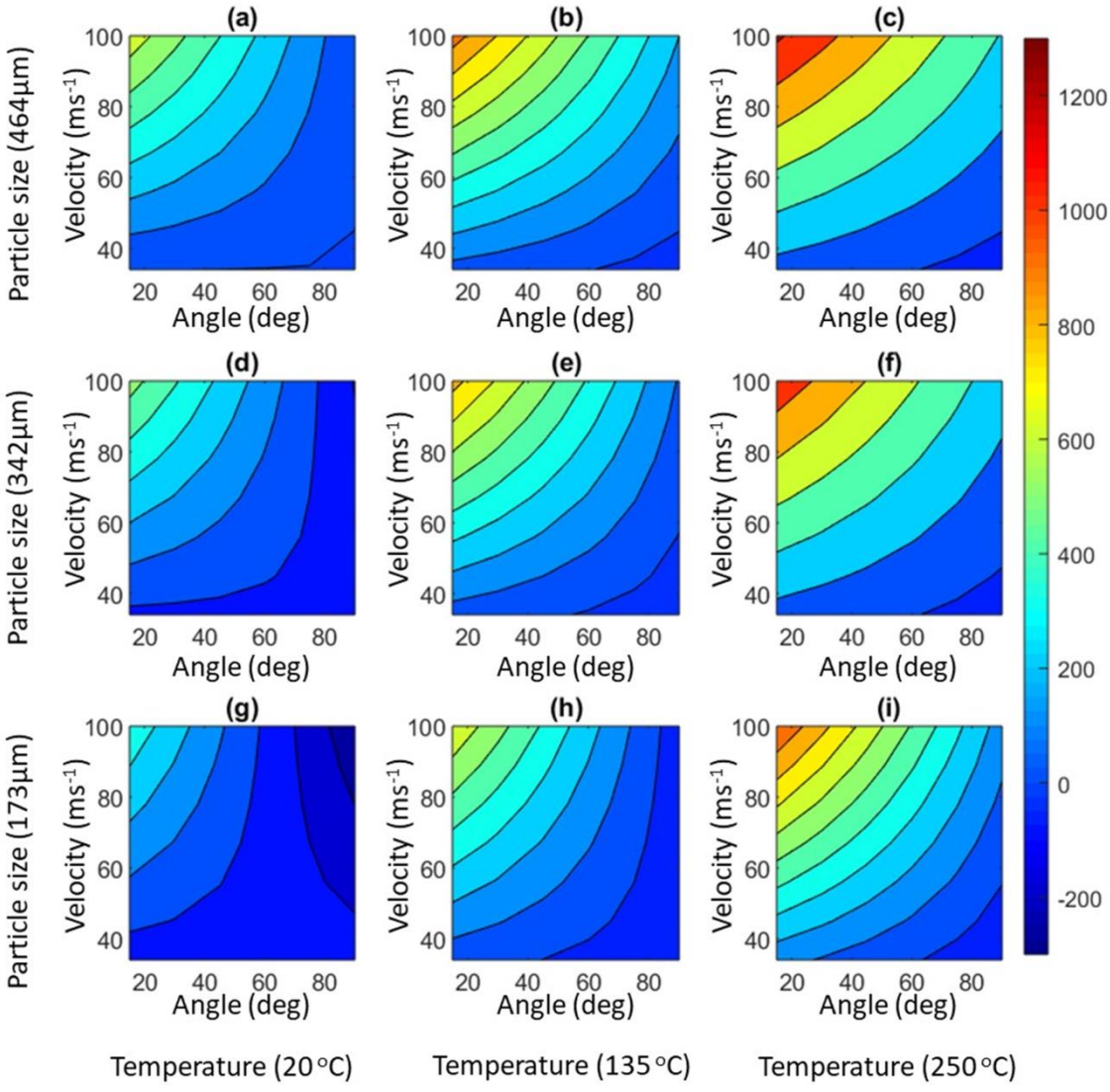

Figure 5.18: Graphical interpretation of influence of main variables on impact erosion. The color scale shows the amount of mass loss in mg.

6 Main conclusion

The main objective of the project was to find the effects of influential variables on impact erosion and to provide a predictive method to illustrate the surface erosion of pneumatic conveying systems in industrial plants. This has been addressed through a systematic experimental research study using a bench-scale sand-blast type erosion tester that enables to study the effects of several parameters simultaneously. The main conclusions of the thesis are provided below:

Literature survey on impact erosion showed that there is still a shortage of information to overcome industrial challenges and lack of established method to accurately predict the amount of erosion under multivariate conditions, though it has been a topic over the years among the research and scientific community.

PAPER 01

Experiments with dolomite on mild steel showed that the mass loss against the particle size increased and then decreased at 30^{o} impact angle after reaching a maximum mass loss. Both conserved kinetic energy in the particles and the number of impacts collectively affect the erosion process where at 30^{o} impact angle, it can be expected that the effect of number of impacts on erosion is more prominent than the kinetic energy for bigger particles. The change of eroded crater profile with the development of the crater resulted in an increase of particle degradation against the exposure time. The shape of the characteristic curve of erosion versus impact angle has changed significantly when the exposure time increased, due to the change of erosion rate at different impact angles. The enlargement of the distance from the nozzle tip to the surface with the growth of the eroded crater, work hardening effects due to particle collisions and the change of impact angle inside the crater (effective impact angle) were proposed as the possible root causes for the change of erosion rate.

PAPER 02

The change of effective impact angle was verified and quantified by profilometry for 15^{o} and 30^{o} initial impact angles. It was observed that the highest mass loss did not coincide with the maximum penetration depth at the same impact angle. While the highest mass loss was attained at 15^{o} impact, the maximum penetration depth was observed at 30^{o} impact at lower exposure times (less than 1 hour). At longer exposure, the effects of erosion were more severe at 15^{o} impact with the maximum penetration as well as the highest mass loss. Based on the transition of maximum penetration, it was concluded that a special attention should be paid to the angle of impact and thickness of the wall material, in addition to the amount of transported bulk material in designing of a pneumatic conveying system.

PAPER 03 and 04

Six influential variables were initially selected for the multivariate analysis. The tested variable space was selected by considering the industrial process conditions in the manufacturing plants. Multivariate analysis was performed using the design of experiment method and the PLS regression method. The effects of the six selected variables on impact erosion were partially identified using a screening design. From these, four significant variables were selected to develop the predictive model for further analysis.

The statistical analysis showed that the variables affecting erosion are highly correlated. It was found that impact angle and impact velocity have a large influence on erosion. Impact velocity showed a higher effect at low impact angles than at high impact angles, indicating interaction between the two variables under multivariate conditions. Further, it was identified that surface temperature and particle size of the bulk material have positive effects on erosion but their influence is lower compared to impact velocity and impact angle. The effect of surface temperature was more pronounced than that of particle size.

The model predictions were not reliable for low mass losses. The validity of the model predictions is limited to the tested conditions and materials. However, the approach proposes a systematic experimental investigation to address the similar challenges of other material handling applications enhancing their reliability in operation, reducing the maintenance cost, avoiding unwanted plant shutdowns, reducing particle emissions to the surrounding, and ensuring occupants' safety and health conditions.

7 Recommendations and future work

The investigation under this study was conducted in a bench scale test rig with one erodent material and one surface material. It can be further extended by focusing on different bulk materials and surface materials. The results found by the bench scale erosion tester are limited in industrial use of other bulk materials. It is necessary to test erosion in a pilot-scale rig and then in an industrial pneumatic conveying system in order to correlate and validate the findings of the bench scale tests. The findings of this study and the correlations with the industrial system could be combinedly used to develop a more comprehensive model.

The results of the eroded craters will assist to enhance the understanding of the dynamic changes at a confined area of surface due to repeated particle collisions. The study of erosion in confined area is inadequate to predict the erosive damage of real life industrial applications. Iteration method or integration of set of confined areas may solve the challenge. It would be interesting to compare the findings of this study with Computational Fluid Dynamics (CFD) and/or Computational Particle Fluid Dynamics (CPFD) simulations. The combination of experimental results with simulation results would be useful to predict mass loss much accurately.

Penetration depth is much more important in prediction of pipe leakage than the mass loss of surface material. Thus, a model with the penetration depth as the response variable would be more relevant in predicting pipe lifetime. Alternative non-invasive methods such as acoustic sensor technology, capacitance tomography should be investigated to measure the variation of pipe wall thickness of industrial pneumatic conveying systems in real time.

References

1. Klinzing, G.E.R.F.M.R.L.L.S., *Pneumatic Conveying of Solids A theoretical and practical approach*. Third ed. Vol. 8. 2010: Springer, Dordrecht.
2. Stokes, J., *The Theory and Application of the HVOF Thermal Spray Process,© Dublin City University*. 2008, ISSN.
3. Stachowiak, G. and A.W. Batchelor, *Engineering Tribology*. 3 ed. 2005: Elsevier Science.
4. Devaraju, A., *A critical review on different types of wear of materials.* Int. J. Mech. Eng. Technol, 2015. **6**(11): p. 77-83.
5. Campo, E.A., *Selection of polymeric materials: how to select design properties from different standards*. 2008: William Andrew.
6. Arabnejad, H., et al., *Development of mechanistic erosion equation for solid particles.* Wear, 2015. **332-333**: p. 1044-1050.
7. Rao, P.V. and D.H. Buckley, *Time effect of erosion by solid particle impingement on ductile materials.* 1983.
8. Finnie, I., *Erosion of surfaces by solid particles.* Wear, 1960. **3**(2): p. 87-103.
9. Finnie, I. *The mechanism of erosion of ductile materials*. in *Proc. of the Third US National Congress of Applied Mechanics, Hagthormthwaite, RM, Ed., ASME, New York*. 1958.
10. Bitter, J.G.A., *A study of erosion phenomena part I.* Wear, 1963. **6**(1): p. 5-21.
11. Bitter, J.G.A., *A study of erosion phenomena: Part II.* Wear, 1963. **6**(3): p. 169-190.
12. Finnie, I., G.R. Stevick, and J.R. Ridgely, *The influence of impingement angle on the erosion of ductile metals by angular abrasive particles.* Wear, 1992. **152**(1): p. 91-98.
13. Gat, N. and W. Tabakoff, *Some effects of temperature on the erosion of metals.* Wear, 1978. **50**(1): p. 85-94.
14. Finnie, I., *Some observations on the erosion of ductile metals.* Wear, 1972. **19**(1): p. 81-90.
15. Hutchings, I.M., *Some comments on the theoretical treatment of erosive particle impacts*, in *5th International Conference on Erosion by Liquid and Solid Impact*. 1979: Newnham College, Cambridge.
16. Oka, Y.I., K. Okamura, and T. Yoshida, *Practical estimation of erosion damage caused by solid particle impact: Part 1: Effects of impact parameters on a predictive equation.* Wear, 2005. **259**(1-6): p. 95-101.
17. Liu, Z., et al., *A numerical study on the effect of particle shape on the erosion of ductile materials.* Wear, 2014. **313**(1-2): p. 135-142.
18. Tegethoff, F.W., J. Rohleder, and E. Kroker, *Calcium carbonate: from the Cretaceous period into the 21st century*. 2001: Springer Science & Business Media.
19. Fan, L.S., et al., *Limestone/Dolomite Sulfation in a Vertical Pneumatic Transport Reactor.* Industrial and Engineering Chemistry Process Design and Development, 1984. **23**(3): p. 538-545.

20. Cenna, A.A., et al., *Wear mechanisms in dense phase pneumatic conveying of alumina.* Wear, 2008. **264**(11-12): p. 905-913.
21. Cenna, A.A., et al., *Generation of transfer film and its effects on wear mechanisms in alumina conveying pipeline of mild steel.* Wear, 2009. **267**(1-4): p. 362-367.
22. Wang, B.-Q. and K. Luer, *The relative erosivity of limestone, dolomite and coal samples from an operating boiler.* Wear, 1998. **215**(1): p. 180-190.
23. Finnie, I., *Some reflections on the past and future of erosion.* Wear, 1995. **186-187**: p. 1-10.
24. Adler, W.F., *Assessment of the State of Knowledge Pertaining to Solid Particle Erosion*. 1979, EFFECTS TECHNOLOGY INC SANTA BARBARA CA.
25. Kleis, I., et al., *Comments on "A two stage mechanism of ductile erosion".* Wear, 1975. **31**(2): p. 403-406.
26. Anand, K., et al., *Flux effects in solid particle erosion.* Wear, 1987. **118**(2): p. 243-257.
27. Levy, A.V. and P. Chik, *The effects of erodent composition and shape on the erosion of steel.* Wear, 1983. **89**(2): p. 151-162.
28. in, et al., *Towards prediction of flux effects in powder blasting nozzles.* Wear, 1998. **215**(1): p. 131-136.
29. Levy, A.V., *Solid particle erosion and erosion-corrosion of materials*. 1995: Asm International.
30. Lindsley, B.A. and A.R. Marder, *The effect of velocity on the solid particle erosion rate of alloys.* Wear, 1999. **225-229**: p. 510-516.
31. Shipway, P. and I. Hutchings, *The role of particle properties in the erosion of brittle materials.* Wear, 1996. **193**(1): p. 105-113.
32. Deng, T., et al., *Effect of particle concentration on erosion rate of mild steel bends in a pneumatic conveyor.* Wear, 2005. **258**(1): p. 480-487.
33. Evstifeev, A., et al., *Experimental and theoretical analysis of solid particle erosion of a steel compressor blade based on incubation time concept.* Engineering Failure Analysis, 2018. **87**: p. 15-21.
34. Hadavi, V., C.E. Moreno, and M. Papini, *Numerical and experimental analysis of particle fracture during solid particle erosion, part I: modeling and experimental verification.* Wear, 2016. **356**: p. 135-145.
35. Islam, M.A., et al., *Effect of microstructure on the erosion behavior of carbon steel.* Wear, 2015. **332-333**: p. 1080-1089.
36. Islam, M.A. and Z.N. Farhat, *Effect of impact angle and velocity on erosion of API X42 pipeline steel under high abrasive feed rate.* Wear, 2014. **311**(1-2): p. 180-190.
37. Oka, Y.I. and K. Nagahashi, *Measurements of plastic strain around indentations caused by the impact of round and angular particles, and the origin of erosion.* Wear, 2003. **254**(12): p. 1267-1275.
38. Tilly, G., *Erosion caused by impact of solid particles*, in *Treatise on Materials Science & Technology*. 1979, Elsevier. p. 287-319.

39. Walley, S. and J. Field, *The contribution of the Cavendish Laboratory to the understanding of solid particle erosion mechanisms.* Wear, 2005. **258**(1-4): p. 552-566.
40. Hagan, J.T., *Cone cracks around Vickers indentations in fused silica glass.* Journal of Materials Science, 1979. **14**(2): p. 462-466.
41. Yoshida, H., M.M. Chaudhri, and Y. Hoshi, *Quasistatic indentation and spherical particle impact studies of turbine-grade silicon nitrides.* Philosophical Magazine A, 2002. **82**(10): p. 2031-2040.
42. Zhou, J. and S. Bahadur, *Erosion-corrosion of Ti-6Al-4V in elevated temperature air environment.* Wear, 1995. **186**(1): p. 332-339.
43. Wang, Y.-F. and Z.-G. Yang, *Finite element model of erosive wear on ductile and brittle materials.* Wear, 2008. **265**(5-6): p. 871-878.
44. Chaudhri, M.M. and M.A. Phillips, *Quasi-static indentation cracking of thermally tempered soda-lime glass with spherical and Vickers indenters.* Philosophical magazine A, 1990. **62**(1): p. 1-27.
45. Sheldon, G. and I. Finnie, *On the ductile behavior of nominally brittle materials during erosive cutting.* 1966.
46. Wensink, H. and M.C. Elwenspoek, *A closer look at the ductile–brittle transition in solid particle erosion.* Wear, 2002. **253**(9-10): p. 1035-1043.
47. Neilson, J. and A. Gilchrist, *Erosion by a stream of solid particles.* wear, 1968. **11**(2): p. 111-122.
48. Ben-Ami, Y. and A. Levy, *Absorbed shear energy during solid particle impact on ductile surface.* Wear, 2016. **368-369**: p. 162-172.
49. Sundararajan, G., *A comprehensive model for the solid particle erosion of ductile materials.* Wear, 1991. **149**(1-2): p. 111-127.
50. Winter, R.E. and I.M. Hutchings, *The role of adiabatic shear in solid particle erosion.* Wear, 1975. **34**(2): p. 141-148.
51. Lindroos, M., et al., *The effect of impact conditions on the wear and deformation behavior of wear resistant steels.* Wear, 2015. **328**: p. 197-205.
52. Hutchings, I., *Wear by particulates.* Chemical Engineering Science, 1987. **42**(4): p. 869-878.
53. Ben-Ami, Y., A. Uzi, and A. Levy, *Modelling the particles impingement angle to produce maximum erosion.* Powder Technology, 2016. **301**: p. 1032-1043.
54. Nguyen, Q., et al., *Effect of impact angle and testing time on erosion of stainless steel at higher velocities.* Wear, 2014. **321**: p. 87-93.
55. Oka, Y.I., et al., *The impact angle dependence of erosion damage caused by solid particle impact.* Wear, 1997. **203**: p. 573-579.
56. Liebhard, M. and A. Levy, *The effect of erodent particle characteristics on the erosion of metals.* Wear, 1991. **151**(2): p. 381-390.
57. Ruff, A.W. and S. Wiederhorn, *Erosion by solid particle impact*. 1979, NATIONAL BUREAU OF STANDARDS GAITHERSBURG MD NATIONAL MEASUREMENT LAB.
58. Stack, M.M., F.H. Stott, and G.C. Wood, *The significance of velocity exponents in identifying erosion-corrosion mechanisms.* Le Journal de Physique IV, 1993. **3**(C9): p. C9-687-C9-694.

59. Sundararajan, G. and P.G. Shewmon, *A new model for the erosion of metals at normal incidence.* Wear, 1983. **84**(2): p. 237-258.
60. Baker, P.J., E.A.J. Barry, and S.T. Bonnington, *A Guide to Slurry Pipeline Systems: PJ Baker, BEA Jacobs, ST Bonnington*. 1979: British Hydromechanics Research Association, Fluid Engineering.
61. Akbarzadeh, E., et al., *The solid particle erosion of 12 metals using magnetite erodent.* Wear, 2012. **282**: p. 40-51.
62. Zhou, J. and S. Bahadur, *High-Temperature Erosion--Corrosion Behavior of Stainless Steels.* Corrosion & Particle Erosion at High Temperatures, 1989: p. 315-333.
63. Yerramareddy, S. and S. Bahadur, *Effect of operational variables, microstructure and mechanical properties on the erosion of Ti-6Al-4V.* Wear, 1991. **142**(2): p. 253-263.
64. Tabakoff, W., *Erosion study of high temperature metals used in turbomachinery.* TMS (The Metallurgical Society) Paper Selection;(USA), 1985. **56**(CONF-840909--).
65. Nguyen, V., et al., *Effect of air-borne particle–particle interaction on materials erosion.* Wear, 2015. **322**: p. 17-31.
66. Tilly, G., *A two stage mechanism of ductile erosion.* Wear, 1973. **23**(1): p. 87-96.
67. Oka, Y. and M. Matsumura, *Erosive Wear Testing Apparatus--Simulation of Erosion Caused by Slurry of Low-Impingement Velocity.* Wear of Materials 1983, 1983: p. 360-366.
68. Levy, A.V., *The platelet mechanism of erosion of ductile metals.* Wear, 1986. **108**(1): p. 1-21.
69. Hutchings, I. and P. Shipway, *Tribology: friction and wear of engineering materials*. 2017: Butterworth-Heinemann.
70. Hornbogen, E., *The role of fracture toughness in the wear of metals.* Wear, 1975. **33**(2): p. 251-259.
71. Deng, T., et al., *Comparison between weight loss of bends in a pneumatic conveyor and erosion rate obtained in a centrifugal erosion tester for the same materials.* Wear, 2005. **258**(1): p. 402-411.
72. Deng, T., et al., *Effect of bend orientation on life and puncture point location due to solid particle erosion of a high concentration flow in pneumatic conveyors.* Wear, 2005. **258**(1): p. 426-433.
73. Laín, S. and M. Sommerfeld, *Numerical prediction of particle erosion of pipe bends.* Advanced Powder Technology, 2019. **30**(2): p. 366-383.
74. Macchini, R., M.S.A. Bradley, and T. Deng, *Influence of particle size, density, particle concentration on bend erosive wear in pneumatic conveyors.* Wear, 2013. **303**(1): p. 21-29.
75. Solnordal, C.B., C.Y. Wong, and J. Boulanger, *An experimental and numerical analysis of erosion caused by sand pneumatically conveyed through a standard pipe elbow.* Wear, 2015. **336-337**: p. 43-57.
76. Mills, D., *Pneumatic conveying design guide*. 1990, London: Butterworths.
77. Sato, S., A. Shimizu, and T. Yokomine, *Numerical prediction of erosion for suspension flow duct.* Wear, 1995. **186**(1): p. 203-209.

78. Portnikov, D., N. Santo, and H. Kalman, *Simplified model for particle collision related to attrition in pneumatic conveying.* Advanced Powder Technology, 2019.
79. Li, H.Z., J. Wang, and J.M. Fan, *Analysis and modelling of particle velocities in micro-abrasive air jet.* International Journal of Machine Tools and Manufacture, 2009. **49**(11): p. 850-858.
80. Deng, T., et al., *A comparison of the gas-blast and centrifugal-accelerator erosion testers: The influence of particle dynamics.* Wear, 2008. **265**(7): p. 945-955.
81. Burnett, A.J., S.R. De Silva, and A.R. Reed, *Comparisons between "sand blast" and "centripetal effect accelerator" type erosion testers.* Wear, 1995. **186**: p. 168-178.
82. Standard, A., *G76-95, Standard Practice for Conducting Erosion Tests by Solid Particle Impingement Using Gas Jets. Vol. 0.302, ASTM, Philadelphia*. Annual Book of ASTM Standards. 1995.
83. Ruff, A.W. and L.K. Ives, *Measurement of solid particle velocity in erosive wear.* Wear, 1975. **35**(1): p. 195-199.
84. foundry, R. *Hot Rolled vs Cold Rolled Steel*. 2021 17/02/2021].
85. Narang, A., et al., *Undergraduate design of experiment laboratory on analysis and optimization of distillation column.* Education for Chemical Engineers, 2012. **7**(4): p. e187-e195.
86. Barrentine, L.B., *An introduction to design of experiments : a simplified approach*, in *An Introduction to Design of Experiments*. 1999, ASQ Quality Press.
87. Alicona, *InfiniteFocus*. 2020.
88. Sympatec. *Laser-diffraction*. [cited 2020; Available from: https://www.sympatec.com/en/particle-measurement/sensors/laser-diffraction/.
89. Sympatec, *Dynamic-image-analysis.* 2020.
90. Zheng, C., et al., *Numerical study of impact erosion of multiple solid particle.* Applied Surface Science, 2017. **423**: p. 176-184.
91. Wass, J.A., *First steps in experimental design--the screening experiment.(Statistical Viewpointd.).* Journal of Validation Technology, 2010. **16**(2): p. 49.
92. Kirk, R.E., *Experimental Design: Procedures for the Behavioral Sciences*. 2013, SAGE Publications, Inc.: Thousand Oaks, California.
93. Breyfogle Iii, F.W., *Implementing six sigma: smarter solutions using statistical methods*. 2003: John Wiley & Sons.

Part B: Published and submitted papers

Paper 01

Mahesh Ediriweera, Jana Chladek, and Chandana Ratnayake. 2019. Effect of impact angle, exposure time, and particle size on impact erosion. Particulate Science and Technology: 1-9. https://doi.org/10.1080/02726351.2019.1663328.

Paper 02

Mahesh Ediriweera, Jana Chladek, Arne Røyset and Chandana Ratnayake. 2020. The progression of impact erosion with exposure time. Submitted to Particulate Science and Technology. Status: Under review

Not available online

Paper 03

Mahesh Ediriweera, Reidar Arneberg, Jana Chladek and Chandana Ratnayake. 2018. Multivariate analysis of impact erosion by Dolomite particles. doi:http://dx.doi.org/10.2139/ssrn.3293018. The International Conference on Conveying and Handling of Particulate Solids (CHoPS, 2018).

MULTIVARIATE ANALYSIS OF IMPACT EROSION BY DOLOMITE PARTICLES

Mahesh Ediriweera[1,2], [1]SINTEF Tel-Tek in Dept. of Process Technology, SINTEF Industry, Kjølnes ring 30, 3918 Porsgrunn, Norway [2]Faculty of Technology, University College of Southeast Norway
mahesh.ediriweera@sintef.no
Chandana Rathnayake[1,2], [1]SINTEF Tel-Tek in Dept. of Process Technology, SINTEF Industry, Kjølnes ring 30, 3918 Porsgrunn, Norway [2]Faculty of Technology, University College of Southeast Norway
Jana Chladek, SINTEF Tel-Tek in Dept. of Process Technology, SINTEF Industry, Kjølnes ring 30, 3918 Porsgrunn, Norway
Reidar Arneberg, SINTEF Tel-Tek in Dept. of Process Technology, SINTEF Industry, Kjølnes ring 30, 3918 Porsgrunn, Norway

Key Words: Erosion, Multi-variate investigation, Design of Experiments, Significant parameters, Dolomite.

Abstract

Erosion on the wall surface due to hard particle impact is a well-known challenge encountered in industrial pneumatic conveying systems. Surface erosion by particle impact depends on many factors. Numerous studies have shown the dependency of erosion on different factors using univariate experiments. However, there have not been many multivariate analyses of erosion with focus on industrial applications. The present study involves multivariate investigation to identify and quantify the effects of six factors on erosion using Design of Experiments (DoE) methodology. A fractional factorial design was selected (2^{6-2} with 3 center points) and analyzed using "Sirius 10.0™" design package. The statistical analysis of the results using ANOVA and PLS allows a closer study of the significance of main factors and interactions. Confounding (also called aliasing) of the main and interaction effects is the price paid for using a fractional design and it may increase the complexity of the analysis. Therefore, additional experiments are needed to isolate the effects of main factors and interaction terms.

1. INTRODUCTION

Impact erosion by solid particles is influenced by numerous factors which can be classified into three main categories: erodent particle properties (shape, size, hardness, etc.), surface material properties (brittleness, ductility, hardness, toughness, etc.) and the process parameters and conditions (impact angle, impact velocity, mass flow rate, temperature, etc.). The objective of the study was to investigate the effect of six different factors which are expected to play a role in impact erosion. The selected factors were size of erodent particles, impact angle, concentration of erodent particles, surface temperature, velocity of erodent particles and amount of erodent particles. The measured response variable was the mass loss from the target material surface. A sand blast type erosion tester was used to perform the experiments. Design of Experiments was employed to study the multivariate behavior of impact erosion with a reduced number of tests. DoE allows us to determine the effects of

the main factors/variables and their interactions. Among the many types of experimental designs, factorial design is the most foolproof design [1]. A two-level, full factorial design with six factors, commonly named as a 2^6 design, implies 64 experiments without counting replicates and center point experiments. The main purpose of the study was screening the main factors and it was therefore decided to start with a smaller/reduced design. A quarter-fractional factorial design (2^{6-2} design) was used instead of a full factorial design, resulting in 16 experiments. The price for reducing the number of runs from 64 to 16 is that aliased (confounded) effects have been generated. Hence, interpreting the results becomes more difficult and riskier. The selected design has a resolution IV, which means that single factors are confounded with three-factor interactions and two-factor interactions are confounded with other two-factor interactions. The confounding structure for the selected design shown in Fig. 1 indicates that, for example, the main factor no. 1 is confounded with three-factor interactions of factors no. 2, 3, and 5 and 4, 5, and 6. The six selected factors were labelled by numbers as follows: 1 - amount of erodent, 2 - impact angle, 3 - impact velocity, 4 - concentration of particles, 5 - surface temperature and 6 - weighted mean particle size.

1 = 1 + 2x3x5 + 4x5x6
2 = 2 + 1x3x5 + 3x4x6
3 = 3 + 1x2x5 + 2x4x6
4 = 4 + 1x5x6 + 2x3x6
5 = 5 + 1x2x3 + 1x4x6
6 = 6 + 1x4x5 + 2x3x4
1x2 = 1x2 + 3x5
1x3 = 1x3 + 2x5
1x4 = 1x4 + 5x6
1x5 = 1x5 + 2x3 + 4x6
1x6 = 1x6 + 4x5
2x4 = 2x4 + 3x6
2x6 = 2x6 + 3x4
1x2x4 = 1x2x4 + 1x3x6 + 2x5x6 + 3x4x5
1x2x6 = 1x2x6 + 1x3x4 + 2x4x5 + 3x5x6

Figure 1 – Confounding structure of the 2^{6-2} fractional factorial design.

Further, the 2-level factorial design assumes there is a linear relationship between each X (independent variable) and Y (dependent variable). Adding center points can help in revealing a curvature (potential non-linearity). It is also important to be aware that the center points do not help in obtaining more precise estimates of model effects. Including center points can provide evidence of curvature but does not identify the nonlinear effects. A total of 19 experiments were performed with center points. The results were analyzed using the software package "Sirius 10.0™".

2. MATERIALS AND METHODS

2.1 Raw material and operating conditions

Dolomite particles ($CaMg(CO_3)_2$) (D10% = 55 µm, D50% = 150 µm, and D90% = 305 µm), kindly donated by Omya Hustadmarmor AS, were used for the tests. Due to low flowability, smaller particles had to be removed using a 150-micron sieve to achieve a stable mass flow rate. The remaining particles (above 150 µm) were

classified into three different size classes using a set of several sieves. The particle size distributions of the resulting size classes are shown in Fig. 2. The tests were run with a sand blast type erosion tester, which accelerates the particles in a stream of compressed air before impact with a target specimen under specified conditions. DOMEX S355MC mild steel bricks (25X25mm and 75X25mm) of 5 mm thickness were used as the target specimens for all the experiments. Low carbon mild steels are known to be ductile materials [2].

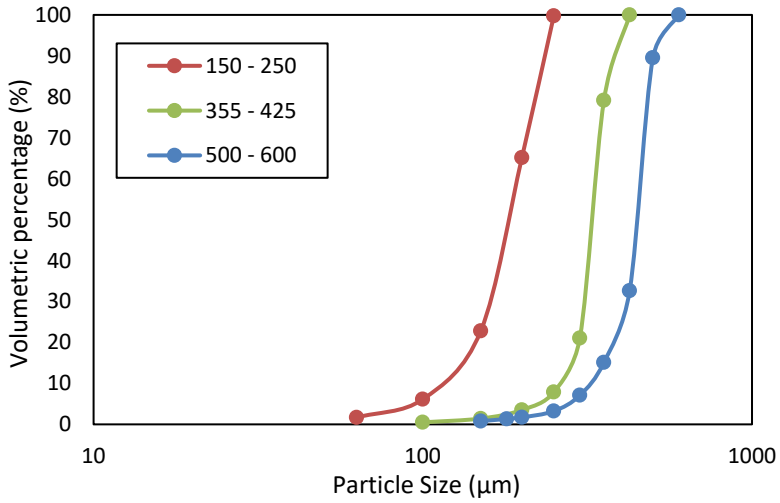

Figure 2 – Particle size distributions of the sieved size classes.

The concentration of particles in the stream of air is given by the Solid Loading Ratio (SLR), the solid to air mass flow ratio. In the experimental test set-up, the solid loading ratio was varied between 0.5 and 1.5. The value of 1.5 was given by the maximum attainable solid mass flow rate in the used erosion tester. SLR values below 15 are typically considered as dilute phase [3, 4] and therefore, the concentration range does not cover the conditions for dense phase conveying. The surrounding temperature of the testing compartment was adjusted to keep the surface temperature of the target plate at the desired levels. The surface temperature of the target material was varied between 20 °C and 250 °C during the tests. A thermocouple which was in-touch with the target material was used to monitor the surface temperature and to ensure that the surface temperature was stable during the tests. It has to be noted that although the surface material reaches the desired temperature, it is not assured that the particles and air have reached the same temperature. It is likely that during the tests at 250 °C, the temperature of the particles and air was lower than the surface temperature of the target material. The impact angle was varied between 15° and 90° using different target specimen holders, which are fabricated to give different inclinations. The particle velocity was calibrated as a function of the supplied air pressure as described below. The mass flow rate of air which is directly proportional to the air supply pressure and inversely proportional to the air temperature was measured by a flowmeter. As shown in Fig. 3, the air supply pressure was used to attain the required air velocity in the tests depending on the particle size. The feed rate of solids (erodent) had to be adjusted in accordance with desired SLR, impact velocity and temperature at given particle size. The amount of erodent material striking at the surface of the target material in one experiment was varied between 2 and 4 kg. Exposure time (i.e., how long the plate was exposed to the particle impact in a test) was given by the time it took to use up 2 to 4 kg of erodent at the fixed feed rate of solids. This implies that exposure time varied in each experiment

depending on the set amount of erodent and the feed rate of solids. Therefore, exposure time could not be used as one of the independent factors, instead amount of erodent was selected and its effect on erosion was investigated. The mass loss from the surface of the target material was calculated by weighing the cleaned surface sample before and after the test. The accuracy of the scale was 0.1 mg.

2.2 Velocity of particles

Particle velocity was calibrated by the double disk motor assembly. Detailed operation of the sand blast type erosion tester and the velocity calibration method were presented in a previous publication [5]. The particles are accelerated by a stream of compressed air. During the calibration, it was observed that the particle velocity varied with the particle size according to the Stokes's law [6]. Larger particles have a higher mass and therefore, they need higher air pressure to achieve the same velocity as smaller particles. Fig. 3 shows the particle velocity plotted against the air pressure for different particle sizes. The relationship between the particle velocity and the air pressure shown in Fig. 3 is also valid for high temperature conditions, however, in high temperatures, the mass flow rate of air needed to attain given pressure is lower than in lower temperatures due to gas expansion.

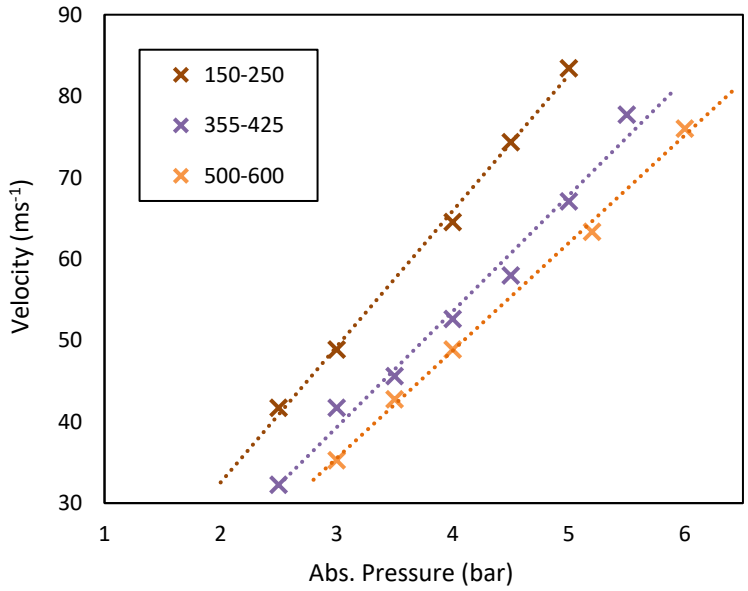

Figure 3 – Particle velocity against air pressure

2.3 Design of Experiments

Design of experiments (DoE) is a simultaneous study of several process variables instead of having separate study for each variable while doing minimum number of experiments [7]. Therefore, the testing time is drastically reduced, and abundance of data is limited. Further, one factor at a time studies cannot detect the effects of interactions between the factors [8]. DoE is useful in estimating which factors and interactions have a significant effect on the response variable and in quantifying the magnitude of these effects. In this experimental set up, the selected variables are expected to have influence on impact erosion [9-13] but the significance of the main effects and interactions is to be determined. Tab.1 shows the six selected variables varied at two levels, given by high

and low values. The values for the variables were pre-decided based on known industrial conditions and limitations given by the erodent material and the instrument. The center points are not at the exact center for the impact angle and the particle size which are discrete variables. Hence, the values for the center point were selected as close as possible to the actual center between low and high values.

Table 1. The range of variables.

Variable	Notation	Unit	Low	High
Amount of erodent	1	kg	2	4
Impact angle	2	°	15	90
Impact velocity	3	ms^{-1}	35	78
Concentration of particles (SLR)	4	-	0.5	1.5
Surface temperature	5	°C	20	250
Weighted mean particle size	6	µm	174	448

3. RESULTS AND DISCUSSION

The resulting mass losses obtained under different experimental conditions in 19 test runs are shown in Tab. 2.

Table 2. Experimental conditions and measured mass losses.

Exp	S. mass (kg)	Angle (°)	Velocity (ms^{-1})	Con (SLR)	Temp (°C)	Size (µm)	Erosion (mg)
Exp 1	2	15	34	0.5	20	174	0.9
Exp 2	4	15	34	0.5	250	174	8.2
Exp 3	2	90	34	0.5	250	448	20.5
Exp 4	4	90	34	0.5	20	448	3.4
Exp 5	2	15	78	0.5	250	448	772.8
Exp 6	4	15	78	0.5	20	448	594.7
Exp 7	2	90	78	0.5	20	174	2.7
Exp 8	4	90	78	0.5	250	174	106
Exp 9	2	15	34	1.5	20	448	30.3
Exp 10	4	15	34	1.5	250	448	230.3
Exp 11	2	90	34	1.5	250	174	0.5
Exp 12	4	90	34	1.5	20	174	0.9
Exp 13	2	15	78	1.5	250	174	578.3
Exp 14	4	15	78	1.5	20	174	237.1
Exp 15	2	90	78	1.5	20	448	7.2
Exp 16	4	90	78	1.5	250	448	143.5
Cent 1	3	45	56	1.0	135	311	108.3
Cent 2	3	45	56	1.0	135	311	103.6
Cent 3	3	45	56	1.0	135	311	96

The results were analyzed using standard methods and tools provided in the design package, that is PLS (Partial Least Square regression) and ANOVA (Analysis of Variance). The effects of the main factors and interactions

were determined, and the potential non-linearity was evaluated using the center points. The regression coefficients of all main factors and interactions are shown in Fig. 4.

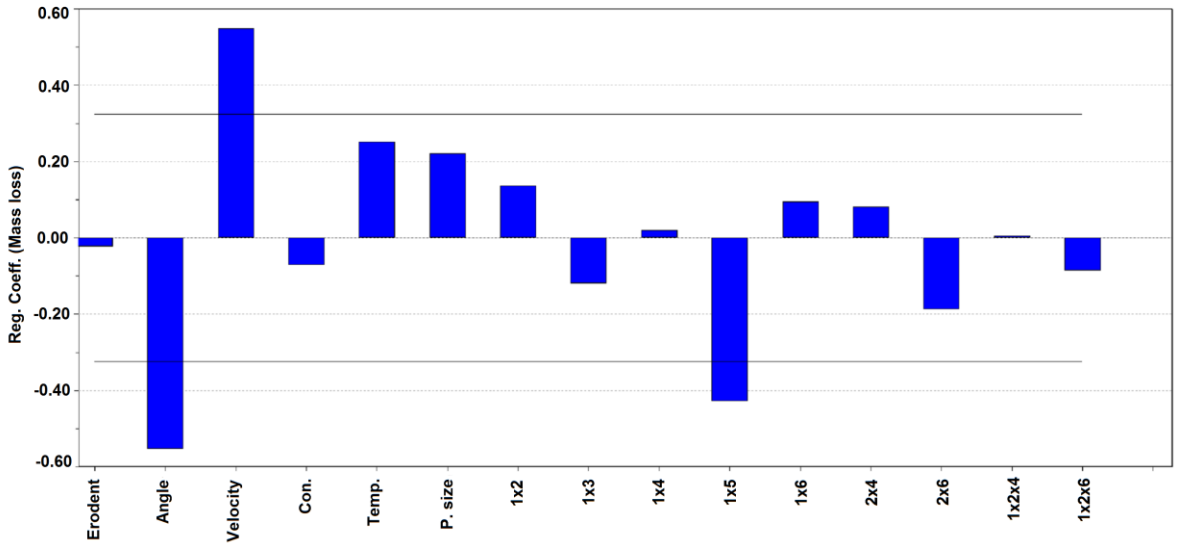

Figure 4 Regression coefficients of main effects and interactions. The Lenth's Margin of Error (ME) is indicated by the horizontal line.

It can be concluded that the effects of the main factors and interactions have different magnitudes. The impact angle and impact velocity have the highest influence on erosion when compared with other main factors. Earlier studies showed that impact velocity has usually an exponential relation with mass loss and it is the most critical variable in erosion by solid particles [9, 14, 15]. The regression coefficient for impact angle has a comparable magnitude with the impact velocity but the value is negative. This means that the amount of erosion is reduced when the impact angle is increased. The results in Tab.2 show that the mass loss is higher at low impact angle (i.e., 15^{o}) than at 90^{o} impact angle. This finding is in agreement with previous studies [10, 16, 17], where ductile surfaces show high mass losses at glancing angles and low mass losses at high angles. Different erosion mechanisms acting on ductile surfaces are responsible for this behavior [18].

Both particle size and surface temperature have a positive effect on erosion, which is approximately half of that for impact velocity or impact angle, based on the magnitude of the regression coefficients in Fig. 4. Temperature has a slightly higher effect than particle size. The mass loss might increase with elevated temperature due to changes in chemical and physical properties of the target material [12]. At high temperatures, the mass loss at glancing angles is dramatically increased. A decrease of hardness with higher temperature might make the material more ductile and thus, the surface damage due to cutting wear could be more severe at glancing angles [19]. For the influence of particle size on erosion, a critical particle size was suggested, above and below which the erosion rate declines [6, 13]. However, those results were based on constant air velocity for different particle sizes. In this study, Fig. 3 shows that larger particles do not follow fluid flow as smaller particles. Hence, higher air velocities had to be used to achieve the same particle (impact) velocity for larger particles.

Concentration of particles has a relatively low influence and is indirectly proportional to mass loss. The results depend to a certain degree on the selected minimum/maximum levels for the various factors. Narrow range of levels may be the reason for the low effect of concentration of particles. Further, a negative impact of concentration of particles was also observed in several other studies [11, 20, 21]. In a highly concentrated particle system, the average distance between the particles is decreased and the degree of interparticle collisions is increased. The particles bouncing from the target collide with the particles approaching the target, diverting their trajectory and preventing them from impact. This will create a shield effect [21] and result in a reduction of erosion.

Amount of erodent, a measure of exposure as explained in the Materials and Methods section has a low effect on erosion compared to other factors, but it is involved in interaction with surface temperature (interaction term 1x5 in Fig. 4) which is highly important. This indicates that the effect of the amount of erodent depends on surface temperature. Due to the use of reduced design, the interaction of 1x5 (amount of erodent x temperature) is confounded with interactions of 2x3 (impact angle x impact velocity) and 4x6 (concentration of particles x particle size) as presented in Fig. 1. This means that it is not possible to distinguish between the effects of two-factor interactions. More experiments are needed to solve this, but looking at the size of the main factors, it is reasonable to expect that the interaction 3x4 (impact angle x impact velocity) is the most important interaction.

Table 3. Analysis of variance table.

Analysis of Variance table						
Source	**Sum of Squares**	**df**	**Mean Squares**	**F Value**	**P Value**	**Regression Coefficients**
Model	819006	5	163801.2	11.652	0.0007	
1. Amount of erodent	93090	1	93089.8	6.622	0.0277	-0.023
2. Impact Angle	293737	1	293736.9	20.896	0.0010	-0.553
3. Impact Velocity	288181	1	288181.1	20.500	0.0011	0.548
5. Temperature	226518	1	226517.6	16.114	0.0025	0.251
1x5	176211	1	176211.1	12.535	0.0054	-0.429
Residual	140573	10	14057.3			
Total	959579	15				

To determine which factors and interactions have a significant impact on erosion, Lenth's method [22] was used as a guideline. This is an objective method for deciding which effects are active in the analysis of nonreplicated experiments, when the model is saturated and hence there are no degrees of freedom for estimating the error variance. The horizontal lines in the graph of Fig. 4 indicate the boundary of significance obtained by Lenth's method. Based on this analysis, the concentration of particles and all interactions including this factor were removed from the model. It is worth mentioning that the amount of erodent is insignificant, but the interaction term with temperature (1x5) is significant according to Lenth's method. Therefore, the main factors, amount of erodent and surface temperature, should also be included in the model. The results in Tab. 3 show the results of an ANOVA analysis which included four main factors (amount of erodent, impact velocity, impact angle and temperature) and one interaction term (amount of erodent x temperature). The resulting model explains 85% of

the measured variation in erosion (mass loss). In comparison, the standard deviation derived from the 3 centre points was approx. 6%.

The degree of non-linearity in the system was evaluated using the results obtained through the center points. It could be observed that the model predicted a mass loss for the conditions at center point at 198 mg. The measured value however varies between 93 mg to 108.3 mg which is approximately half of the predicted mass loss. The deviation at the center point between the predicted and the measured values indicates a potential non-linearity which is not captured by the model.

4. CONCLUSIONS

The impact angle and impact velocity showed significant main effects. Two-factor interaction terms were also significant, most likely, the interaction of impact angle x velocity. Due to the complexity of the negative influence for the impact angle and the positive influence for the impact velocity and the interaction between these two factors, it is not straightforward to interpret the results even if we resolve the aliasing structure by just looking at the regression equation. The screening model is valid only for the tested values (e.g., the selected minimum/maximum values). The deviation of the center points from the model illustrates potential non-linearity in the relationship between the independent variables (experimental conditions) and the dependent variable (actual erosion). The experiments and analysis presented above should be used as a starting point for more detailed designs, such as full factorial design for the four significant factors (impact angle, impact velocity, surface temperature and amount of erodent) and central composite design including 5 levels for each factor.

5. ACKNOWLEDGMENT

The authors are grateful to Research Council of Norway, Omya Hustadmarmor, Hydro Aluminium and GE Power Norway for funding the project and providing relevant information from production plants.

6. REFERENCES

1. Institute, S.A.S., *JMP 11 Design of Experiments Guide*, in *Design of experiments guide*. 2013, SAS Institute.
2. Knowles, P.R., *Design of Structural Steelwork*. 1987: London.
3. Klinzing, G.E.R., F. Marcus, R. Leung, L.S., *Pneumatic Conveying of Solids A theoretical and practical approach*. Third ed. Vol. 8. 2010: Springer, Dordrecht.
4. Mills, D., *Pneumatic conveying design guide*. 1990, London: Butterworths.
5. Ediriweera, M., C. Ratnayake, and J. Chladek, *SCIENTIFIC INVESTIGATION ON INFLUENCE OF PARTICLE SIZE ON EROSIVE WEAR BY CaCO3*, in *RELPOWFLO V*. 2017: Skien.
6. Nguyen, V.B., et al., *Effect of particle size on erosion characteristics.* Wear, 2016. **348-349**: p. 126-137.
7. Narang, A., et al., *Undergraduate design of experiment laboratory on analysis and optimization of distillation column.* Education for Chemical Engineers, 2012. **7**(4): p. e187-e195.
8. Barrentine, L.B., *An introduction to design of experiments : a simplified approach*, in *An Introduction to Design of Experiments*. 1999, ASQ Quality Press.
9. Lindsley, B.A. and A.R. Marder, *The effect of velocity on the solid particle erosion rate of alloys.* Wear, 1999. **225-229**: p. 510-516.

10. Islam, M.A. and Z.N. Farhat, *Effect of impact angle and velocity on erosion of API X42 pipeline steel under high abrasive feed rate.* Wear, 2014. **311**(1-2): p. 180-190.
11. Deng, T., et al., *Effect of particle concentration on erosion rate of mild steel bends in a pneumatic conveyor.* Wear, 2005. **258**(1): p. 480-487.
12. Zhou, J. and S. Bahadur, *Erosion-corrosion of Ti-6Al-4V in elevated temperature air environment.* Wear, 1995. **186**(1): p. 332-339.
13. Macchini, R., M.S.A. Bradley, and T. Deng, *Influence of particle size, density, particle concentration on bend erosive wear in pneumatic conveyors.* Wear, 2013. **303**(1): p. 21-29.
14. Okonkwo, P., et al., *Erosion Behaviour of API X100 Pipeline Steel at Various Impact Angles and Particle Speeds.* Metals, 2016. **6**(10): p. 232.
15. Ruff, A.W. and S. Wiederhorn, *Erosion by solid particle impact*. 1979, DTIC Document.
16. Liu, B., L. Bao, and A. Xu, *Effect of fabric orientation and impact angle on the erosion behavior of high-performance thermoplastic composites reinforced with ductile fabric.* Wear, 2016. **352-353**: p. 24-30.
17. Ben-Ami, Y., A. Uzi, and A. Levy, *Modelling the particles impingement angle to produce maximum erosion.* Powder Technology, 2016. **301**: p. 1032-1043.
18. Bitter, J.G.A., *A study of erosion phenomena part I.* Wear, 1963. **6**(1): p. 5-21.
19. Shimizu, K., et al., *High temperature erosion characteristics of surface treated SUS410 stainless steel.* Wear, 2011. **271**(9): p. 1349-1356.
20. in, et al., *Towards prediction of flux effects in powder blasting nozzles.* Wear, 1998. **215**(1): p. 131-136.
21. Anand, K., et al., *Flux effects in solid particle erosion.* Wear, 1987. **118**(2): p. 243-257.
22. Lenth, R.V., *Quick and Easy Analysis of Unreplicated Factorials.* Technometrics, 1989. **31**(4): p. 469-473.

Paper 04

Mahesh Ediriweera, Maths Halstensen, Reidar Arneberg, Jana Chladek and Chandana Ratnayake. 2019. Multivariate modelling of key variables in solid-particle erosion. Submitted to Tribology - Materials, Surfaces & Interfaces. Status: Under review

Not available online

Appendices

Appendix I: Product information - Technical data of particles

The tests of multivariate analysis (section 5.3) were carried out using the particles in Appendix I.

Norwegian Talc AS
NO-5355 Knarrevik

ISO 9001 Certified

Product Information - Technical Data

Microdol 40/200

MINERALOGY

Major mineral

Dolomite, $CaMg(CO_3)_2$, 99,4%

Minor mineral

Mica.

MINERAL RELATED PHYSICAL PROPERTIES

pH	10	ISO 787-9
Refractive index	1,62	
Hardness	3,5	Moh's scale
Density	2,85 g/ml	ISO 787-10
Loss on ignition	47,3%	ISO 3262-1
Moisture ex. works	<0,2 %	ISO 787-2

PRODUCT RELATED PHYSICAL PROPERTIES

Specific surface	0,1 m^2/g	BET, ISO 4652
Oil absorption	-----	ISO 787-5
Tamped density	1,94 g/ml	ISO 787-11
Electrical conductivity	$5,3x10^{-5}Ohm^{-1}xcm^{-1}$	DIN 53208
Acid insoluble	0,6%	ISO 3262-2
Soluble in H_2O	0,07%	ISO 787-3
Whiteness		
Rx	-----	Elrepho 450X, DIN 53163
Ry	-----	
Rz	-----	
Particle Size		
Weight% < 595 µm	99,9	Dry sieving, ISO 787-7
Top cut, D_{98}	500 µm	
Med. part. size, D_{50}	150 µm	
Weight% < 75 µm	16	Dry sieving, ISO 787-7

Particle size distribution

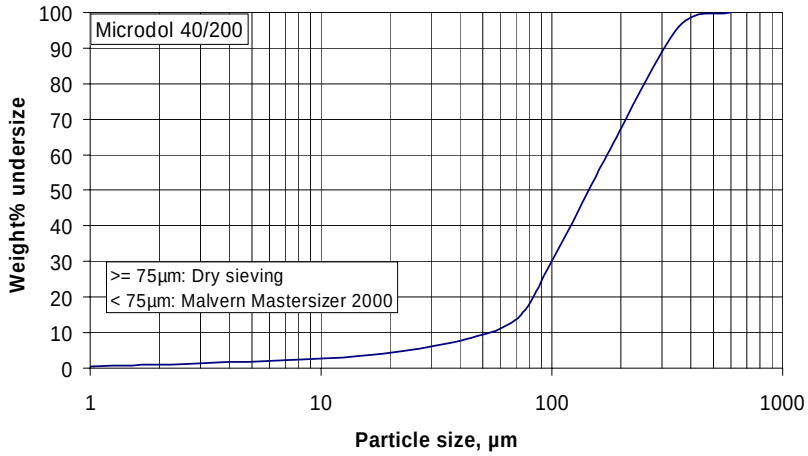

CHEMICAL ANALYSIS

Main elements (XRF)

CaO	30,0%
MgO	23,4%
SiO_2	0,3%
Al_2O_3	0,1%
Fe_2O_3	0,1%

The values in this information sheet are typical average data and may not be looked upon as specifications.

Appendix II: PSD curve of particles in the range of 0-5000 micron

The preliminary tests (section 5.1) were carried out using the particles in Appendix II.

Particle size distribution of $CaCO_3$ (Ball mill feeder) from Omya.

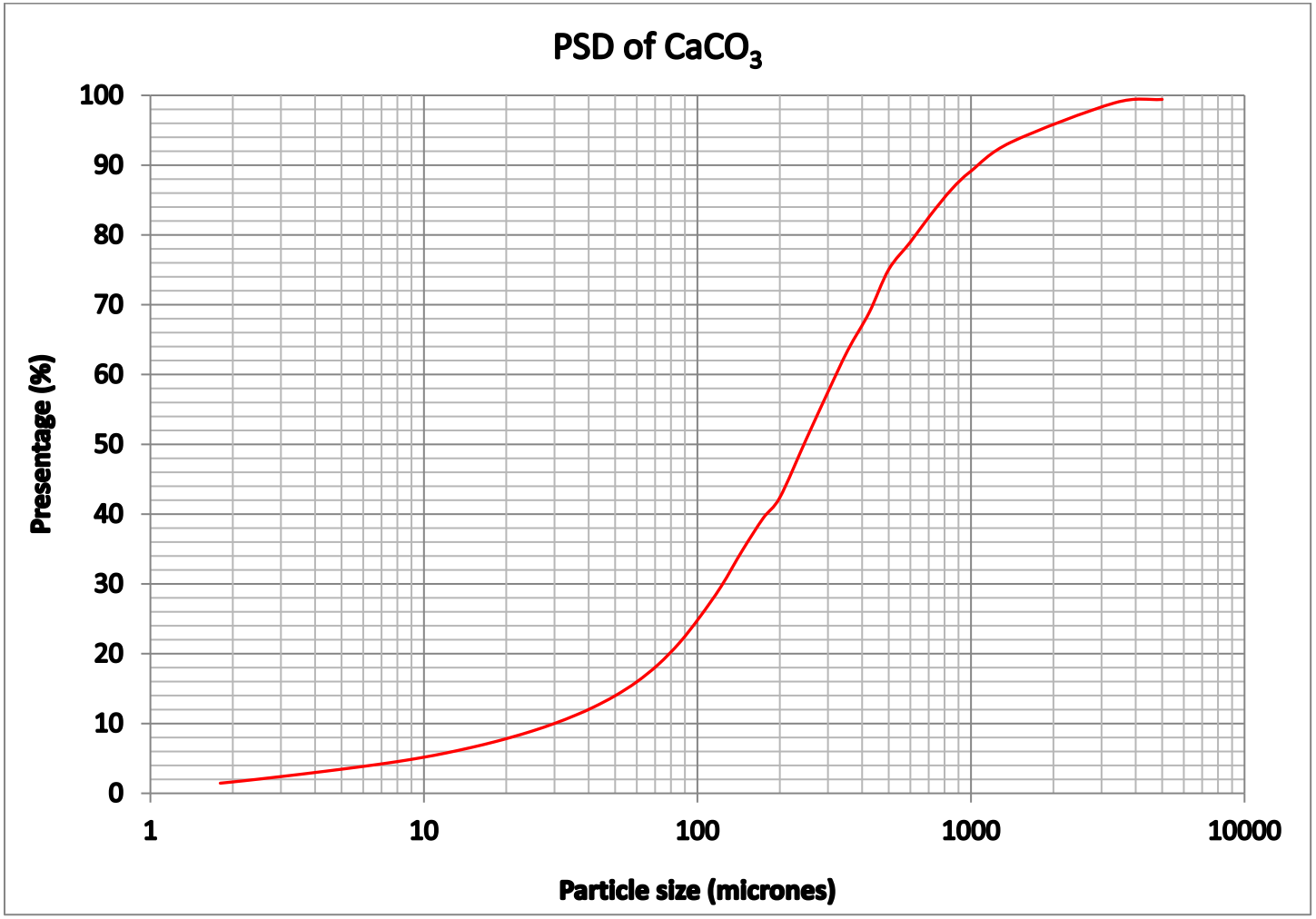

Appendix III: Target material properties

NORSK STÅL

CO #	Item #	Del #	Heat	Lot	Your art #	Qty	Description
	100	RP4367 9	299686			5	VV PL DX 355MCD B/O 4,0X1500X3000 MM

This document is electronically reproduced and is identical to the original.

100

SSAB

SSAB EMEA AB, SE-781 84 BORLÄNGE, Sweden

Inspection certificate A02	Issuing department A05	Purchaser order no A07	Our order no A08	Invoice no A19	Certificate no and date A03
EN 10 204 - 3.1	Quality inspection	46033833-2005	860979-2	2725768	15703992 2015-11-23

Purchaser A11
45280

NORSK STÅL A/S
POSTBOKS 123
NO-1378 NESBRU
NORGE

Product B01
HR pickl. wide strip in sheets

Marking B06
Manufacturer, MATERIAL ID

Standard/rules B02
SSAB
Steel grade DOMEX 355 MC D*)

Quantity B08	Dimensions [mm] B09-B11	Weight [kg] B12	Deliv. Cond. B04	Internal code B16
182	T 4 W 1500 L 3000	25900		

Consignee A06
NORSK STÅL A/S POSTBOKS 123 NO-1378 NESBRU NORGE

Customer marks B15

MATERIAL ID B07
29-9686-709329-01 , 29-9686-709329-02 , 29-9686-709329-03 , 29-9686-709329-04 , 29-9686-709329-05 , 29-9686-709329-06 , 29-9686-709329-07 , 29-9686-709329-08 , 29-9686-709329-09 , 29-9686-709329-10 , 29-9686-709329-11 , 29-9686-709329-12 , 29-9686-709329-13 , 29-9686-709329-15

Chemical composition C71-C92

Heat no	C	Si	Mn	P	S	Cr	Ni	Mo	V	Ti	Cu	Al	Nb	B	N	Cekv
29-9686	.064	.01	.64	.009	.004	.02	.03	.00	.01	.00	.01	.034	.023	.0001	.002	.18

Carbon equivalent etc C93-C99
Cekv = C + Mn/6 + (Ni + Cu)/15 + (Cr + Mo + V)/5

Testtype C04	Millcode C00	Specimen position C01	Direc-tion C02	Treat-ment B05	Specimen type C10	Temp [degr C] C03	Test results
Tensile test	CCG991	Top end	Longitudinal	Delivery condition	Rectangular 380x40		C11 Reh [MPa] 390 / C12 Rm [MPa] 479 / C13 A5 [%] 37.5
Bend test	CCG992	Top end	Transvers	Delivery condition	Rectangular 300x25		C50 The_test_is satisfactory -

*) S355MC EN 10149-2

Production time: 2015-11-19

Customer article no: 27233

It is hereby certified that the material described above complies with the requirements of the order. Z02

This certificate is produced with EDP and valid without signature Z01

Material Testing/ L Smedh/ L Söderqvist/ S Forsström/ M Eriksson

A22

A04
DOMEX® HIGH STRENGTH STEEL
www.domex.com

PROV 1.0 (45280)

Doctoral dissertation no. 101
2021

—

Impact erosion by solid particles in gas-particle flows

Dissertation for the degree of Ph.D

—

Mahesh Ediriweera

—

ISBN: 978-82-7206-608-5 (print)
ISBN: 978-82-7206-609-2 (online)

usn.no